POLITECNICO DI MILANO

School of Industrial and Information Engineering

Master degree in Materials Engineering and Nanotechnology

FIELD EFFECT TRANSISTORS BASED ON $Sp^2 - Sp$ CARBON MOLECULES

Supervisor: Prof. Carlo S. Casari

Co-supervisor: Mario Caironi

Tommaso Losi

ID 882507

Academic Year: 2018 – 2019

Contents

Abstract

Carbon-based materials have gathered a lot of attention during the last years in many scientific and technological fields because of the wide range of possible structures assumed. They possess tuneable physical properties that vary with size, geometry and hybridization, making them versatile in many applications. Nowadays the most investigated materials are based on sp^3 and sp^2 hybridization. For what concerns *sp*-carbon based materials, even if a lot of theoretical work has already been done, only few experimental studies have been performed because of their high instability due to their tendency to crosslink. Nevertheless, outstanding properties, including high electrical conductivity, have been theoretically predicted that make them appealing in many fields of science and engineering.

The aim of this work was to test the thin-film electronic properties of a small *sp*-carbon based molecule named *[3]ph* (tetraphenyl butatriene) as a case study to assess the potentiality of an hypothetical completely new class of π conjugated materials for molecular electronics. This was done by adopting the thin films as active material in Field − Effect Transistors (FETs) in a Bottom gate − Bottom contacts (BGBC) configuration. A self-assembling monolayer of pentafluoro tiophenol (PFBT) was used to improve charge injection. The transistors produced at the beginning by drop-casting were shown to work, but with low performances and poor stability, mainly because of the low film-forming properties of *[3]ph* that tends to form a deposit of isolated randomly disposed needle-like crystals. For this reason, many deposition-tests were performed, changing various processing parameters, in order to obtain a film with good uniformity and coverage. In particular, the effects of deposition technique, processing temperature, solvent, concentration and type of substrate were considered, as well as the possibility of blending the semiconductor with an insulating polymer (atactic polystyrene). After many trials, the best condition, among those explored, turned out to be the deposition by bar-coating of a solution of *[3]ph* with PS (1:1) with concentration of 20 mg/ml in 1,2-dichloro benzene (DCB) at temperatures higher than 50°C. Under these conditions, crystalline films with good uniformity, reproducibility and coverage were obtained. Depending on the processing temperature, the morphology was

observed to change a lot, from small single crystals to highly oriented fibers or spherulite-like domains. The films were characterized by many techniques such as: optical polarizing microscopy and scanning electron microscopy (SEM), to study film morphology; mechanical profilometer, to get information about the surface profile and state of roughness; and UV-vis spectroscopy, to study solid state interactions. Also X-ray diffraction and SERS measurements were performed, to obtain informations on the crystalline structure and the mechanism of charge transfer between metal electrodes and active material. For the transistors produced by bar-coating *[3]ph* with PS, a net improvement of electrical performances was observed, including an increase of field-effect mobility of two orders of magnitude, reaching a maximum of 0,05 cm^2/Vs. In particular, the devices showed a constant non-bias dependent mobility, with a reliability factor higher than 70% and a steep subthreshold swing around $0,2 - 0,1$ V/dec. Even the stability in air of the material was improved, thanks to the encapsulation effect of the polymer. Furthermore, at the end of this work, an attempt was made to change device architecture, by passing to a Top gate − Bottom contacts configuration (TGBC) was done. The transistors produced in this way showed an improved stability and device ideality with respect to the BGBC configuration, eliminating unwanted electrical features like the presence of a hysteresis cycles.

This work, studying for the first time the electrical properties of *sp*-carbon-based materials in transistors, has been able to demonstrate the great potential of these systems in organic electronics.

Riassunto

Negli ultimi anni, i materiali a base di carbonio hanno catturato l'attenzione della comunità scientifica, per via della vasta gamma di strutture che possono assumere. Essi hanno proprietà fisiche ingegnerizzabili che possono cambiare variando dimensioni, geometria e ibridazione, rendendo questi sistemi versatili in diversi campi scientifici e tecnologici. I materiali più studiati, che trovano una reale applicazione, sono quelli basati su ibridazione sp^3 e sp^2. Per quanto riguarda quelli ibridizzati sp, anche se sono state fatte diverse indagini teoriche, sono stati condotti ancora pochi studi sperimentali, poiché questi sistemi sono altamente instabili a causa della loro tendenza a reticolare. Tuttavia le loro proprietà eccezionali, tra cui l'elevata conducibilità elettrica, rendono questi materiali interessanti in diversi campi scientifici e ingegneristici.

Lo scopo di questo lavoro è stato quello di testare le proprietà elettroniche in film di una piccola molecola a base di carbonio ibridizzato sp denominata *[3]ph* (tetraphenyl butatriene) come caso studio, per valutare le potenzialità di un'ipotetica nuova classe di materiali π coniugati. Ciò è stato fatto utilizzando i film sottili come materiale attivo in transistor a effetto di campo (FET), con configurazione Bottom gate − Bottom contacts (BGBC). Un monostrato auto-assemblante di pentafluoro tiophenol (PFBT) è stato usato per migliorare l'iniezione di carica. I transistor prodotti inizialmente mediante drop-casting, hanno dimostrato di funzionare, ma con basse prestazioni e scarsa stabilità, principalmente a causa delle inadeguate capacità del *[3]ph* nel formare un film uniforme e compatto. Di fatto, esso tende a formare un deposito di cristalli isolati, simili ad aghi, disposti in modo casuale. Per questo motivo, dopo i primi dispositivi, sono stati eseguiti numerosi test di deposizione, durante i quali sono stati modificati diversi parametri di processo al fine di ottenere un film con buona uniformità e copertura. In particolare, sono stati considerati gli effetti dovuti al tipo di tecnica di deposizione, temperatura di lavorazione, genere di solvente, concentrazione e tipo di substrato, nonché la possibilità di miscelare il semiconduttore con un polimero isolante (polistirene atattico). Dopo molte prove, la migliore condizione, tra quelle esplorate, si è dimostrata essere la deposizione mediante bar-coating di una soluzione di *[3]ph* e PS (1:1) con concentrazione 20 mg/ml in 1,2-diclorobenzene (DCB) a temperature superiori a 50°C.

In questa condizione, sono stati ottenuti film cristallini con buona uniformità, riproducibilità e copertura. A seconda della temperatura di lavorazione, è stato osservato che la morfologia può cambiare parecchio, passando da piccoli cristalli a fibre altamente orientate o domini simili a sferuliti. I depositi prodotti sono stati caratterizzati mediante: microscopia a polarizzazione ottica e microscopia elettronica a scansione (SEM), per studiare la morfologia; profilometro meccanico, per ottenere informazioni sullo stato superficiale; e spettroscopia UV-vis, per studiare possibili interazioni a stato solido. Sono state effettuate anche misure di diffrazione a raggi X e SERS. Le prime per ottenere informazioni sulla struttura cristallina, le seconde per studiare il meccanismo di trasferimento di carica che avviene tra elettrodi metallici e materiale attivo. Per i transistor prodotti deponendo una soluzione di *[3]ph,* con PS, mediante bar-coating, è stato osservato un netto miglioramento delle prestazioni elettriche, incluso un aumento della mobilità a effetto campo di due ordini di grandezza, raggiungendo 0,05 cm^2/Vs. In particolare, i dispositivi hanno mostrato mobilità costanti e indipendenti rispetto al voltaggio di gate, con un fattore di affidabilità superiore al 70% e subthreshold swing intorno a 0,2 - 0,1 V/dec. Anche la stabilità del materiale in aria è migliorata, grazie all'effetto di incapsulamento del polimero. Inoltre, alla fine di questo lavoro è stato effettuato un tentativo in cambiare l'architettura del dispositivo, passando a una configurazione Top gate – Bottom contacts (TGBC). I transistor prodotti in questo modo, hanno dimostrato di funzionare, di avere una migliore stabilità e idealità del dispositivo rispetto alla configurazione BGBC e di riuscire a eliminare caratteristiche elettriche indesiderate come la presenza di un ciclo di isteresi.

Questo lavoro, approfondendo per la prima volta gli studi delle proprietà elettriche di materiali a base di carbonio *sp* nei transistor, ha dimostrato la grande potenzialità di questi sistemi nell'elettronica organica.

1. *Sp* – carbon based materials

## 1.1 Introduction to *sp* − hybridization: polyynes and cumulens

In the last years, carbon based materials have played a crucial role in science and technology advancement (1). Carbon is the only element able to produce a large variety of materials with different structures and properties depending on the type of hybridization assumed: sp^3, sp^2 and *sp*. To describe the electronic structures of these materials mixed hybrid orbitals given by a proper linear combination of the pure valence orbitals *2s* and *2p* coming from each isolated carbon atom have to be considered. This can be done since the 2s and *2p* have slightly different energy and can be treated, in first approximation, as degenerate. These hybrid orbitals are used because their special orientation in space very well describes the three different types of geometries of carbon that are experimentally observed: tetrahedral, trigonal planar and linear. Hence, with them it is possible to distinguish carbon based materials depending on the structure assumed.

While in sp^3 hybridization all the *2p* orbitals are mixed to form σ molecular orbitals, leading to an insulating character, in the case of sp^2 hybridization, thanks to the left *2p* orbital orthogonal to the molecular plane, it is possible to form π-conjugation with the formation of π molecular orbitals, which are delocalized and more polarizable, resulting in a semiconducting character. For this reason, sp^2 carbon based materials have gathered a lot of attention in these years especially in electronic and optoelectronic applications due to the possibility of tuning electrical, optical and thermal properties by changing the chemical composition, structure and dimensionality of the system.

In principle also *sp* hybridization is able to sustain π-conjugation since two hybrids are used to form σ orbitals while two *2p* atomic orbitals can be used to form two different

sets of π molecular orbitals orthogonal to each other (2). For this reason, *sp* carbon based materials would have a great potentiality of application in all the fields in which sp^2 hybridization is used since they should display semiconducting and conducting properties. In particular, in recent years these systems started to be considered as possible alternative to normal π conjugated materials in molecular electronics, where single molecules or monolayer ensembles are at the base of electronic devices (1). In Fig.1 the three different types of hybridizations of carbon with the related hybrid orbitals and geometries are presented.
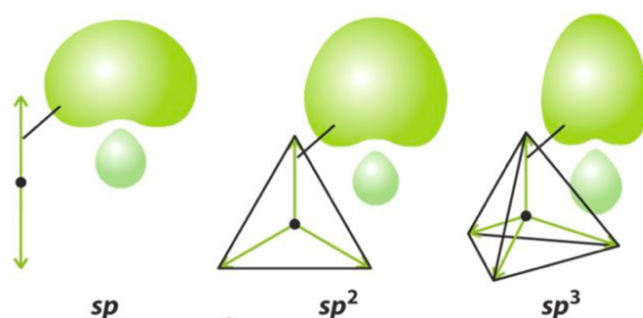
Figure 1. Hybrid atomic orbitals of carbon and the corresponding geometries in space.

The hypothetical bulk material based on *sp* carbon, called carbyne, should be constituted by many long atomic linear chains weakly interacting by Van der Waals forces. The existence of such material has been subject of debates until today. It is generally thought that carbyne would be highly unstable upon crosslinking. However, isolated finite molecules with different lengths and terminations have been synthetized.

The ideal infinite system constituted by a linear chain of carbon atoms hybridized in *sp* configuration is called carbon atomic wire (CAW) and it presents two possible resonant structures, shown in Fig.2, which display semiconducting or metallic behaviour. The first one is called polyynic structure and it is characterized by an alternation of single and triple bonds, while the second one is the cumulenic structure characterized by an equalized chain made of a successive alternation of double bonds. A useful parameter that allows to distinguish between these limiting cases is the so-called bond length alternation (BLA – difference in bond length between two adjacent carbon atoms) which is zero for the cumulenic case and different from zero for the polyynic one.
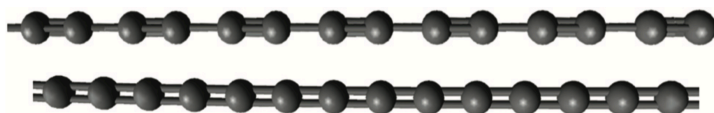
Figure 2. Structures of an ideal infinite carbyne: polyyne and cumulene.

In the framework of the Linear Combination of Atomic Orbital (LCAO), using Tight – binding methods or Hückel theory, it is possible to explain the electronic properties of these systems and why the band gap will change while changing the BLA (3). In case of an infinite cumulene, the Hamiltonian matrix for the π electrons will be described just by a single value of tunnelling integral -*t* as first off-diagonal elements (since all the bonds are equals as also the interactions among atoms) and one value of on-site energy ε_0 (diagonal elements). All the other elements are zero according to the first neighbour approximation. Then, applying periodic boundary conditions, recognizing the cyclic structure of the matrix and solving the corresponding eigenvalues problem it is possible find the π electronic band structure (4):

$$E^{\pi}(j) = \varepsilon_0 - 2t\cos(\theta_j)$$

In the latter expression, θ_j is a scalar phase factor connected to the electronic wave vector and the size of the unit cell: $\theta_j = \overline{k_j} \cdot \overline{a}$. Then, since there is just one π electron for each *2p* orbital and since the unit cell is formed by only one carbon atom, there will be two degenerated conduction bands (one for the *2p$_z$* and one for the *2p$_y$* orbitals) half occupied leading to a metallic character. In Fig.3 the dispersion relationship is shown, where the effect of tunnelling integral variation is also demonstrated.
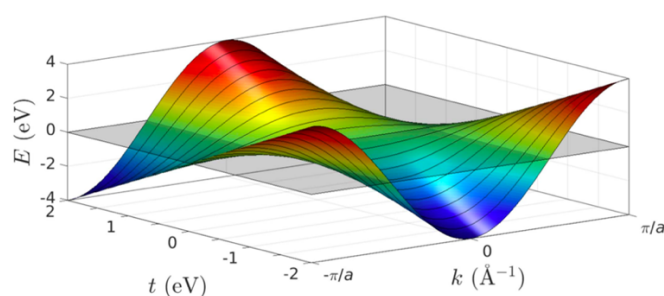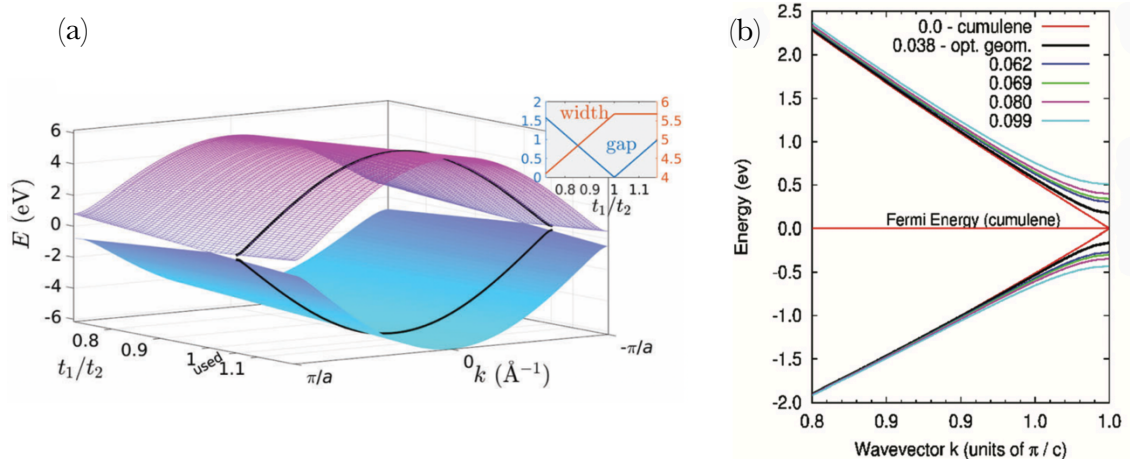

Figure 3. Dispersion relationship of an infinite cumulene with BLA equal to zero and variable value of tunneling integral (5).

In case of an infinite polyyne, two values of tunnelling integral $-t_1$ and $-t_2$ must be considered for the single and triple bonds. In this case, the matrix will be similar to the one for cumulenes but in form of blocks. The diagonal blocks $\overline{\overline{A}}$ will represent interactions within the unit cell (composed by two atoms), while the off-diagonal blocks $\overline{\overline{B}}$ will represent interactions between adjacent cells. $\overline{\overline{A}}$ will contain both ε_0 (along the diagonal) and $-t_1$ (as off-diagonal elements) while $\overline{\overline{B}}$ will contain just one non-zero element equal to $-t_2$. Solving the corresponding eigenvalues problem in cyclic form, in this case two non-degenerated bands for both *2p$_z$* and *2p$_y$* orbitals are obtained; one will be the conduction band and the other the valence band (4):

$$E^{\pi}(j) = \varepsilon_0 \pm \sqrt{t_1^2 + t_2^2 + 2t_1 t_2 cos(\theta_j)}$$

Since the number of electrons is equal to the one of cumulenes, but the unit cell is composed by two carbon atoms, in this case the valence band will be completely filled, while the conduction one will be empty, resulting in a semiconducting character. The band gap is directly related to the difference between the absolute values of t_1 and t_2 or, in other words, to the difference in bond length between adjacent bonds (BLA). If the number of carbon atoms tends to infinite, E_g will tend to $\sim 2(t_2 - t_1)$. For a perfect alternated polyyne these two values should be chosen in such a way to reflect the presence of a perfect single and triple bond. In Fig.4(a) it is possible to see the dispersion relationship and the trend of the band gap as a function of the ratio between t_1 and t_2. As we can see, as the ratio increases up to 1 (cumulenic phase), the band width and band gap linearly increases and decreases respectively. Then, for ratios larger than 1, the gap starts to increase, while the width remains almost constant. These results could be interpreted also in terms of a change in the BLA instead of a change in the ratio between t_1 and t_2 since the two quantities are directly related, as shown in Fig.4(b).

Figure 4. (a) Dispersion relationship for an infinite polyyne with variable ratio between tunneling integrals related to the single and triple bonds (4). (b) Dispersion relationship for an infinite polyyne with different BLA values (6).

For an infinite CAW, the cumulenic configuration is actually unstable upon bond deformation and tends to pass in its alternated counterpart. This is attributed to Peierls distortion, as in the case of sp^2 polyacetylene (2). In Fig.5 it is possible to see the metal – semiconductor transition for an infinite CAW as a function of the BLA, which is a useful distortional parameter to characterize the system. The curve was derived by quantum mechanical calculations applying periodic boundary conditions to the system (7).
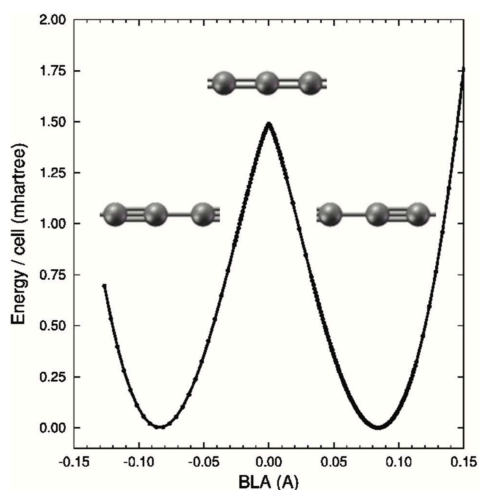

Figure 5. Total energy of an infinite CAW as a function of the BLA (7).

However, for finite systems, the end groups play a fundamental role in determining the actual value of the BLA and consequently the nature of the chain, especially when the wire gets shorter. In fact, Peierls distortion becomes effective only in very long chains (*n*

> 52), since it is rigorously defined for an ideal infinite system (2) and up to now, wires with lengths more than 50 atoms have not been synthetized. This is the reason why also cumulenic-like molecules can be effectively produced. Hence, the BLA can assume different values ranging from two limiting cases: the perfect infinite equalized cumulene (BLA=0) and fully infinite alternated polyyne depending on the terminations. BLA values exactly equal to zero has not been reached yet, but it is possible in any case to distinguish between cumulenes and polyynes when the value is closer to one of the two extremes. To model real finite systems and predict electronic properties such as band gap, it is still possible to use the infinite chain model but with an appropriate value of BLA (2).

Thanks to the BLA-modulating effect of end groups, there is the possibility of tuning electronic properties by controlling the molecular structure of the chain using different terminations. This is very appealing for technological applications. Some end groups stabilize the cumulenic phase while others the polyynic one, for a given value of chain length. Usually di-substituted chains assume an equalized structure while mono substituted chains will have an alternated one. An example is reported in Fig.6(a), (b) and (c) showing a comparison between different *sp* carbon molecules with the same chain length but different terminations. As shown in Fig.6(c), while H-endcapped wires have a finite BLA, $-CH_2$ terminated wires are expected to have an almost equalized structure with very low value of bond length alternation. In Fig6.(b) the same concept is represented but in terms of how the bond length changes moving along the chain. These results were derived by DFT calculations performed by Milani et al. (8).

(a)   (b)   (c)
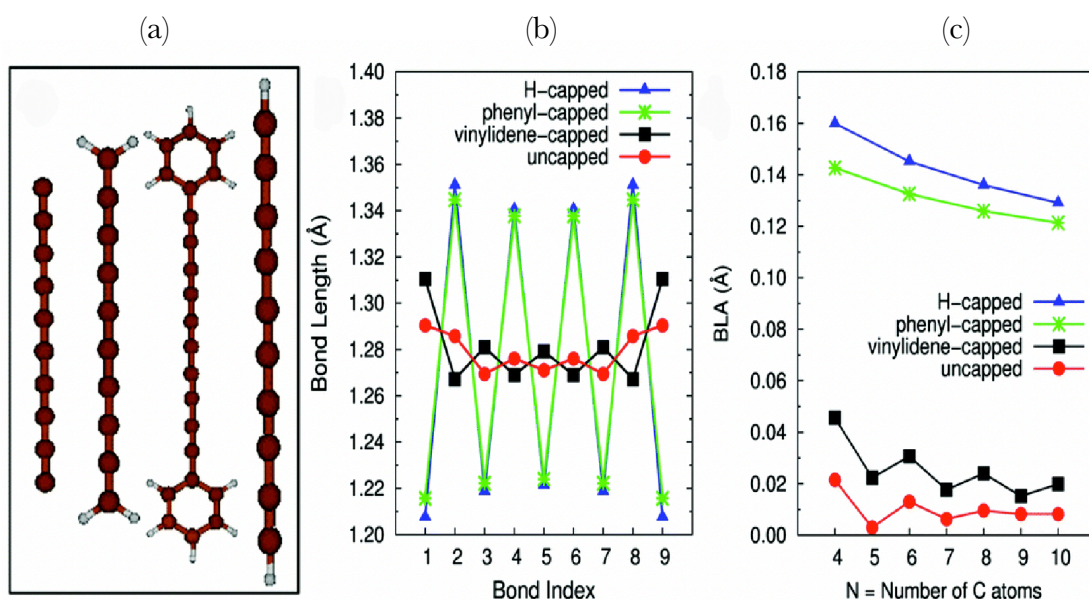
Figure 6. (a) Example of finite CAW molecules. (b)-(c) Changes in bond length along the chain and BLA values as a function of chain length for the molecules presented in (a) (8).

Based on these results, it is possible to understand that with a proper molecular design the properties of CAWs can be largely tuned, even more than sp^2 based materials. This possibility makes these systems very versatile in a vast variety of application fields.
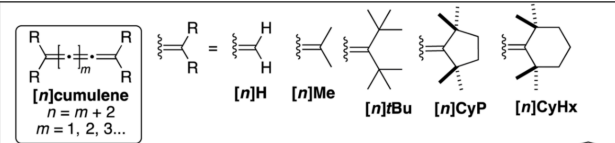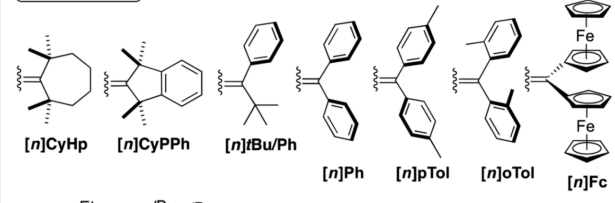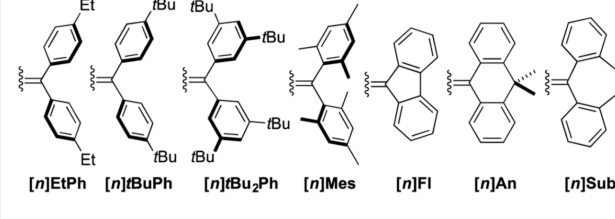
1.2 Synthesis and characterization

Carbon wires can be produced with both physical and chemical processes. Two examples of physical methods are the production of hydrogen endcapped polyynes by means of submerged arc discharge, as presented in the work done by F. Cataldo et al. (9), and laser ablation of solid carbon targets in liquid, producing a solution of polyyne-like chains with an even number of carbon atoms. These techniques offer also the possibility to control chain termination with the selection of suitable solvents (1). Liquid environments are preferred for the synthesis since they ensure a relatively good stability of the wires preventing intermolecular interactions as long as the concentration is kept low. For what concerns chemical methods, two main approaches have been used so far, both in solution. The first one is based on polymerization techniques such as dehydrohalogenation of polymers, dehydropolycondensation of acetylene and polycondensation reactions of halides (10), (11), while the second one is based on the dimerization of ethynyl groups with specific length and terminals (12). Other more complicated chemical reactions with different precursors have been used, depending on the particular chain length and end groups desired. Some examples of cumulene synthesis can be found in the work of Tykwinski et al. (12).

In general, polyynes, and even more cumulenes, are difficult to be produced due to their high intrinsic reactivity and tendency to crosslink, losing the *sp* character of carbon and moving toward a more stable sp^2 configuration. Different solutions to this problem have been adopted to improve the stability of these systems. An example is the use of Ag nanoparticles in a solution of H-terminated polyynes that proves stability in ambient

conditions for several months (1). Another approach adopted in chemical methods is the incorporation of bulky end-groups able to prevent chain-to-chain interactions. Thanks to the latter approach, the longest CAW produced so far has 44 carbon atoms (13). In Table.1, a list of cumulene-like molecules that has been synthetized so far with different chain lengths and terminations is presented (12). Cumulenes are more instable than polyynes and the incorporation of large sp^2 aromatic groups is fundamental to ensure stability.

Table 1. List of cumulenes that have been synthetized so far with different terminations and lengths (12).

	[3]	[4]	[5]	[6]	[7]	[9]
[*n*]Fc	√	√	√	√		
[*n*]CyHx	√	√	√		√	√
[*n*]Fl	√		√		√	
[*n*]An	√		√		√	
[*n*]Ph	√	√	√		√	√
[*n*]oTol	√		√		√	√
[*n*]Mes			√		√	√
[*n*]*t*Bu$_2$Ph	√		√		√	√

To characterize both polyynes and cumulenes many spectroscopic techniques can be used, such as IR, Raman and UV-vis spectroscopy. In particular, Raman spectroscopy is largely used to investigate both electronic and vibrational properties of carbon-based materials, due to their peculiar response thanks to which is possible to distinguish in an efficient way the different carbon structures. The Raman signal of carbon is in fact very sensitive to the type of hybridization, confinement effects, dimensionality, size, structure and topology of the system. Hence, it is possible to recognize some unique features in the Raman spectra and perform peak assignment for the different carbon materials. For this reason, Raman can be adopted also to investigate *sp* systems. Indeed, as it is possible to see in Fig.7(a), while the first order Raman signal of sp^2 carbon materials ranges between ~1300 to 1600 cm^{-1} depending on the particular system considered

(graphite, graphene, carbon nanoribbons, carbon nanotubes and fullerenes), the signal of CAWs falls in a region completely uncovered by other carbon systems (signals beyond 2400 cm^{-1} are due to second order Raman scattering). This allow to consider the Raman peaks at ~1800 to 2300 cm^{-1} as markers of the presence of *sp* carbon (1). In Fig.7(b) it is possible to see how Raman is able to distinguish very well polyynes with different size and end groups.
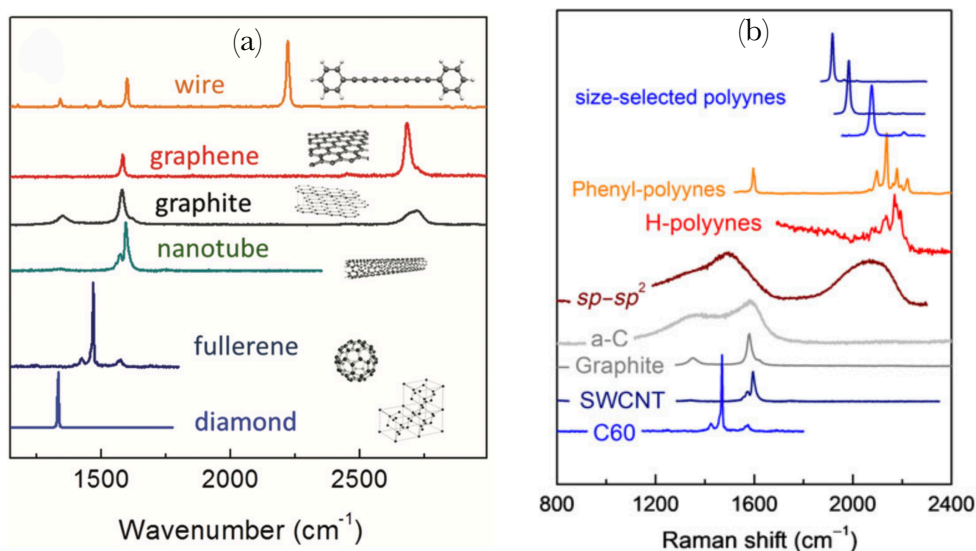
Figure 7. (a) Raman spectra of different types of carbon structures (2). (b) Raman spectra of some carbon based materials with *sp^2* and *sp* hybridization (2).

The peak assigned to *sp* carbon should correspond to a collective stretching vibration of the carbon atoms in the main chain, which can be interpreted also as a collective oscillation of the BLA. This vibrational mode is typically called "effective conjugated coordinate" or simply ECC mode. Based on the results predicted for the infinite carbyne and the general properties of polyconjugated systems, with increasing chain length, the degree of conjugation increases too, resulting in a red shift and in an increase of intensity of the ECC mode (2). This interplay between electronic and vibrational properties is due to the strong vibronic coupling of π conjugated systems, which means that changes in the BLA will affect both electronic and vibrational states. In Fig.9 the correlation between BLA, bang bap and vibrational frequency of the ECC mode is shown (in terms of LO phonon wave number) for an infinite chain derived by quantum mechanical calculations. To obtain this result, the vibronic coupling was included in the formulation of the matrix elements of the Hessians used to solve the vibrational problem

as follows (2), (3):

$$K_{ij} = \delta_{ij} k_{ij}^{\sigma} + 4 \left(\frac{\partial t}{\partial r} \right)^2 \alpha_{ij}$$
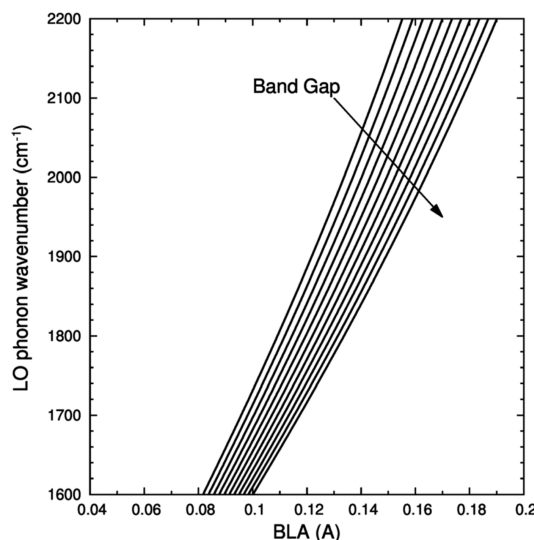

Figure 8. Correlation between BLA, Band gap and vibrational LO phonon wave number related to the ECC mode (14).

In the previous equation, α_{ij} is the polarizzability tensor, k_{ij}^{σ} are the force constants of the σ bond and $\partial t / \partial r$ is the vibronic coupling parameter that relates the change in the tunneling integral of Hückel theory along the chain. This model can be used also for finite chains where the effect of end-groups is fundamental in determining the real value of the BLA, as already said in the previous section. Thus, it is easy to understand how Raman spectroscopy is not only able to distinguish between different types of CAWs, but is also able to give information about the electronic properties, such as the energy gap.

Another important technique used to characterize these materials and to study the physics of charge transfer processes that occur between *sp* molecular wires and metal electrodes is SERS (Surface Enhanced Raman Spectroscopy) (15). With this technique, thanks to the formation of an organometallic complex with the metal substrate used to enhance the Raman signal, and the wire, it is possible to observe a charge transfer from(to) the metal to(from) the molecule followed by a structural change of the system. The understanding of the direction of charge transfer and the distribution of the excess of charge can be useful to model what happens in real devices like field effect transistors or solar cells where mobile charges are injected and collected from(to) metal contacts

to(from) the semiconductor. Milani et al. investigated charge transfer processes between silver nanoparticles (used both as SERS substrate and to stabilize the molecules in solutions) and polyynes terminated with N,N-dimethylanilo (DMA) groups with different chain lengths: two (C2) and eight (C8) carbon atoms (15). Comparing the Raman and SERS spectra of the two systems in the *sp* region, it is possible to notice the appearance of a new peak for C8 below 2000 cm^{-1} at typical frequencies of cumulenic systems. This was attributed to an induced molecular change due to electron transfer from the nanoparticle to the wire, which will behave as an acceptor. DFT calculations support this hypothesis thanks to the good agreement between the experimental SERS spectrum and the simulated Raman spectrum of a negatively charged molecule, as shown in Fig.10(a). However, for C2, no change in the spectrum was observed in the typical region of *sp* carbon, but rather in a frequency range below 1600 cm^{-1}, where several bands arise with the appearance of completely new spectral features. Thus, while for the C8 the excess of charge is expected to be more localized on the *sp* chain, leading to a change in the BLA, for C2 charge transfer involves mostly the end-groups, since the changes in the spectra are associated to peaks related to the terminations. Moreover, by comparing the experimental results and the simulations, it was possible to see that in this case the wire will behave as a donor, becoming positively charged. To support these interpretations, the ionization energy of the metal-wire complex was estimated in the two configurations, Ag$^+$/CAW$^-$ and Ag$^-$/CAW$^+$, for different chain lengths ranging from 2 up to 8 carbon atoms. As it is possible to see in Fig.10(b) there is an inversion moving from C2 to C8.

(c)

C2   C8
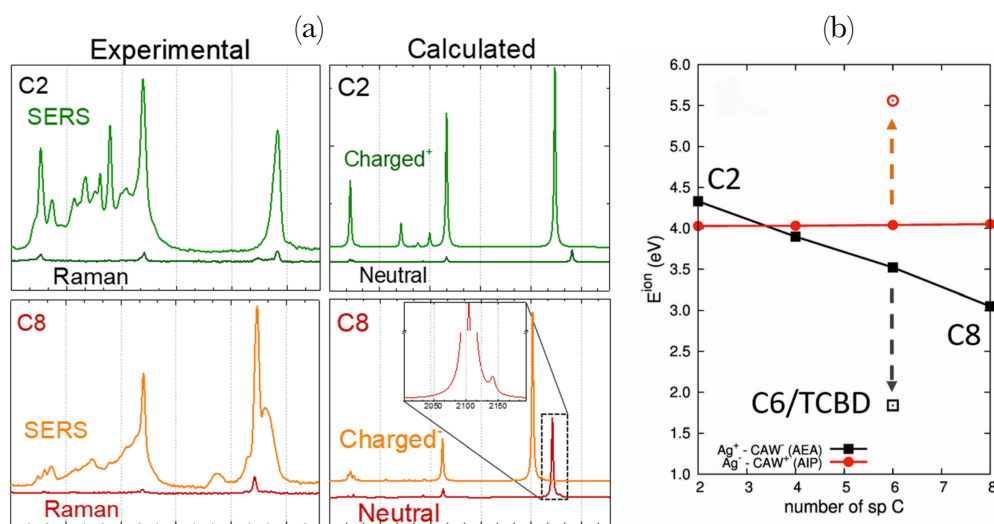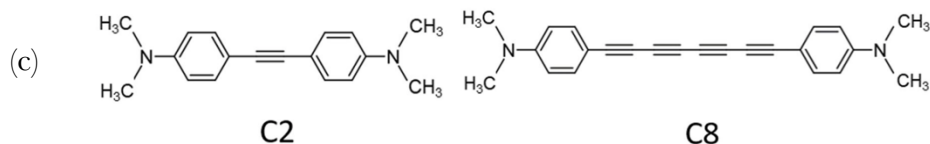
Figure 9. (a) On the left the experimental Raman and S.E.R.S spectra for C2 and C8 are shown, while on the right the calculated Raman spectra for the neutral and charged molecules are presented (15). (b) Ionization energy for two systems: Ag+/CAW- and Ag-/CAW+ changing the length of the wire (15). (c) Lewis structures of C2 and C8.

1.3 Potential applications

As mentioned before, CAWs in principle possess a great potentiality in many applications due to the high tunability of physical properties such as electrical and optical but also mechanical and thermal ones. The range in which they can change is very large due to the strong influence of end-groups, which are able to set the value of the BLA, affecting directly all the properties of the wire. As said before, these materials should display a conducting character, which can be brought closer to the metallic or semiconducting one, depending on the degree of conjugation. This makes these systems the perfect candidates in electronics and optoelectronics as semiconducting active media due to band gap engineering. Potential applications of finite wires can be found in the fields of organic semiconductors such as solar cells, photo detectors, light emitting diodes, lasers, field effect transistors and thermoelectric devices. Hence it could be possible to find a new family of π conjugated organic materials, in addition to the one constituted by sp^2 carbon, that could further improve the actual performances of carbon based devices. However, very limited experimental works have been performed. L. Ravagnan et al. performed conductivity measurements of an amorphous film with sp/sp^2 hybridization (with atomic fraction of sp carbon higher than 20%) produced by supersonic cluster beam deposition. The relative ratio between sp/sp^2 was observed to change as a function of the substrate temperature, affecting the electrical properties of the deposit (20). In the field of molecular electronics, isolated long CAWs have been considered as conducting atomic bridges between two metals electrodes. Few theoretical studies have been performed which predict unique electrical behaviours of a single

CAW. Lang et al. theoretically demonstrated (16) an oscillatory response with the chain length of the conductance of a hypothetical wire attached between two gold contacts. They modelled also charge transfer processes and intrachain transport supposing chemisorption of the wire on the electrodes. The conductivity values of such systems are predicted to be close to the maximum hypothetical one of $2G_0$, where G_0 is the quantum of conductance according to the Landauer formula (valid in case of quantum ballistic transport regime). In particular, even number of carbon atoms are predicted to have lower values of conductance than odd ones due to the behaviour of the DOS in correspondence of the Fermi level of the metal. Vasilii I. Artyukhov et al. have demonstrated the possibility of modulating the band gap of an ideal CAW with a mechanical stimulus inducing a metal to semiconductor transition (17). Another interesting system is represented by the hypothetical graphene-wire-graphene, appealing for nanoscaling of electrical devices and realization of pure carbon electronics. One of the few experimental studies of the properties of isolated wires is the work of La Torre et al. (18). They were able to create and measure transport properties of single CAWs connected between graphene edges. The system was produced using transmission electrical microscope (TEM) starting from graphitic aggregates. In particular, depending on the internal state of stresses, they were able to observe a change in the $I - V$ characteristic curve of the device indicating a metal − insulting transition, as shown in Fig.10. The "S" shape is attributed to a Schottky contact and a semiconducting character (polyynic chain), while a more linear curve is attributed to an ohmic contact and a metallic character (cumulenic chain).
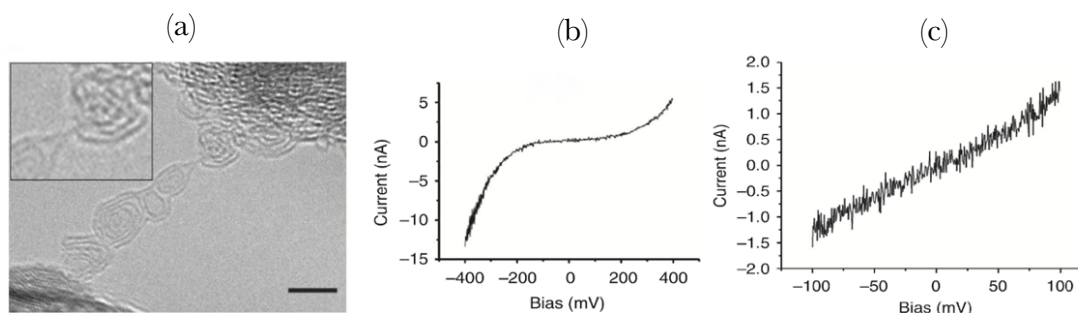
Figure 10. (a) TEM image of a CAW formed between graphitic contacts (18). (b)-(c) $I - V$ curves for a strained and unstrained CAW (18).

Yuya Tanaka et al. experimentally demonstrated the possibility of "doping" polyynic chains with d-transition metals (Ru fragments) that, interacting with the molecule, form

an organometallic complex able to change the frontier orbitals and prevent crosslinking (19). This work is fundamental because it illustrates the possibility to realize stable metal-to-wire junctions thanks to the presence of bulky groups. The molecules used are metallo-polyynes with AP(OMe)$_3$ groups as terminations and length from 2 to 4 carbon atoms. They are schematically represented in Fig.11. The end-groups are fundamental to form C-Au(electrode) covalent bonds. These systems have shown conductance of 10^{-2} - 10^{-3} G$_0$. These values were measure by STM – break junction technique.
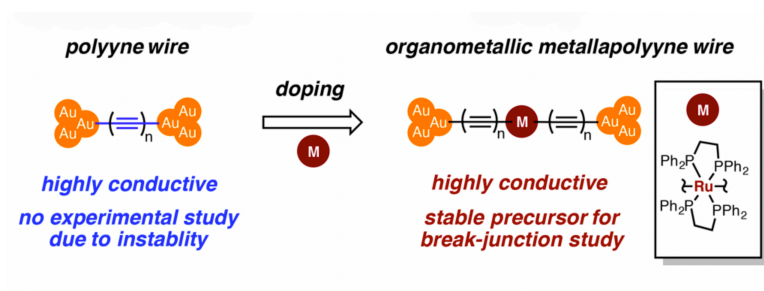
Figure 11. Comparison between undoped and doped wires with Ru fragments (19).

According to their structures, CAWs should also have excellent mechanical properties in terms of mechanical strength, which might be even higher than the one of nanotubes and graphene if one considers an ideal long chain. Thus, they have a great potentiality also in mechanical applications, especially the field of composite materials, as possible reinforcing phase.

2. Organic Field Effect Transistors

## 2.1 Working principle and architectures

An organic field effect transistor (OFET) is an electrical device whose working principle is quite similar to the one of its inorganic counterpart, which is the common metal-oxide-semiconductor field effect transistor (MOSFET). Also in this case we exploit a field effect to tune the conductivity of a semiconducting active material by controlling the charge carrier density thanks to the application of a bias voltage. In this way it is possible to modulate the intensity of the current flow between two electrodes (source and drain) with the application of a voltage to a third one, called gate. A schematic representation of a MOSFET is shown in Fig.12 underlining the most important geometrical parameters: L (channel length), W (channel with) and t (dielectric thickness).
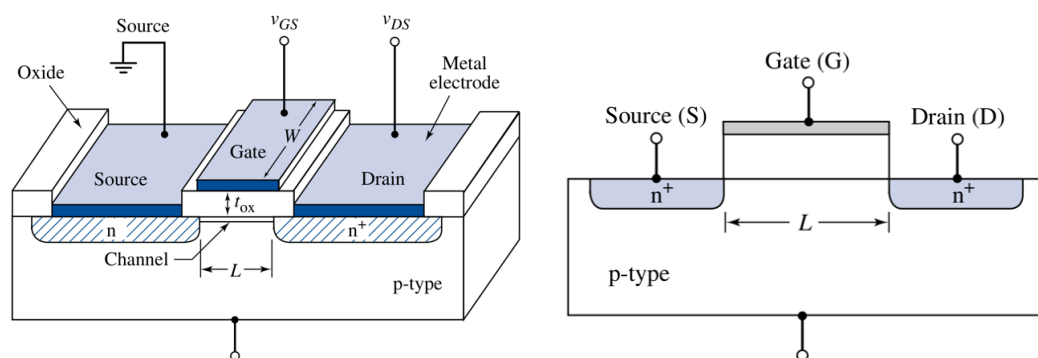
Figure 12. General architecture of a MOSFET.

As we can notice, the whole device can be seen as a capacitor made of the gate electrode, the dielectric and the semiconductor. Let's imagine for a moment that the last one is a p-type material, like silicon doped with an element of the V group, so that it will preferentially show hole conductivity. In this case, by applying a positive vertical voltage

at the gate, we generate an electric field that penetrates in the dielectric, polarizing it, and in the semiconductor. The field, created by the induced positive charges at the gate, will repel holes which are majority carriers, moving them away from the semiconductor-dielectric interface, and attract electrons, which are the minority carriers. Hence, increasing the gate voltage, a negative space-charge region will be created. At a certain point, if the positive bias is large enough, the density of minority carriers at the interface will be comparable to the one of majority carriers, creating the so-called electron-inversion layer. This layer, or channel, is able to connect two n-doped regions below source and drain so that, if a voltage is applied between these two terminals, a current can flow with an intensity determined by the conductivity of the conducting channel, which will increase by increasing the gate voltage. For an n-type semiconductor the principle is the same but the bias applied at the gate will be negative to create a hole-inversion layer. This particular operating mode is called enhancing mode. There is also the accumulation mode in which instead of creating an inversion layer of minority carriers, an accumulation layer of majority carrier is formed, applying an opposite bias. In Fig.13 the two operating modes of a MOSFET are shown.
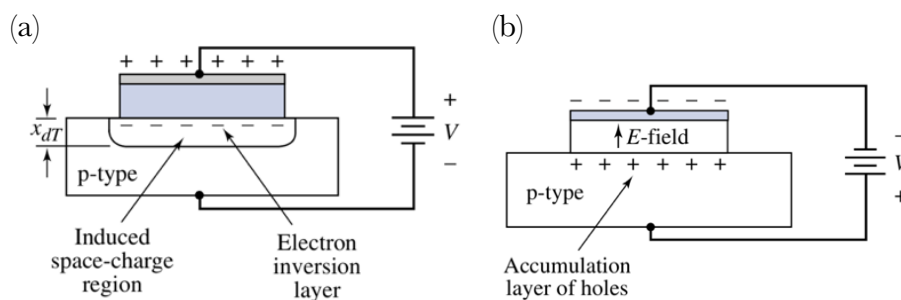
Figure 13. The two operating modes of a p-type MOSFET: (a) enhancing mode, (b) accumulation mode.

In case of an OFET, the major difference with respect to a MOSFET is that the active material is an organic semiconductor. Also in this case it is possible to tune the conductivity of a thin layer of material that acts as conducting channel by applying a voltage. However, to create the channel, unlike for usual inorganic semiconductors, we work in accumulation regime, forming a region close to the interface, usually of few nanometres, in which the carrier density of majority carriers is increased by field effect, so that the material will become more conductive. For example, a channel of positive charges, let's say holes for simplicity, will be formed applying a negative bias at the gate with respect to the source. In this case, the material behaves as p-type. On the contrary,

if a positive voltage is applied at the gate, a channel of electrons is created and the material behaves as n-type. In principle all the organic semiconductors can behave in both ways since they are ambipolar. The mechanism by which the channel is created is different with respect to the one for common inorganic materials like silicon, even if in both cases it occurs through the application of a voltage that accumulates charges at the interface with the dielectric. For organic semiconductors the mechanism by which that happens can be seen as a sort of reversible doping process called charge − injection doping. Instead, in case of silicon, it occurs thanks to the electrostatic repulsion/attraction between electrons/holes and the electric field generated in the semiconductor, which causes a simple physical diffusion of carriers. To explain better this concept, it is necessary to explain what we mean by doping for organic semiconductors. From a microscopic point of view, it can be seen more as a chemical process rather than a physical one, unlike for inorganic semiconductors. In this case, it is not a physical diffusion of dopant elements that donate extra holes or electrons, but it is the creation of charged molecules thanks to charge transfer processes, which are, from a chemically perspective, redox reactions that take place between a donor and an acceptor specie. There are different ways to do so depending on the kind of device that we are considering. Some of them can be seen more as physical methods while other more as chemical methods. However, all the doping processes share the same fundamental principle: exploit redox chemical reactions between donor and acceptor. For example, in case of smart windows, which can be schematized as electrochemical cells, the doping will be reversible and performed thanks to a current that flows between anode and cathode (electrochemical doping). Another method, more "chemical" let's say, is instead the use of external substances to oxidize or reduce the material (chemical doping). In this case, the process is irreversible and the material remains charged. A list of doping processes is presented in Table2. with related advantages and disadvantages.

Table 2. List of type of doping methods used for organic semiconductors with advantages and disadvantages.

| Doping Method	Controlled Variables	Advantages	Disadvantages
Chemical doping	Vapor pressure, Exposure time to dopant	Simple way to obtain doping upon exposure of the sample to a vapor of the dopant or immersion into a solution with the dopant	Performed as slowly as possible to avoid inhomogeneous doping
			The doping levels obtained are not stable with respect to time
			Unexpected structural distortion may cause electrical conductivity decay
			Doping/de-doping shows low reversibility
Electrochemical doping	Amount of current passed	Doping level can be easily controlled by using an electrochemical cell with a controlled amount of current passed	Unexpected structural distortion may cause electrical conductivity decay
		Doping/de-doping is highly reversible and clean polymer can be retrieved	
		Can be achieved with many dopant species	
Photo doping	Radiation energy of light beam	Charge carrier is formed without chemical compound (dopants)	The electrical conductivity disappears rapidly when irradiation is discontinued due to recombination of electrons and holes
		No distortion of the material structure	
Non-redox doping	Protonic acid strength	Number of electrons generally does not change	Depends on the degree of oxidation of CPs and degree of protonation of the material
			Low conductivities are observed for some CPs
Charge-injection doping	Applying an appropriate potential on the polymer structure	Does not generate counter ions. Minimized distortion	Coulombic interaction between charge and dopant ion is very strong and can lead to change in the energetics of the system

The major differences are the methods by which doping is performed, determining the reversibility of the processes and the possible presence of counter ions given by the reduction (or oxidation) of the oxidizing (or reducing) agent. Charge − injection doping is carried out by applying a voltage difference without the use of any external substance. As the electrochemical and the photo − doping, it is reversible.

Thanks to doping, it is possible to introduce charges in the material that for the moment can be considered as electrons or holes for simplicity, leading to an increase of charge carrier density. For this reason, the charged material will show increased conductivity with respect to the typical high resistivity of the pristine material. The p-doping process will add positive charges, while the n-one negative charges, so the former will be an oxidation while the second one a reduction.

An important distinction has to be done regarding p-type and p-doped or n-type and n-doped materials. For common inorganic semiconductors usually there is no difference and the two concepts coincide. This because there is an intrinsic low concentration of both holes and electrons which can be increased selectively after doping, determining what are the majority and minority carriers and the type of conduction. For example, silicon, as it is, is neither a p- nor an n-type material. Then, when it is doped, the

number of electrons in the conduction band, or holes in the valence band, is increased, leading a p or n-type character.

For an organic semiconductor the two concepts are different. When we speak about p- and n-type materials, usually we are saying that there is a higher tendency to undergo a p- or n-doping process, even if the material is theoretically ambipolar and can conduce both electrons and holes. To be a p-type material the fundamental requisite is to have a high HOMO − easily oxidized, while to be an n-type it has to have a low LUMO − easily reduced. Hence, the term "doped", is referred to the charged material.
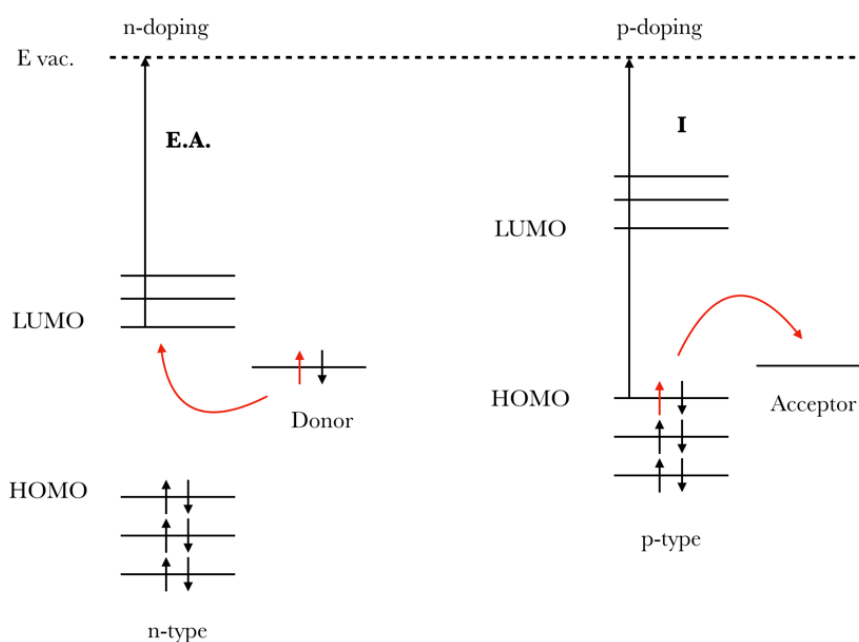
Figure 14. Energy scheme for an organic semiconductor when a p or n-doping process is performed.

Since the conductivity of the pristine (not charged) material is quite low, we don't need to use two reverse doped regions below source and drain to have a very low OFF current.

The common mathematical description of a FET is rather simple and leads the following equations, also called Schottky equations:

$$I_D = \frac{WC\mu}{L}\left[(V_G - V_T)^2 V_{DS} - \frac{V_{DS}^2}{2}\right] \quad V_D < V_D(sat)$$

$$I_D = \frac{WC\mu}{2L}(V_G - V_T)^2 \qquad\qquad V_D > V_D(sat)$$

$$\text{Capacitance of the capacitor} \quad C = \frac{\varepsilon_0}{t}$$

These equations are called current − voltage characteristic curves and they refer to the linear and saturation regimes. I_D is the current that flows between source and drain, while V_D is the voltage difference between them, called also drain voltage, and V_G is instead the voltage applied at the gate. V_T is the so-called threshold voltage that for inorganic semiconductors is defined as the bias that has to be applied at the gate to create an inversion channel of minority carriers with density equal to the one of majority carrier in the bulk. In other words, it is the value of V_G needed to create a conducting channel with enough conductivity to "turn-on" the device, so that a non-negligible current between source and drain can be observed. A threshold voltage a can be identified also for organic semiconductors, even if we cannot use the previous definition to define it. In this case, it represents the value of V_G needed to dope the material enough to have enough conductivity in a thin layer at the interface that connects source and drain. For MOSFETs, V_T is positive for p-type devices and negative for n-type ones. For OFETs, since the operating mode is the accumulation, V_T is negative for p-type devices and positive for the n-type.

In the linear regime there is a direct proportionality between I_D and V_D for a given gate voltage, hence the semiconductor channel behaves as an ohmic resistance and the slope of the curve is connected to the resistance R_{CH} of the channel. Obviously, if one increase V_G, the conductivity of the channel will increase too, leading a lower resistance and a higher slope. However, as the drain voltage V_D increases, the voltage drop across the dielectric close to the drain terminal decreases, leading to a decrease of the charge density. This causes a deviation from linearity and the I_D − V_D curve starts to bend. When V_D reaches a value for which the voltage difference across the dielectric at the drain is equal to V_T, the condition of "pinch − off" is reached.

$$V_G - V_D(sat) = V_T$$

Now, the transistor enters in the saturation regime where, in an ideal device, the value of I_D becomes independent on V_D, reaching a plateau. By increasing the gate voltage, the current keeps increasing quadratically with V_G. The passages from linear to saturation regime when increasing V_D in an ideal FET are illustrated in Fig.15.
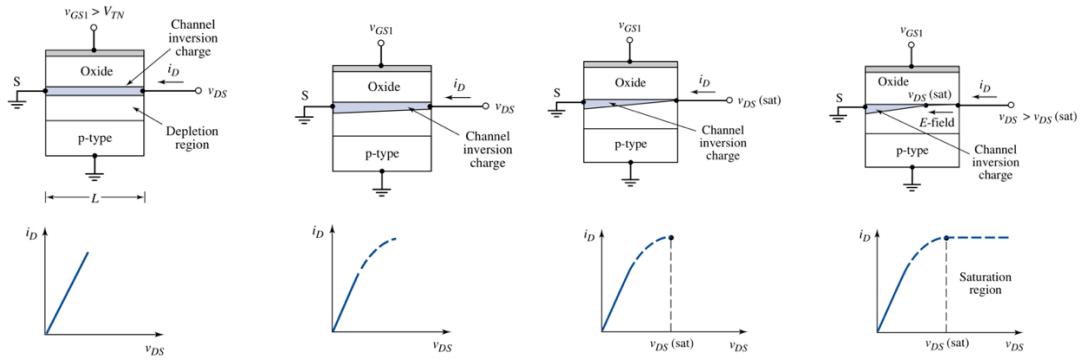
Figure 15. Evolution of the output characteristic with the drain voltage for a fixed gate bias.

Different families of $I_D − V_D$ curves for different values of gate bias are shown in Fig.16(a); this plot is called output curve or output characteristic of the device. Experimentally the plot is obtained by recording I_D as a function of V_D, for different V_G values. Another way to represent graphically the previous equations is in form of transfer curve or transfer characteristic. In this case I_D is plotted as a function of V_G for a fixed drain voltage. An example of a transfer curve is shown in Fig.16(b). Experimentally the transfer curve is obtained recording I_D as a function of V_G typically for two different value of V_D, one for the linear and one for the saturation regime.
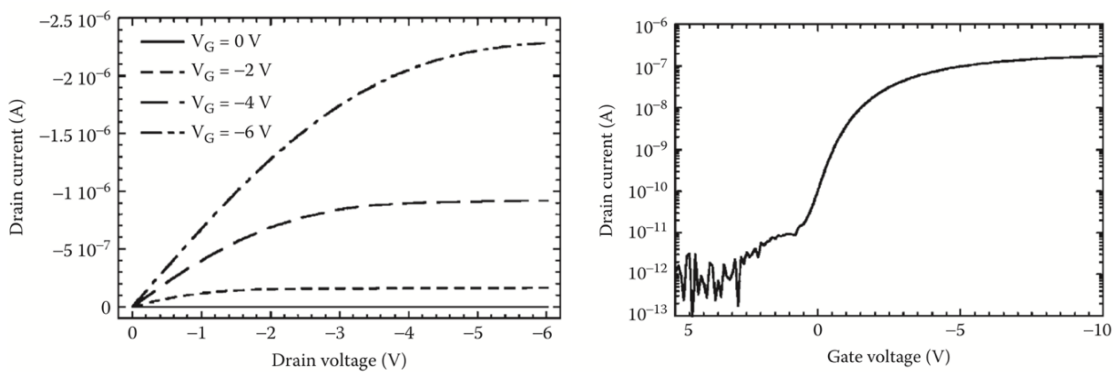
Figure 16. Output and transfer characteristic curves for a general OFET.

The transfer curve is the most common way to represent the electrical characteristic of the device. This because it is easier to extract experimentally material and device parameters, like mobility and threshold voltage, from this data rather than from the ones coming from an output curve.

It is important to mention that the previous equations used to model a field effect transistor are derived with some assumptions (21), (22):

1. The transverse electric field associated to V_G and/or V_D is much higher than the longitudinal one (gradual channel approximation).
2. The mobility is constant all over the channel and not bias dependent.
3. Charges are injected/extracted via ohmic contact (negligible contact resistance).
4. Transport is not limited by the presence of traps.

The first assumption is a direct consequence of device geometry and the fact that source – drain distance is often much larger than dielectric thickness. The second one is usually far from true in organic semiconductors. Moreover, the value of contact resistance is often very large (non-ohimc contacts), becoming one of the most limiting factors, together with the presence of different types of charge traps. For these reasons, the use of the previous equations to extract field effect mobility and other parameters could lead to a wrong estimation. The reliability of the parameters extracted is connected to the concept of ideality of the device. This concept will be explained more into details later on in Chapter 4.

For what concerns the architectures of OFETs it is possible to distinguish between four different configurations, shown in Fig.17, with related advantages and disadvantages.

1. **Top gate – Top contacts** (**TGTC**) Fig.17(a): the semiconductor is deposited on top of a substrate that acts as a support. Then, over the active material, source, drain and the dielectric are deposited. Finally, on top of the dielectric there is the gate terminal.

2. **Top gate – Bottom contacts** (**TGBC**) Fig.17(b): the architecture is similar to TGTC but source and drain are deposited on the substrate before the semiconductor that will be formed on top of them.

3. **Bottom gate – Top contacts** (**BGTC**) Fig.17(c): in this case, first there is a substrate, that usually acts also as gate terminal, over which the dielectric material and the semiconductor are deposited. Then, on top of the last one, there are the source and drain terminals.

4. **Bottom gate – Bottom contacts (BGBC)** Fig.17(d): the configuration is the same of BGTC but source and drain are deposited over the dielectric before the semiconductor, which will be on top the two terminals.

The three terminals, source, drain and gate, usually are metallic electrodes made of gold, silver or aluminium. Also highly doped semiconductors can be used, both inorganic materials such as a silicon substrate n⁻ or p⁺⁺, and doped organic polymer blends, like PEDOT:PSS. The dielectric material can be both an inorganic insulator like silicon dioxide, as well as a polymeric material.
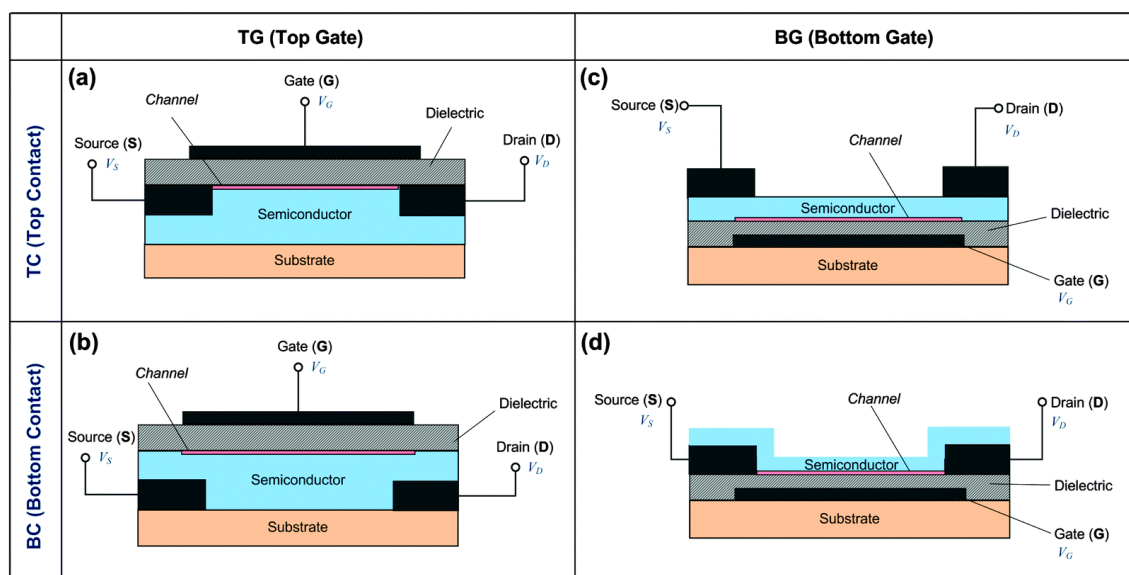
**Figure 17.** Possible architectures of OFETs (23).

In bottom gate (BG) configurations the active material is directly exposed to the external environment. This can limit the performances, since usually organic semiconductors are quite sensitive to the atmosphere, temperature, moisture, light and can be easily oxidized and degraded. They are reactive toward oxygen and water. For this reason, if the considered material is highly unstable, BG architectures are avoided while the top gates (TG) are preferred.

Bottom contacts (BC) configurations offer the advantage, with respect to top contacts (TC), to avoid the deposition of metal electrodes on the semiconductor, avoiding possible degradation phenomena. The deposition of the dielectric is usually not a problem since polymeric materials can be used, and they can be processed by solution techniques.

32

Depending on the type of semiconductor, one architecture could be better than the other. It depends on the semiconductor sensitivity and reactivity toward many processing and environmental parameters. The configuration that offers more advantages could be the TGBC one, if the deposition of the dielectric is not too invasive, due to the limited exposure toward the environment. However, to perform first studies of charge transport of new materials, usually the BGBC configuration is adopted, working in inert atmosphere or in vacuum. This because nothing is deposited on top of the semiconductor, avoiding any possible degradation.

2.2 Solution processed OFETs

Electronic and optoelectronic devices such as FET, light emitting diodes (LED), sensors, and solar cells based on solution processable organic semiconductors are rapidly increasing both their performances and reliability (24). They offer different advantages with respect to those processed with vacuum technology. For example, since the deposition does not require vacuum, it is cheaper and simpler. Moreover, manufacturing can be performed at low temperatures limiting the energy consumption and avoiding side effects like substrate degradation. Then, many techniques, especially the printing based manufacturing processes, are relatively easy to be scaled for large area production. On the other hand, it is more difficult to control precisely and in a systematic way the microstructure of the active material, leading to higher energetic disorder (25). Hence, the formation of the film will be more affected by the processing conditions. However, nowadays the values of field-effect mobility for solution-processed devices are approaching those obtained for OFETs produced with vacuum technology, especially in recent years. The progress of mobility values in OFETs over the years, comparing solution and vacuum processes, is reported in Fig.18(b) (22). In Fig.18(a) it is possible to see the comparison between p and n-type devices.
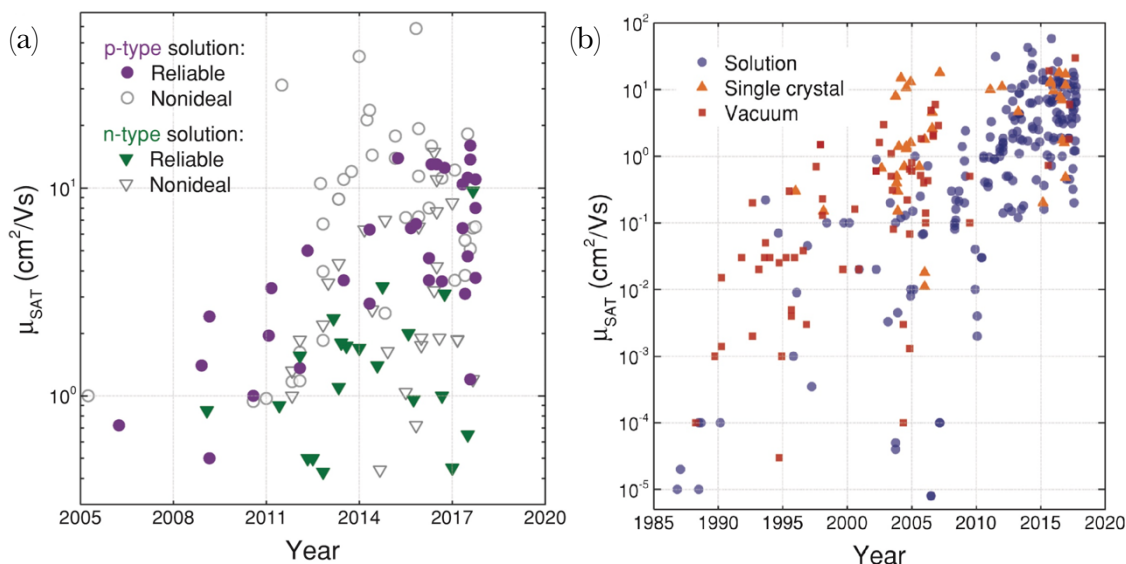
Figure 18. Trend of field effect mobility over the years, indicating which values are reliable and which not, due to non-ideality of the device. (a) Comparison between p- and n-type devices for solution processed OFETs (22). (b) Comparison between solution and vacuum technology, indicating also when the material is in form of single crystal (22).

2.2.1   Polymeric materials

There is a wide variety of semiconducting polymers but usually they are constituted by a main backbone formed of aromatic rings such as benzene or thiophene. Alkyl chains are often added as lateral substituents to increase the solubility, limiting π-π interactions thanks to good chain flexibility. The most common polymer is P3HT (poly(3-exhylthiophene)) and its thiophene derivatives (both homopolymers and copolymers). In Fig.19 (23) we can see some other examples.
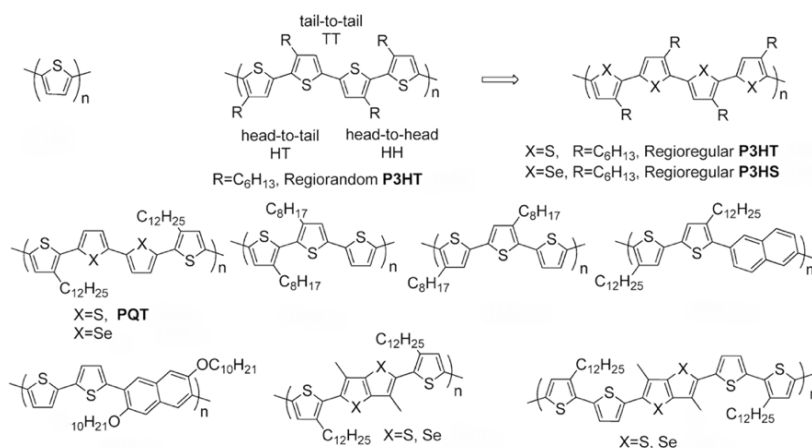
Figure 19. Examples of common thiophene based semiconducting polymers.

Semiconducting polymers have the advantage to exhibit high viscosity due to their high molecular weight. This makes it easy to process them when they are deposited with many techniques like spin coating, blade coating, bar coating and inkjet printing. However, the mobilities reached are lower with respect to small molecules. This is usually attributed to the fact that they cannot be fully crystalline due to kinetic effects. So there will always be a given amorphous content that limits charge transport efficiency. Another advantage of using polymers is that they have good mechanical properties, which is an important requirement for flexible electronics.

It is possible distinguish two main approaches to realize OFETs based on solution-processed polymers (24):

1. **Amorphous-like films**: in this case the aim is to produce a uniform film with good reproducibility in terms of morphology, avoiding any abrupt change in the structure and energy site fluctuation. Obviously the carrier mobility is often limited to low values (around 10^{-3}-10^{-2} cm^2/Vs). However, good environmental stability has been demonstrated. Examples of amorphous-like polymers are regioirregular polytiophenes.

2. **Semicristallyne films**: here the goal is to achieve a film with high degree of order and crystallinity to optimize charge mobility, which nowadays reaches values up to few cm^2/Vs. Depending on processing conditions many packing configurations and degree of crystallinity can be obtained affecting a lot the performances.

2.2.2   Small molecules

With small molecules it is possible reach relative high mobilities, comparable to the ones obtained with vacuum technology. This because they have a high tendency to crystallize thanks to strong π-π interactions and limited conformational disorder. Nowadays values higher than 10 cm^2/Vs have been reached. The disadvantage of small molecules is the limited film formability. One famous class is constituted by acenes and derivatives,

which are characterized by good intermolecular π interaction and overlap, leading to high transfer integrals (23). They are characterized by two different packing modes that depend on their specific molecular structures. In normal acenes, due to the balance between the π-π interactions and electrostatic repulsion, a herringbone configuration is thermodynamically favoured. However, if polar groups are introduced, a new balance can be achieved with a change in the packing, for example, from herringbone to lamellar stacking (23). The usual requirement form small molecules is to have good conjugation and molecular planarity to facilitate intermolecular interactions. Usually they are oligomeric compounds constituted by phenyl and thienyl rings fused together or separated by single bonds. Other hetorocycles can be found with oxygen and nitrogen. Lateral substituents are added to adjust the position of the energy levels in order to improve stability and tune ionization potential and electron affinity. Sometimes, as for polymers, alkyl chains (with 4-6 carbon atoms typically) are introduced to improve the solubility of the molecules and make them more processable without altering the ability to π-stack. Bridges made of single and triple bonds can be incorporated to force planarity and limit molecular distortion (Fig.20) (23).
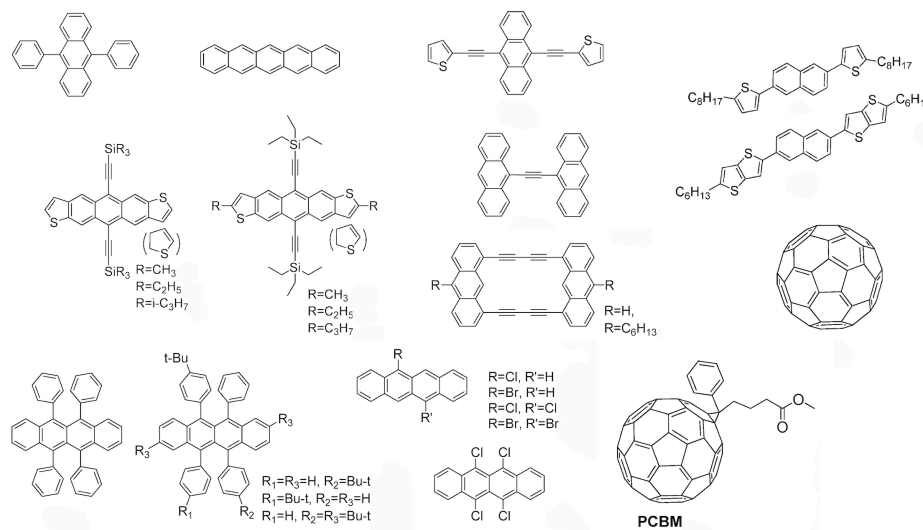
Figure 20. Examples of common semiconducting small molecules used in OFETs.

2.2.3   Semiconducting blends

A recent and emerging approach to increase the performances of solution-processed OFETs is the use of semiconducting blends. In this case the active material will be

constituted by a mix of different components. The blends that are more studied are constituted by two materials (bi-components), even if in literature also more complicated mixtures are present like three-components blends.

There are many examples of blends formed by a mixture of two semiconducting polymers. However, the most intriguing case is the one in which a small molecule and a polymer are combined. The idea beyond this concept is to exploit both the high mobility of small molecules and the processability of polymeric materials that can act as sort of binder to create a film with good uniformity. This strategy can be effective in contrasting morphological anisotropy and device-to-device performance variation, which are the drawbacks of small molecules films.

It is possible to list two main approaches used in binary small molecules/polymer blends (23):

1. **Blending a small molecule with an insulating polymer** will improve film formability resulting in better electrical properties and stability thanks to a vertical phase segregation.

2. **Blending a small molecule with a semiconducting polymer** often result in a further increase in mobility, especially if some requirements are satisfied, such as energy level matching. In this case, the polymer may not only improve film-forming properties and provide a sort of encapsulation, but it can also participate actively in the charge transport, in different ways depending on the structure of the film. For example, it might reduce the resistance at grain boundaries where usually it usually segregates in the layer richer of small molecules.

With these approaches, some of the best values of mobility for solution deposited semiconductors have been obtained (>10 cm^2/Vs), in addition to an improved environmental stability thanks to the polymer encapsulation properties. Furthermore, device ideality can be increased as an effect of a reduced disorder. Alexandra F. Peterson et al. (27) obtained mobility exceeding 13 cm^2/Vs using 2,7-dioctyl[1]-benzothieno[3,2b] [1]benzothiophene C_8-BTBT as small molecule and indacenodithiophene-benzothiadiazole C_{16}IDT-BT as polymer, with $C_{60}F_{48}$ as p-dopant compound. Julianna Panidi et. al demonstrated mobility of 8 cm^2/Vs using diF-TES

ADT as small molecule with poly(triaryl amine) PTAA plus a Lewis acid that acts as p-dopant (BCF). The same group reported also value of 11 cm^2/Vs for C$_8$-BTBT with poly(indiacenoditiophene-co-benzothiadiazole) C$_{16}$IDT-BT (26). Junshi Soeda et. al obtained values of 17 cm^2/Vs using C$_{10}$ -DNBTD-NW with PMMA producing single crystal films of small molecules with phase segregation (28). Some of the most reliable values of mobility reached in recent years using blend technology are listed in Table.3 (22).

Table 3. List of recent values of field effect mobility for solution processed OFETs based on small molecules/polymer blends.

	Blend materials			Max. μ_{h_sat} [cm^2 V^{-1} s^{-1}]	Dielectric	Geometry	Solution deposition technique
	Small molecule	Polymer	Dopant				
Ternary blend	C$_8$-BTBT	C$_{16}$IDT-BT	–	4.7	Cytop or PTFE	TG-BC	Spin coating
	C$_8$-BTBT	C$_{16}$IDT-BT	C$_{60}$F$_{48}$	13	Cytop or PTFE	TG-BC	Spin coating
	C$_8$-BTBT	C$_{16}$IDT-BT	BCF	11	Cytop	TG-BC	Spin coating
	diF-TES ADT	PTAA	–	2.4	Cytop	TG-BC	Spin coating
Binary blend	diF-TES ADT	PT-FAA	–	5	Cytop	TG-BC	Spin coating
	diF-TES ADT	PTAA	BCF	8.0	Cytop	TG-BC	Spin coating
	TIPS-pentacene	PTAA	BCF	3.7	Cytop	TG-BC	Spin coating
	diF-TES ADT	PS	–	6.7	SiO$_2$	BG-BC	Blade coating
	TIPS-pentacene	PTAA	–	1.1	Cytop	TG-BC	Spin coating
	TIPS-pentacene	PS	–	4.6	SiO$_2$	BG-BC	Blade coating
	PS	DNTT precursor	–	4.7	SiO$_2$	BG-TC	Spin coating
	PSS	C8-BTBT	–	10.4	SiO$_2$	BG-TC	Spin coating
	C$_{10}$-DNBDT–NW	PMMA	–	17	SiO$_2$/PMMA	BG-TC	Edge casting

One of the reasons why small molecules/polymer blends are very attracting is that they offer a wide range of morphologies compared to each single material of the system. The structure assumed depends on many factors such as chemical composition, molecular weight and self-assembling properties of the polymer, relative amount of polymer/small molecules, viscosity of the solution, solubility of both polymer and small molecule, evaporation rate, post-processing treatment, etc. (22), (29). The polymer has a fundamental role in the film growth, determining its kinetics and final structure in terms, for example, of grain size, orientation and crystallinity. Microstructures may be dominated by the solvent-solute or solute-solute interactions. In the first case evaporation of solvent from the top surface leads to a higher solute concentration and therefore preferential accumulation of the more soluble component at this interface. This concentration gradient leads to a vertically segregated film. In the second case, the order in which the two components solidify affects the microstructure and the solvent

evaporation less strongly affects the liquid-liquid phase separation. For example, the first component to solidify may be expelled to the interfaces as the second solidifies (30).

An example of these concepts can be found in the work by K. Singsumphan et al., where the change in morphology of a film deposited by drop-casting from toluene of a blend constituted by TIPS-anthracene with PS in different proportions was monitored: the concentration of TIPS-anthracene was varied from 0.25 to 1 wt% (31). As it possible to see from Fig.21(a),(b),(c) and (d), the shape and size of crystals change. A similar work is the one by Jeremi Smith et. al, in which a blend of diF-TES ADT with PTAA was deposited by spin-coating with different concentrations. In the optical polarized images (Fig.21(e)) crystallisation of a diF-TES ADT rich phase is evident in compositions exceeding 37.5 wt.% of diF-TES ADT, with grain sizes of the crystals formed being of the order of 50 μm. Above 75 wt.%, the thin-films started to become non uniform, with some regions of the substrates found to be not fully covered. At 95 wt.% diF-TES ADT, the films severely de-wetted from the substrates, resulting in only small semiconducting islands (32).
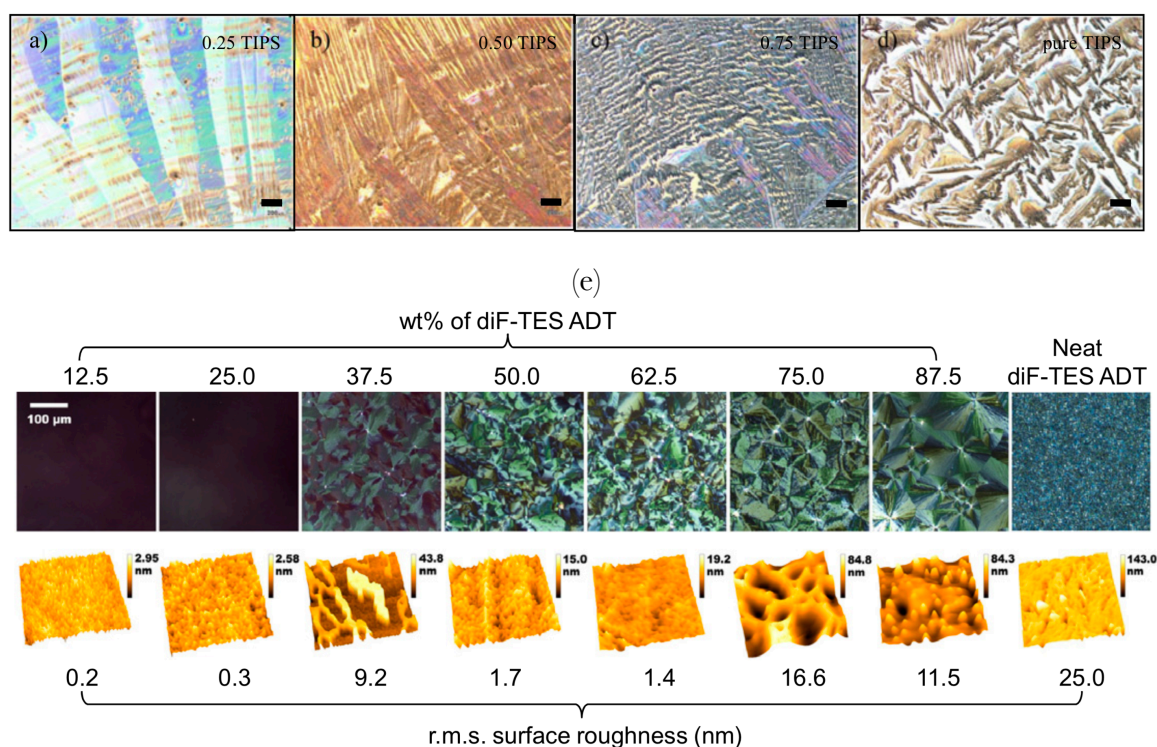
Figure 21. (a)-(b)-(c)-(d) Different morphologies obtained for a blend of TIPS-pentacene:PS deposited by drop-casting with different concentrations of TIPS-pentacene: 25, 50, 75 and 100 % (31). (e) Effect of concentration of diF-TES ADT in a small molecule/polymer blend with PTAA deposited by spin-coating (32).

In literature it is shown that, in proper working conditions, vertical phase segregation can be obtained forming one layer richer of semiconducting small molecules and one richer in polymer. Sometimes this occurs at both interfaces (top and bottom) leading to a stratified structure, while in other cases just at one of them. In most cases, such separation is not sharp, but gradients in the relative concentrations are typically formed. To control phase segregation in order to obtain a semiconducting crystalline layer at the dielectric interface, different parameters must be taken into account, such as type of polymer and molecular weight, solubility of the components in the solvent, surface energy at the two interfaces, viscosity of the solution and evaporation rate (31), (22).

Fig.22(a),(b) and (c) are related to concentration profiles obtained by neutron reflectivity measurements and polarized optical microscope images for a blend of diF-TES ADT with three different polymers deposited in the same conditions: (a) PαMS, Fig (b) PMMA and (c) syndiotactic PS (33). Another example of vertical phase segregation for a blend of TIPS-pentacene with PTAA is shown in Fig.23. This study was done by Richard Hamilton et. al (34) using dynamic secondary ion mass spectroscopy (DSIMS), exploiting the presence of at least one type of characteristic element for each compound. It is possible to notice the formation of a top layer rich of TIPS-pentacene at the dielectric interface, allowing good charge mobility in a Top gate − Top contacts configuration.
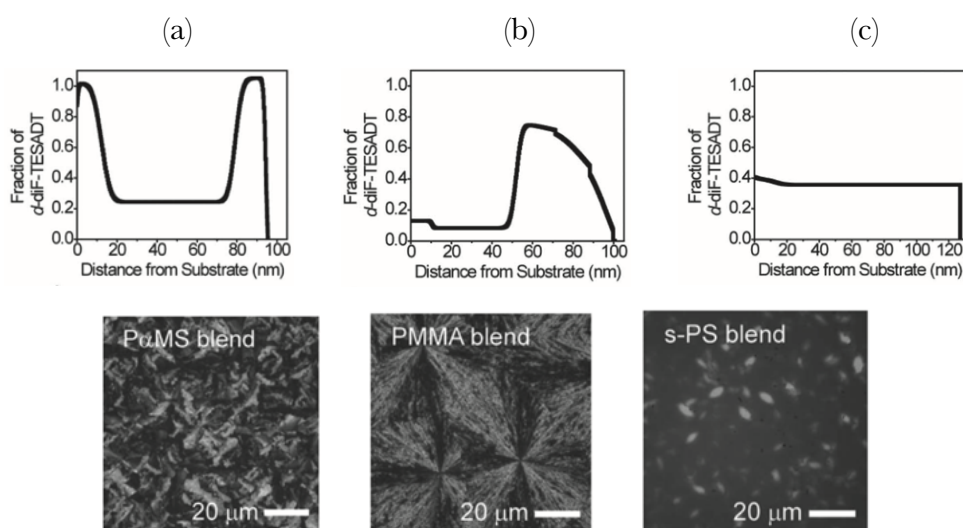
Figure 22. Concentration profiles and optical images of a small molecule/polymer blend formed by diF-TES ADT with three different polymers: (a) PαMS, (b) PMMA and (c) s-PS (33).
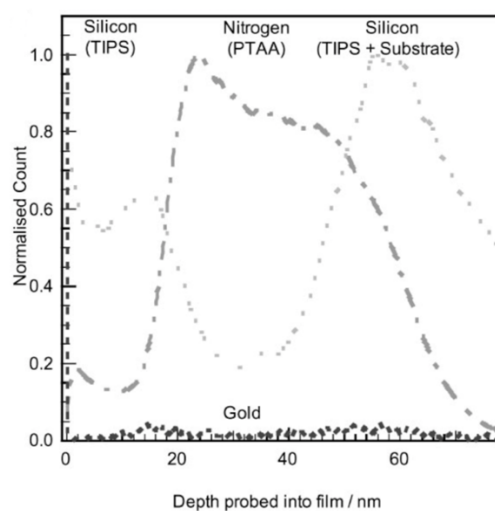
Figure 23. Concentration profile of a blend formed by TIPS-pentacene with PTAA (34).

2.3 Charge transport in organic semiconductors.

Charge transport in organic semiconducting materials is completely different with respect to the one of common crystalline inorganic semiconductors such as monocrystalline silicon and it is one of the main reasons for such discrepancy in values of carrier mobility (35). The room temperature mobility of highly purified rubrene or pentacene, which are among the organic semiconductors with the highest charge carrier mobility, is a few tens of cm^2/Vs, while the value of monocrystalline silicon is an order of magnitude larger. The fact that room temperature charge mobility has never exceeded 50 cm^2/Vs among the thousands of molecules synthesised, strongly suggests that there is a strong difference in the transport mechanism between the two systems (35).

The most important difference is that organic semiconductors are molecular materials formed by many molecules weakly interacting by Van der Waals forces, unlike covalent inorganic semiconductors that are constituted by an ideal infinite network of chemically bonded atoms. Hence, the transport properties will depend on the chemical nature of the molecules, how they interact and how they are arranged in space (packing mode).

41

Moreover, the degree of crystallinity and the presence of impurities, especially at the dielectric interface in an OFET device plays a fundamental role.

A short review of the mechanism of charge transport in molecular materials follows, underlining the most important concepts and the key factors necessary to understand better the relationship between structure and properties.

2.3.1 Nature of charge carriers in π – conjugated materials

Due to the structural difference between molecular and covalent semiconductors and due to the strong coupling between molecular vibrations and electrons, the nature of charge carries is completely different. In this case, the usual band-like transport description fails and electrons cannot be described by delocalized wave functions extended over the whole solid in which they move almost freely, in the framework of the effect mass approximation, without caring too much of what happens to the nuclei fails. In molecular solids, electrons are preferentially localized on the molecules and have to overcome a barrier to move from site to site. When electrons move, a big change in molecular electron density occurs both on the molecule they leave and on the one they transfer to, always causing a deformation, since the molecules won't be in their equilibrium states any more. As such, the movement of electrons will be always associated to vibrations. This is true for any organic material. Moreover, in π-conjugated systems this coupling, also called vibronic coupling or electron-phonon coupling, will be very strong thanks to the presence of an extended electronic cloud of π electrons, that strongly connects all the atoms of the molecule. This can be experimentally observed doing UV-vis spectroscopy. In the case of organic materials, there will never be pure electronic transitions, but the change of electronic state will always be accompanied by a change of vibrational states. This can be theoretically seen, comparing the potential energy surface of two electronic states, for example the ground state and the first excited one. Differently from covalent solids, for which the two potential wells are very similar, resulting in a week electron-phonon coupling, the two potential curves for molecules will be very different, with a change in curvature and a shift of the equilibrium position. This suggests that electronic transitions always involve

vibrations. This is easy to understand this if one looks at the matrix element of transitions in case of UV-vis spectroscopy:

$$V_{if} \propto <i|\,\mu|f> = \mu_{if} \approx \mu_{ge} <\underline{0}\,|\,\underline{n}>$$

μ_{ge} is the transition dipole moment related to the electronic transition from the ground state $<g|$ to an excited state $<e|$. $<\underline{0}\,|\,\underline{n}>$ is the overlap between the total vibrational ground state and the total vibrational excited state in which a given number of normal modes are excited from the lowest energy level $n = 0$ to an excited state $n \neq 0$. If the two potential wells are very different, the normal modes of the two electronic states will be too. This leads to a non-zero overlap even for $n \neq 0$. Therefore, the vibrational states of the initial and final electron states can be different.

Since electrons and vibrations are connected, while an electron is moving in the material, it is easy to imagine that molecular vibrations will move with it. This is true for both inter- and intra-chain transport. Consequently, charge carriers are not simple electrons but they are rather composed particles of different types such as soliton, polaron, bipolaron (depending on the molecular system) formed by a charge dressed with phonon cloud (36). This is quite similar to the description of cooper pairs for superconductors in the BCS theory.

The different types of charge carriers that can be found in organic semiconductors will be described more in details in the following paragraph. Doing this, it will be also possible to explain the intra-chain transport mechanism. A chemical description will be given rather than a physical one, since it is more immediate and allows to understand the main features.

To introduce the type of carriers, let's consider the simple case of polyacetylene (PA) and let's assume that some "defects" are formed, due to rearrangement of double bonds, like a radical (actually two radicals are formed but since they are not correlated we can consider just one of the pair). The unpaired electron separates the chain in two parts A and B. In the special case of PA these two resonance structures are isoenergetic and correspond to the two minima in a plot, as the one presented in Fig.24(a), where the energy of the system changes with the BLA. The radical is instead an high energy species (very reactive) and it will correspond to the maximum of the plot. Moreover, as

any energetic defect, it can be associated to a discrete singly occupied level between HOMO and LUMO. The radical along with its energy state is called soliton: a specie with zero charge and spin ½. When the radical is formed, it is never localized on one site but it will spread with a given extent over some number of carbon atoms, leading to a more stabilized system. The region over which the radical is delocalized will have BLA equal to zero.

Since the energy of the two configurations A and B is the same, the movement of the soliton along the chain will be very fast without any energy dissipation, even if it will cause a molecular deformation. However, it is experimentally observed that the charge carriers in polyacetilene are spinless. For this reason the soliton cannot be the main responsible of charge transport in PA. To introduce the actual charge carriers we have to immagine to perform an electron transfer process caused by, for example, doping, through which an electron is added (removed) to (from) the system. In this case the species that are formed are called positive or negative solitons and correspond to a positive or negative charge localized on the molecule where there was the radical. From an energetic point of view it is possible to associate an empty or doubly occupied energy level to these species. The positive or negative solitons, differrently from the neutral one, are characterized by charge +/-1 and zero spin. All the types of solitons are rapresented in a schematic way in Fig.24(c).
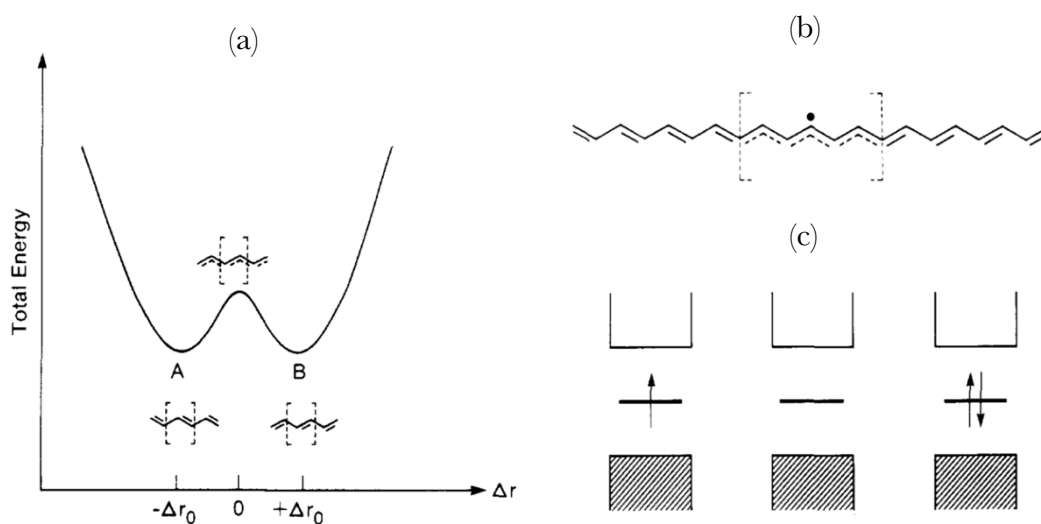
Figure 24. (a) Plot of the total energy of polyacetylene as a function of the BLA (37). (b) Schematic representation of a neutral soliton (37). (c) Energy diagram of all the type of solitons (neutral, positive and negative) (37).

As for the neutral soliton, also the positive and the negative ones move in the chain without energy dissipation. In addition, owing to Coulomb repulsion, if more charges are created on the same molecule, the solitons will tend to move faster.

Solitons, however, exist only in polyacetilene, where the two structures formed by rearrangement of double bonds are isoenergetic. In common π-conjugated systems, when a radical is formed, the two structures A and B are very different in energy. For example, we can go from an aromatic structure to a quinoidal one, which is less stable. For this reason, the radicals cannot be formed spontaneously by a rearrangement of bonds but thanks to a doping process. For these reason, instead of creating two radicals, a radical and a postive or negative charge are formed, depending if the electron is added or removed. These two species are called positive or negative polarons and will be characterized by charge +/-1 and spin ½. From the energetic point of view it is possible associate to polarons two descrete energy levels that correspond to the combination of the one of the radical (neutral soliton level singly occupied) and one of the charge (charged soliton level empty or doubly occupied).

In case of discrete level of doping also bipolarons can be observed. To describe them we have to immagne to perform a second doping process to a polaron, adding or removing a further electron, creating a second positive or negative charge. They are characterized by charge +/-2 and zero spin. Two descrete empty or fully occupied levels in the gap are associated to them. In Fig.25(a) and (c) the formation of a positive polaron and bipolaron and the corresponding energy diagrams are shown. For an high doping level we can also immagine the formation of polaronic bands, filled or empty depending on the nature of the charge carriers.
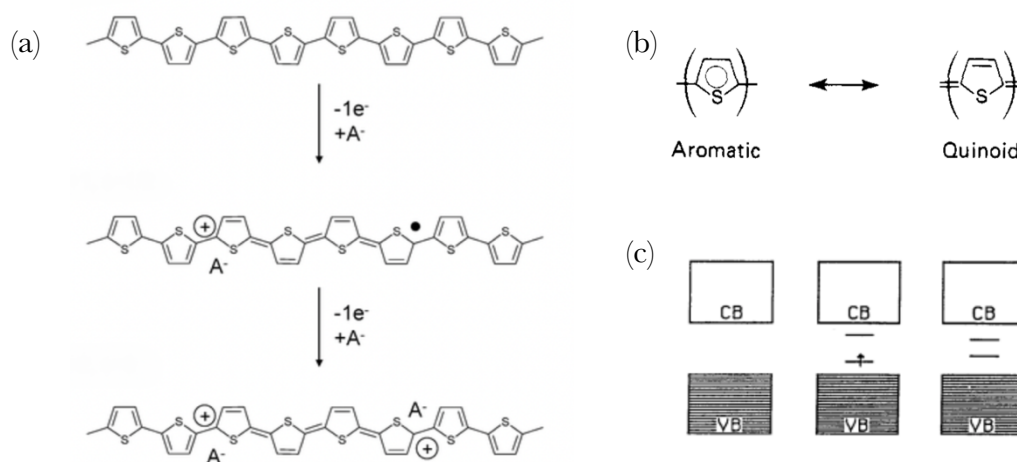
Figure 25. (a) Formation of a positive polaron and bipolaron in case of polytiophene (36). (b) Possible molecular structures originated due to polaron formation in polytiophene (36). (c) Energy diagram for the pristine state, positive polaron and positive bipolaron (36).

Unlike for soliton, in the case of polarons and bipolarons the part of the molecule that goes from structure A to B is limited to few atoms and depends on the energy balance between Coulomb repulsion between same charges and the increase of energy passing from aromatic to quinoid structure. For this reason the two charges of a bipolaron, or the charge and the radical of the polaron, are strongly correlated. However, they can still move in couple along the chain without energy dissipation if we consider the actual carrier as the whole set of the two chrges, or one charge plus the radical, bounded by a molecular deformation rapresented by the quinoid part between them. Again we can see the similarity between soliton, polaron and bipolaron and cooper pair: also in this case the charge carriers are electrons or holes bonded with a vibration that move with no dissipation.

2.3.2   Electron transfer processes and intermolecular transport

Electrical transport in molecular materials is the result of two contributions, intra- and inter-chain ones. Intra-chain transport can be relevant in polymers, while is negligible in case of small molecules. In general conditions, it is never the limiting factor for charge transport, even for long polymer chains, since it is very fast. The mechanism that mainly determines the conduction in semiconductors is the inter-chain one. For this reason, at least at room temperature, the overall transport can be seen as a hopping process of carriers from site to site. From a chemical perspective, it corresponds to a series of electron transfer processes that are substantially redox reactions between two molecules, where one will behave as donor and the other as acceptor.

Due to the strong vibronic coupling, whenever an electron is removed (oxidation/p-doping) or added (reduction/n-doping), the molecule is no more in its equilibrium geometry. After the formation of the charged molecule, for example due to an ionization, there must be a relaxation process by which the system goes in the new equilibrium configuration, according to the potential curve of the ionized state. Hence, the whole process can be seen as an instantaneous ionization at frozen nuclei in the equilibrium geometry of the pristine state followed by a geometry relaxation in the excited state (37). These two processes correspond to process (1) and (2) in Fig.26(a),

where $E_{IP\text{-}g}$ is the ionization energy of the ground state non-distorted and E_{rel} is the so-called relaxation energy of the ionized state. To calculate these quantities, it is necessary to know the geometry and electron density at equilibrium of the pristine state and ionized state, and in the distorted configuration of the ionized state. Since the ionized state is more difficult to be modelled, it is better to imagine the process in a reverse way: first we distort the molecule so that it will assume the geometry of equilibrium in the ionized state. This will cost a given distortional energy E_{dis}. Then, there will be an ionization in the distorted configuration with energy cost $E_{IP\text{-}d} < E_{IP\text{-}g}$ (37). The two processes correspond to process (3) and (4) in Fig.26(a). In this case, to estimate E_{dis} and $E_{IP\text{-}g}$ we do not need to know the distorted geometry of the ionized state but the one of the pristine state, which is more predictable.
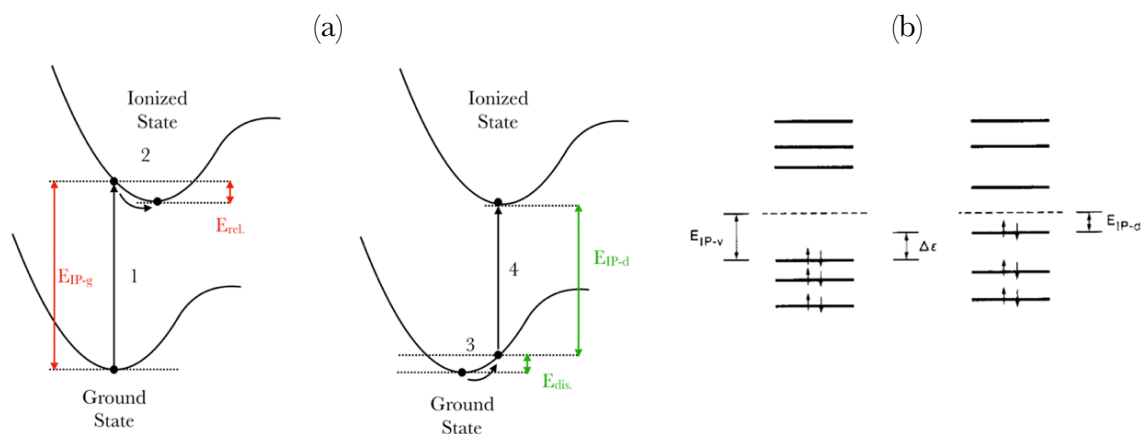
Figure 26. (a) Potential wells of the neutral and charged molecule. (b) Change in ionization energy of the neutral molecule upon molecular deformation (37).

The difference between the two ionization potentials is due to the change of molecular orbitals when the molecule passes from the equilibrium geometry of the ground state to the distorted geometry, as illustrated in Fig.26(b). $E_{IP\text{-}d}$ will be lower than $E_{IP\text{-}g}$ since the molecule is preparing the nuclei in a proper way so that it will be easier remove or add electrons. The change in orbital energy between equilibrium and distorted state is called $\Delta\varepsilon$ and it can be related to the relaxation and distortional energy just doing the energy balance:

$$E_{IP-g} = E_{IP-d} + E_{dis.} + E_{rel.}$$

$$\Delta\varepsilon = E_{IP-g} - E_{IP-d} = HOMO_{eq.} - HOMO_{dis.} = E_{dis.} + E_{rel.}$$

$$\rightarrow \quad E_{rel.} = \Delta\varepsilon - E_{dis.}$$

The relaxation energy is strongly connected to the polaron binding energy imagining again the carrier as a charge bonded with its associated molecular deformation and it is directly related to the strength of the vibronic coupling. Obviously it must be larger than zero to form a polaron, leading to $\Delta\varepsilon > E_{dis.}$. In other worlds, the reduction in ionization potential upon distortion must balance the large distortional energy required to ionize the molecule (37).

The picture of transport as a series of thermally activated tunnelling processes between diabatic states (which consist in the charge being localized on the donor while the acceptor is neutral) is true in the limit of strong electron-phonon coupling, where strong means higher than the electron-electron coupling. In this case the molecule undergoes a large geometry relaxation. This is the usual condition encountered in π-conjugated systems (21), (38). In this case it is possible to relate the hypothetical mobility of the material to charge transfer processes with a proper formulation of an electron-transfer rate. The simplest formulation is the Marcus rate which was introduced to describe redox reactions in solutions (21). The equation can also be derived applying first order perturbation theory between diabatic states. The final result is the following:

$$k_{ij} = \frac{2\pi}{\hbar} \frac{|V_{if}|^2}{\sqrt{4\pi\lambda_{if}k_B T}} exp\left[-\frac{\left(\Delta E_{ij} - \lambda_{if}\right)^2}{4\lambda_{if}k_B T}\right]$$

In the expression above, k_{ij} is the rate or probability per unit time of transition related to electron transfer processes. V_{if} is the matrix element of transition, which is called also transfer integral or electronic coupling, and is related to the interaction strength between diabatic states and to the overlap between molecular orbitals of the donor and acceptor. λ_{if} is the so called reorganization energy, which is a molecular parameter similar to the relaxation energy E_{rel}. ΔE_{ij} is related to difference in on-site energy for example due to polarization effects caused by intermolecular interactions. The latter contribution is often neglected, especially when dealing with systems formed by identical molecules. The usual assumption is that the site energies of identical molecules are the

same. However, this assumption can be wrong when intermolecular interactions are taken into account (36). A usual way to estimate the transfer integral is through the "Energy Splitting in the Dimer Method" (ESDM). It relies on the concept that in any perturbation theory the splitting between energy levels as a consequence of an interaction between two "entities" is a direct measure of the strength of the interaction itself. So, V_{if} is estimated as the splitting of LUMO (or HOMO) levels of neighbour molecules upon dimer formation (36).

$$V_{if} = \frac{E_{L+1[H]} - E_{L[H-1]}}{2}$$
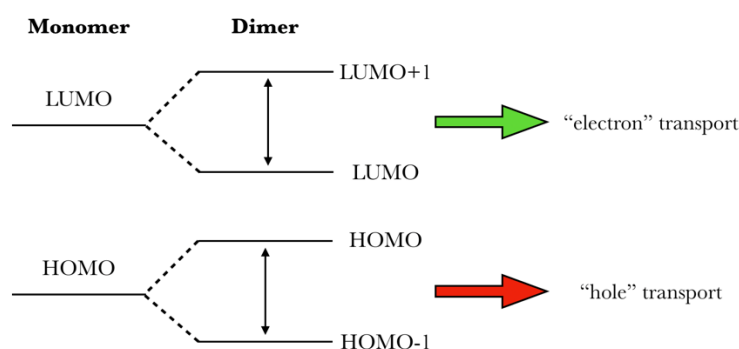
Figure 27. Split of the frontiers energy levels (HOMO and LUMO) of adjacent molecules upon dimer formation.

2.3.3 Role of morphology and processing conditions

In the previous section, important concepts about transport in organic semiconductors have been introduced. However, we must take into account that several factors determine macroscopic quantities such as the charge carrier mobility: the molecular electronic structure, the relative positions and orientations of neighbouring molecules, and spatial inhomogeneities in the morphology, which limit charge carrier pathways on a macroscopic scale. As said before, if nuclear dynamics is much slower than the dynamics of charge carriers and electronic coupling is weak, charge transport can be described by the hopping processes between localized states. In this picture, hopping rates depend on the electronic structure and on the relative positions and orientations of

molecules. Hence, in order to evaluate the rates, material morphology must be known with atomistic resolution. This can be achieved by performing molecular dynamics simulations using proper force-fields and DFT calculations. It is also possible to use experimental results to predict better material morphology. Then, considering a list of pairs of molecules (neighbours), Marcus type hopping rates are calculated based on transfer integrals, reorganization and on-site energies. Finally, it is possible solve the corresponding master equation using the Monte Carlo method, able to simulate charge dynamics of non-steady-state systems (39).
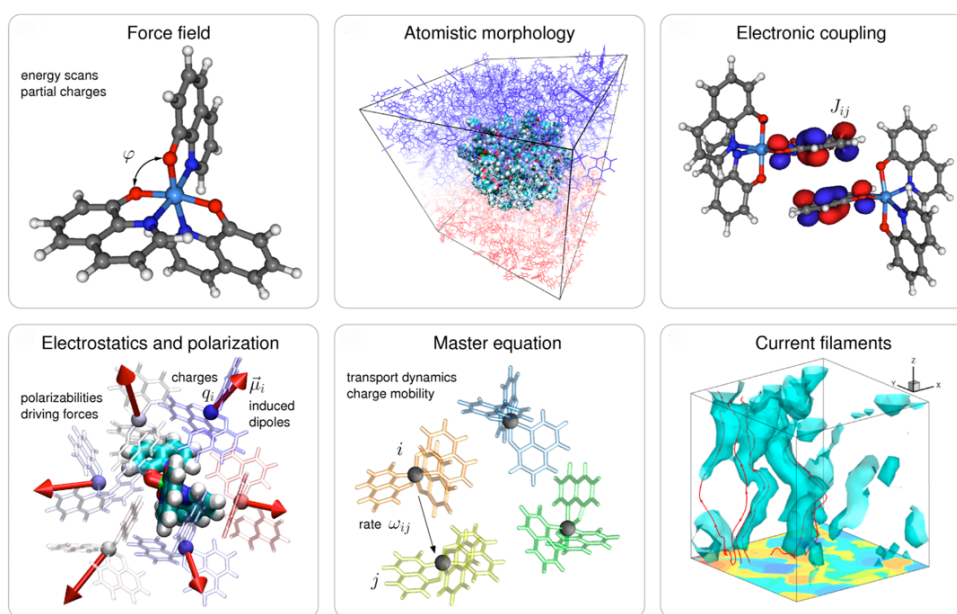
Figure 28. Fundamental ingredients for transport simulations in organic semiconductors (39).

However, even if nowadays charge transport simulations are increasing their reliability also for organic semiconductors, they are not able to predict in a systematic way transport phenomena that occur in real electrical devices like OFETs. This is because simulations are able to give a hint about the intrinsic transport of the material, which could be enough if we had an ideal single crystal without any defect. However, what we have to consider in a real device is not the intrinsic material, but rather an active film that, at the macro scale, is characterized by a high level of complexity for what concerns its structure and morphology. For example, at the macro scale it is possible to have different segregated phases with different compositions in which many types of crystalline domains are present, separated by grain boundaries. Then, inside a crystalline domain, we could have different crystalline structures organized in a well-

defined way, separated by disordered amorphous regions. Also inside each single crystal we could have structural inhomogeneities and defects which can act as charge traps and limit the transport. For this reason, the transport at the macro scale cannot be fully predicted yet. Additionally, this hierarchical structure strongly depends on the processing conditions like temperature, solvent, humidity, concentration, deposition rate, surface energy, etc. So, intrinsic properties of the material are difficult to be experimentally measured, and extrinsic factors are often dominant in devices electrical characteristics.

In case of an OFET, additional factors to be taken into account are contact resistance, charge injection mechanism, type of contacts, type of dielectric, structure at the semiconductor-dielectric interface in terms of defects and traps.

Finally, the transport is also affected by environmental factors that can degrade the material because of interactions with light, moisture and oxygen.

2.4 Charge Injection

In OFETs, once the conducting channel is created with the application of the gate voltage, to have a current flow between source and drain when a bias is applied, mobile charges must be injected and collected from(to) the metal contacts with a good efficiency. For this reason, charge injection is one of the fundamental steps for the functioning of transistors, along with the transport in the active material. Both of them have a high impact in the final performance.

2.4.1   Origin of the contact resistance

To have a good injection of carriers from the metal to the semiconductor there must be a good matching between the energy levels of the two materials. In particular, if a hole has to be injected, what is important is the relative position between the Fermi level of the metal E_F and the HOMO of the semiconductor. If an electron has to be injected the relative position of the LUMO with respect to E_F is instead considered. A rough but good estimation of the injection barrier is given by the difference between these levels as

shown in Fig.29(a), in which pentane is taken as an example of semiconductor and gold as metal electrode.

$$Injection\ barrier\ for\ holes \sim |E_F - HOMO| = \ \Phi - IP$$

$$Injection\ barrier\ for\ electrons \sim |E_F - LUMO| = \ \Phi - E.A.$$

The formation of the barrier is a complex process that depends on many factors such as metal work function Φ, ionization energy IP or electron affinity E.A. of the semiconductor (HOMO and LUMO positions), reduced transport gap within the first 2 nm from the interface, presence of polaronic states inside the gap related to charged molecules in the semiconductor, broadening of energy states due to energetic and positional disorder (HOMO and LUMO levels are statistically distributed according to a Gaussian or an exponential distribution with a width of about 100 meV) and presence of interfacial dipole moments at the interface (21), (40). All these parameters contribute to the formation of the actual injection barrier. The interfacial dipole shifts the vacuum level of the metal as well as the work function and the relative position of the Fermi level with respect to the HOMO and LUMO, increasing or decreasing the barrier height of a given amount. The mechanisms by which this happens can be many and depend on the type of interactions between metal and semiconductor, which can range from simple physisorption, when organic molecular orbitals do not hybridize with metal electrons wavefunctions, to strong and weak chemisorption, with the formation of covalent bonds (40). Moreover, when E_F approaches the LUMO or HOMO level, sizeable, integer charge transfer between metal and semiconductor takes place, causing the storage of charges in the semiconductor and resulting in a bending of energy levels, with the LUMO levels acquiring a negative curvature and the HOMO a positive one. An example of an energy diagram for hole injection in case of pentacene with gold contacts is shown in Fig.29(b).
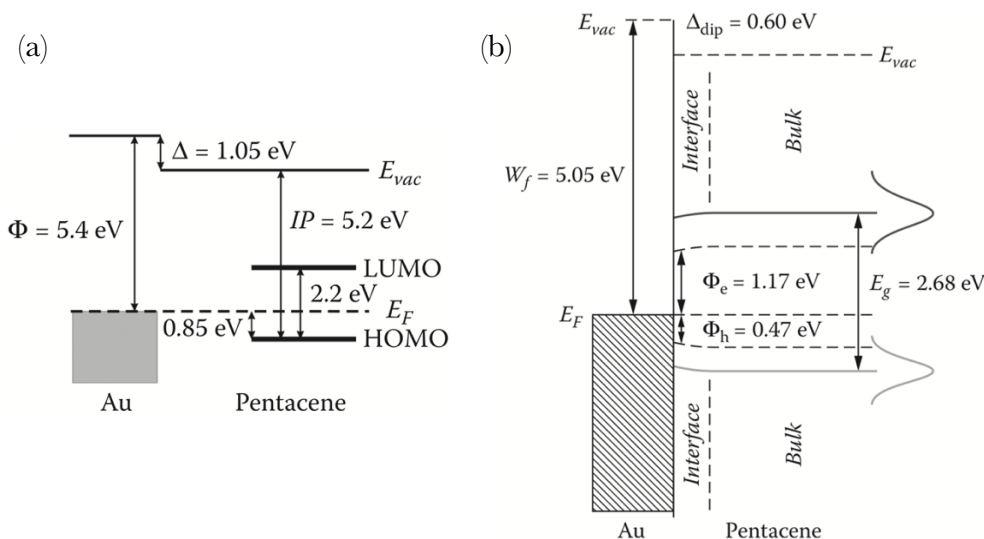
Figure 29. (a) Schematic representation of the energy diagram for a metal-semiconductor interface of gold and pentacene when the two materials are not in contact (21). (b) Formation of injection barrier for a gold-pentacene junction (21).

Let's discuss now the different types of metal/semiconductor interactions that result in a vacuum level shift originated by an interfacial dipole which changes the work function of the metal.

1. **Physisorption**. In this case, due to the physical absorption of organic molecules at the surface of the metal, there will be a modification of the metal work function. In fact, if one considers an isolated metal, the electronic charge density does not abruptly drop to zero at the surface but "leaks" into vacuum, giving rise to a surface dipole that contributes to the total work function. When organic molecules are physisorbed at the surface, the metal electron tail is pushed back closer to the metal surface by π-electron clouds, modifying the surface dipole of the metal and ultimately decreasing the work function (40).

2. In case of **weak chemisorption**, the contact between metal and organic molecules results in metal-hybridization of molecular orbitals, which broadens and ultimately gives rise to a continuum distribution of states in what used to be the energy gap. This Induced Density of Interfacial States (IDIS) is filled with the electrons of the isolated and neutral molecule up to the so-called charge neutrality level. The relative position of the latter with respect to E_F of the metal determines charge transfer which leads to a shift of the vacuum levels after that

thermal equilibrium is reached. This extreme situation that happens only in case of ultra clean surfaces with no contaminants (40).

3. The third case is the one of **strong chemisorption**, where the formation of metal/organic covalent bonds occurs. The situation is typical of Self Assembly Monolayers (SAMs), whose anchoring groups (e.g. thiols) give rise to chemisorption even toward nonreactive metals like gold. Since chemical bonds can be accompanied by partial charge transfer, an interface dipole may develop leading to a shift of the vacuum level. Moreover, in the case of SAMs, the molecule end-group can have an intrinsic dipole due to its donor or acceptor nature, leading to an additional shift of the Fermi level (40).

It is important to mention that other parameters can affect the injection; they are responsible of the discrepancy between theoretical values of injection barriers and the experimentally observed ones. Two examples are given by the presence of structural disordered regions of semiconductor near the contacts and the presence of contaminants (21). Finally, there are different mechanisms by which carriers are injected from the metal electrodes. The simplest one is by thermionic emission, where a carrier overcomes the energy barrier thanks to thermally activated excitations. The second one is called field-emission and consists in a tunnelling process by which carrier tunnel through the barrier. This process can be active along with thermionic emission, especially when the gate voltage is sufficiently high, since it reduces the width of the barrier. A third possible mechanism is a defect-assisted injection in which carriers are able to "bypass" the barrier through mid-gap states (21). In Fig.30 all types of injections are summarized.
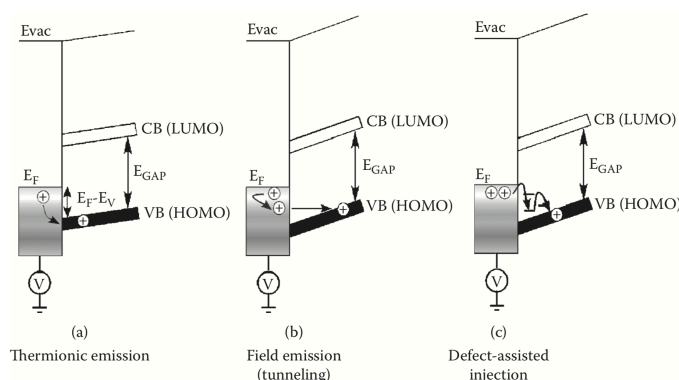
Figure 30. Different types of charge injection mechanisms that can be active during charge injection (21).

54

2.4.2   Contact engineering

The injection barrier at the contact-semiconductor interface is responsible of the origin of the so-called contact resistance R_C, which is important for both the final performances of the device and the reliability of the values of field effect mobility. The contact resistance enters the equations of an OFET operation because the source-semiconductor-drain circuit can be represented by three resistors connected in series. The resistances associated with charge injection and collection can be gathered into an overall contact resistance R_C, while the resistance associated with crossing the conducting channel length is called channel resistance R_{CH}. Hence, the total source-drain resistance is:

$$R_{TOT} = \frac{V_D}{I_D} = R_C + R_{CH}$$

Usually the contact resistance in OFETs is high and in some cases can even become larger than the channel resistance. In fact, the channel resistance scales as the ratio between channel length and width L/W, but the contact resistance scales as 1/W (it does not depend on L). This means that the contact resistance is potentially very important in short channels (L<5µm usually), since it will contributes more to the total resistance. In this case the transport is described as contact limited.

To avoid limitations given by the contact resistance, in order to exploit better the potentiality of the active material, it is possible to perform contact engineering, tuning the injection barrier for carriers. There are different ways to do so. The first one is with the application of SAMs thanks to which it is possible to modify the work function of the metal due to the formation of an interfacial dipole. Moreover, these molecules have lateral groups with strong electron withdrawing or donating character (donor or acceptor) to which we can associate an additional dipole that causes a further change depending on the nature of the functional group. The change in injection barrier can be expressed as (41):

$$\Delta\varphi = -N\left(\frac{\mu_{M-s}}{\varepsilon_0 k_{M-S}} + \frac{\mu_{SAM}}{\varepsilon_0 k_{SAM}}\right)$$

Where N is the grafting density of the SAM molecules, μ_{M-s} and μ_{SAM} are the dipole

moments of the M–S bond and of the SAM due to the presence of functional groups, ε_0 is the permittivity of free space, and k_{M-S} and k_{SAM} are the dielectric constants of the M–S bond dipole and SAM molecule, respectively. The first term is strongly dependent on the metal species (e.g., the Ag–S dipole moment is larger than the Au–S dipole moment) and the second part is determined by the SAM chemical nature. Although the first term has an almost fixed sign and magnitude depending on the metal, the latter can be positive or negative and its magnitude dominates in the total dipole moment. In Fig.31 a list of examples of SAMs used to perform contact engineering is presented. The most common ones are molecules with the –SH group that is able to form dative bond with noble metals such as silver and gold. Aromatic and alkyl chains are added to decrease the work function, while halogens, due to the high electronegativity, are used for the opposite purpose (41).
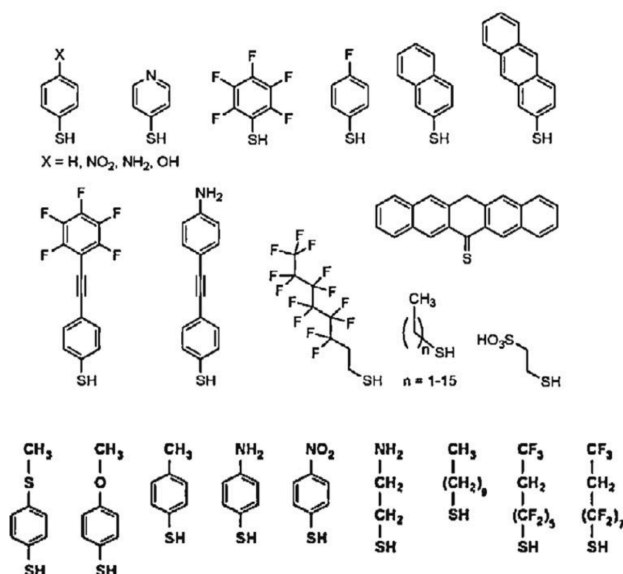
Figure 31. Examples of SAMs molecules used for contact engineering (41).

Another possibility, less employed, is given by the use of salts of transition metal oxides which behaves as interlayers to facilitate the injection. They can be deposited both with solution and vacuum techniques (41).

2.5 Hysteresis and threshold voltage instabilities

There are different ways to assess whether an OFET behaves in an ideal way or not. One marker of non-ideality and possible degradation is the formation of an hysteresis cycle in the transfer characteristic during the forward and backward sweeps of the gate voltage V_G, which may lead to also a shift of the threshold voltage. In Fig.31 the two types of hysteresis are illustrated. In the first case (a), the back sweep current is higher than the forward sweep current (higher BSC hysteresis) while in (b) it is the opposite (lower BSC hysteresis).
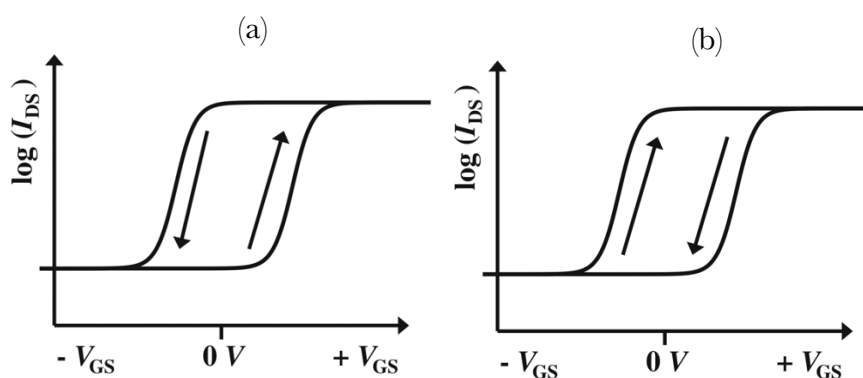
Figure 32. Types of hysteresis cycles in OFETs. (a) Higher BSC hysteresis. (b) Lower BSC hysteresis.

The origins of hysteresis in OFETs can be many (42):

1. **(A1) Charge trapping of majority carriers in the channel close to the semiconductor-dielectric interface.** Traps of charge carriers due to impurities or defects originated during operation close to the dielectric can lead to hysteresis if the rate of release is lower than the one of the voltage sweep so that thermal equilibrium cannot be reached. Oxygen and water can act as source of this kind of traps when dielectrics such as silicon dioxide are used. In this case, $-OH$ groups, which are known to behave as electron traps, are formed at the surface. To overcome this problem, SAMs can be used (e.g. silanes). Charge trapping of majority carriers usually leads to a lower BSC hysteresis: when the scan starts from the off state, the traps are empty. During the off-to-on sweep many carriers are quickly trapped, but this is compensated by the higher number of induced charges formed while V_G increases. Then, during the on-to-

off sweep, the trapped carriers are not able to contribute to the current since they are slowly released. Thus, as V_G decreases, other carriers will be trapped, leading to a lower current. If multiple scans are performed in succession, when all the traps are occupied the hysteresis is eliminated but, with time, the trapped charges will be released and hence hysteresis can appear again.

2. (**A2**) **Charge injection from the semiconductor into the dielectric.** The mechanism is quite similar to the one of charge trapping, but with a different traps location. For this reason, also in this case a lower BSC hysteresis is expected.

3. (**A3**) **Counter ions effects.** If mobile counter ions (e.g. charged impurities) are present, these might stabilize the carriers (polarons) neutralizing their charge. The complex formation with counter ions may cause a lower BSC hysteresis.

4. (**A4**) **Mobile ions in the semiconductors.** Ions in the semiconductor with the same polarity as majority carriers can cause lower BSC hysteresis since the total number of charges in the channel is fixed and determined by the applied voltages. Hence, ions, moving slowly with respect to majority carriers, reduce the number of mobile charges in the channel.

5. (**B1**) **Ferroelectric dielectrics.** In this case, the remaining polarization of the dielectric (caused by an external applied electric field) is responsible of an additional electric field that will sum up to the one induced by the gate, resulting in a higher number of induced charges and consequently an higher BSC hysteresis.

6. (**B1**) **Quasi-ferroelectric dielectrics.** When the dielectric contains polar groups that can be oriented due to an external electric fields an effect quite similar to the one of ferroelectric materials can occur, leading an higher BSC hysteresis.

7. (**B2**) **Mobile ions in the dielectric.** In the on-state (e.g. negative V_G to the gate for p-type devices), mobile anions will move toward the semiconductor

interface. Then, during the back sweep, the ions will stay there compensating the diminishing field and causing higher BSC hysteresis

8. (**C**) **Charge injection from the gate into the dielectric.** If charges are injected from the gate electrode into the dielectric, a higher BSC hysteresis is expected. For example, for a p-type device, in the on-state electrons are injected into the dielectric. They will stay at the semiconductor interface stabilizing the hole accumulation layer, also during the back sweep, leading an higher current.

In Fig.33 all the possible mechanisms that can lead to the formation of an hysteresis cycle are shown in a schematic way.
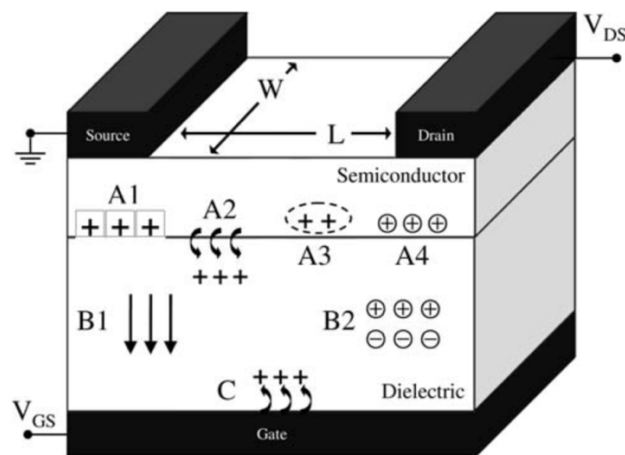
Figure 33. Schematic representation of the different types of mechanisms that can lead to an hysteresis cycle (42).

3. Material and methods

3.1 Semiconducting blend *[3]ph* − PS (tetraphenyl butatriene : polystyrene)

The active material used in the electrical devices is constituted by a small molecule/polymer blend. In particular, as small molecule, tetraphenyl butatriene, called also *[3]ph*, was used (where three is the number of subsequent double bonds in the main chain while "*ph*" indicates the nature of the end groups, which are two phenyl rings at both ends). This is a cumulene-like molecular system in which the two central carbon atoms are hybridized in *sp* configuration, while the other two at the extremities of the chain are forced to be hybridized as sp^2 since they are connected by single bonds to two aromatic rings. Even if the chain length is very small, this molecule was chosen to investigate the thin film electronic properties of *sp* carbon based molecular materials in field-effect transistors, before using more complex systems. Even if the cumulene configuration is highly unstable, thanks to the limited extension of the chain, compared to the size of the end-groups, the stability of the system is improved both in solution and in form of powder in the solid state. This allows an easy storage of the material and prevents crosslink for several months, if the exposure to light is limited (43). The system is stable enough also to permit deposition in air and at high temperatures, leading to functioning electrical devices. From a DSC analysis performed by Tykwinski et al. it was shown that the material should start to degradate very suddenly at temperatures around 150°C.

In Fig.34 the molecular structure of the *[3]ph* is shown. As others "odd" cumulenes, its geometry should be planar. However, as it is possible to see, due to steric hindrance, the molecule cannot lie on a plane. There is a distortion which can be correlated to the

angle between the planes of each phenyl ring and the one associated to the cumulenic chain. The four angles are 27,9, 27,4, 41,8 and 38,5 ° for rings A,B,C and D respectively, as previously investigated by diffraction experiments (44). The molecule does not possess exactly 222 point symmetry due to differences in torsion angles between the aromatic rings. Moreover, the cumulenic chain is not perfectly linear but it is slightly bent, removing any possible centre of inversion. This was experimentally observed by X − ray diffraction measurements and it is a feature found also in other cumulenic systems (44). However, the degree of bending is negligible and significantly lower with respect to the one of polyynic systems (12).
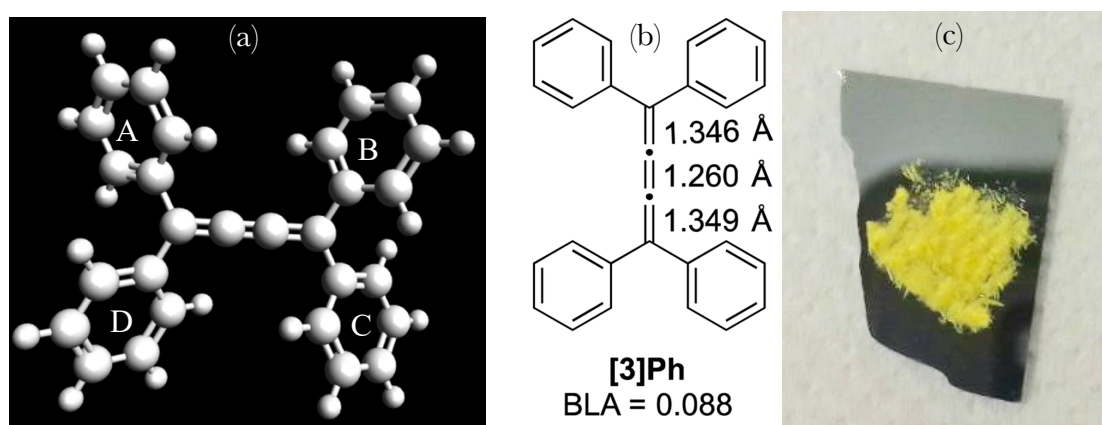
Figure 34. (a) Molecular structure of *[3]ph* calculated by Avogadro using MMFF94 as force field. (b) Lewis structure of *[3]ph* showing also the value of the BLA and bond lengths of the carbon-carbon bonds in the chain. (c) *[3]ph* in form of powder.

The molecule was produced by Tykwinski et al. with a procedure illustrated in reference (12). They performed UV-vis spectroscopy and X − ray diffraction measurements to quantify the BLA and the optical band gap. The value of $\lambda_{max.}$ obtained is 418 nm (maximum of the main peak), while wavelength corresponding to the onset of the lowest energy absorption is around 454 nm ($\lambda_{onset.}$), meaning that the material absorbs in the blue − violet of the visible region. The corresponding value of band gap is 2,73 eV, hence the material is expected to be a semiconductor. The estimated value of the BLA is 0,088 as reported in the previous figure, together with the value of bond length for the three C − C bonds present in the chain. From DFT calculations performed by Milani et al. the energy of the frontiers molecular orbitals was calculated and a band gap equal to 2,5 eV is obtained, slightly lower than the experimental one. These data were confirmed by electrochemical measurements performed by Tykwinski et al. In Table.4 the values

of energy levels for *[3]ph* obtained experimentally by optical spectroscopy and cyclic voltammetry along with the theoretical ones are shown while in Fig.35 the shape of the HOMO and LUMO is presented.

Table 4. In the first two tables the energy values of the frontier molecular orbitals of *[3]ph* obtained by Tykwinski et al. are listed (on the left electrochemical measurements while on the right the optical ones). In the second table, the results of DFT calculation performed by Milani et al. using HSE06/cc-pVTZ as functional are listed.

E^1_{red} (V)	E^2_{red} (V)	E^1_{ox} (V)	E_{HOMO} (eV)	E_{LUMO} (eV)	E_{gap} (eV)	$\lambda_{max.}$ (nm)	λ_{onset} (nm)	E_{gap} (eV)
-2.01	-2.45	0,71	-5.81	-3,10	2.72	418	454	2,73

$HOMO-1$ (eV)	$HOMO$ (eV)	$LUMO$ (eV)	$LUMO+1$ (eV)	E_{gap} (eV)
-6,85	-5,141	-2,63	-0,80	2,51
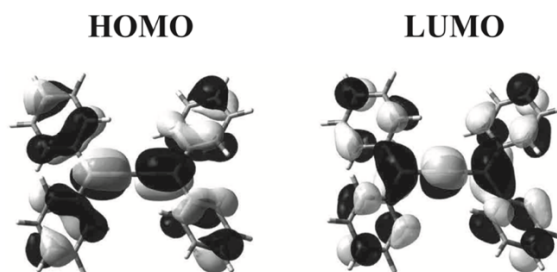
Figure 35. Shape of HOMO and LUMO molecular orbitals of *[3]ph* (43).

Atactic polystyrene (a-PS) with a molecular weight of 2.000.000 g/mol was chosen as polymer. The material was purchased from Sigma-Aldrich. Since it is an insulator, it won't actively participate into the electrical transport. In principle, choosing a semiconducting polymer the final performances could be better, but in this case, since the goal is to study the potentiality of *[3]ph* as active media in transistors, it won't be useful to add another conducting material because it would be difficult to understand what are the relative contributions of the two. PS was used just to affect the film growth and increase the processability of the material, so that it can be deposited with techniques for which high viscosity is required, such as bar-coating and spin-coating. The polymer will act as a binder to create a uniform and reproducible deposit, avoiding de-wetting phenomena, morphological anisotropy and low coverage. Moreover, PS was exploited to increase the stability of the film toward the external environment since the

semiconductor is less exposed, limiting its degradation.

Since the polymer lacks in regioregularity, it won't be able to crystallize, remaining in its amorphous state. This was exploited to easily distinguish the two materials when an optical polarized microscope is used (only the crystalline part of the film, constituted by *[3]ph*, will be visible, while the amorphous regions, formed by a-PS, will be dark).

Moreover, the amorphous state could be preferable when the blend is deposited at temperatures below the phase transitions of polystyrene (T_g or T_m) in order to avoid fast crystallization of the polymer which can hinder the crystallization of the *[3]ph* limiting the molecular mobility and the kinetics of film growth.
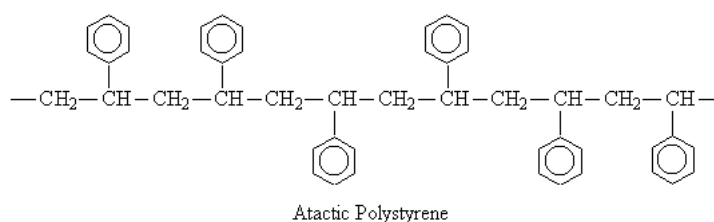
Figure 36. Chemical structure of atactic polystyrene.

3.2 Device configuration and fabrication

In this section all the methodologies used to realize the electrical devices will be illustrated, starting from the cleaning processes of the substrates up to the complete production of the transistors. All the procedures were carried out in clean room to avoid contaminations. The configuration adopted at the beginning was the Bottom gate – Bottom contacts (BGBC) one, which is also the most common used to perform first studies on new semiconductors. This because, no material is deposited on the active layer avoiding any possible degradation due to processing. However, since the semiconductor is directly exposed to the atmosphere, this architecture is not good to perform electrical measurements in air. For this reason, the electrical tests were carried out in controlled environment inside a glove box. Then, an attempt in changing configuration has been done, moving to a Top gate – Bottom contact one, which should improve device stability.

3.2.1 Bottom gate – Bottom contacts (BGBC)

The BGBC devices were prepared starting from prefabricated substrates produced by Fraunhofer institute. They are formed by a heavily n-doped silicon substrate (Si n⁻⁻) which acts also as gate electrode, with electron density equal to $\sim 3 \cdot 10^{-17}$ cm⁻³. On top of it, there is a thin layer (230 nm) of thermally grown silicon dioxide (SiO_2) as dielectric. Then, an interdigitated pattern of gold contacts is created by lithographic processes. Between the gold electrodes and the dielectric, a thin layer of 10 nm of ITO is deposited to improve adhesion toward SiO_2. In Fig.37(a) there is a schematic representation of the transistor architecture. To protect the substrates, a protection resist AZ7217 is deposited on the whole wafer, which contains 60 chips (15 cm² x 15 cm²). In each chip, there is a total of 16 transistors, four for each channel length equal to 2.5, 5, 10 and 20 μm as shown in Fig.37(b) and (c). For a given value of L, the four devices are disposed at the vertices of a square, alternating the orientation of 90 degrees, so that it can be possible notice anisotropic effects in the electrical transport. The value of channel width W is equal to 1 cm for all the transistors.
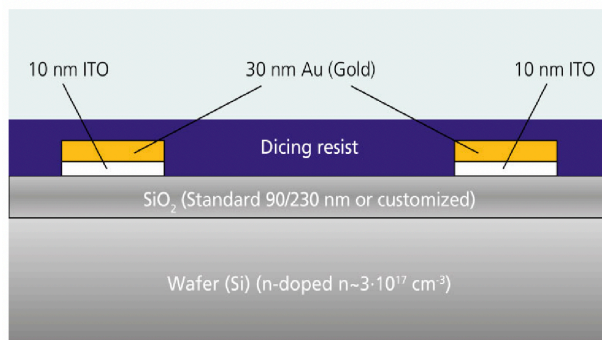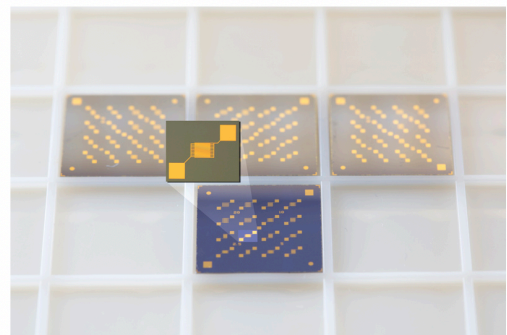
(a)   (b)
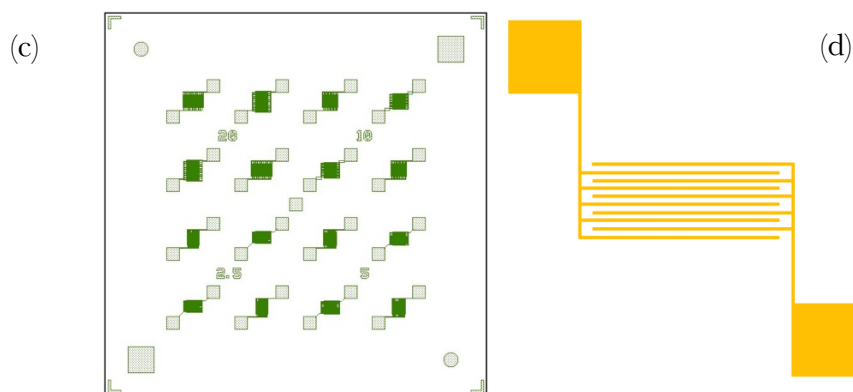
Figure 37. (a) Schematic representation of the device architecture. (b) Prefabricated substrates (chips). (c) Disposition of the 16 transistors in a single chip. (d) Geometry of the interdigitated pattern of gold contacts for a single transistor.

3.2.1.1 Substrate preparation

Before depositing the active material on any kind of substrate, a specific cleaning protocol was followed to remove the protective resist, if present, and any possible contamination, which can strongly affect the film growth. This protocol was used for both the realization of transistors and for the deposition-tests. For BGBC devices the substrates are prefabricated chips, while for TGTC transistors and for the deposition-tests, corning glasses with lithographed gold patterns are used.

During the cleaning process, first the substrates were washed manually in acetone to remove the greatest part of the resist, if present. Then, they were put in an ultrasonic bath for 10 minutes, first in acetone and then in IPA. Acetone was used to eliminate completely the resist and the large part of contaminants while IPA was used to remove any residue of acetone. All the solvents were purchased from Sigma-Aldrich. Then, after a drying step with nitrogen, the substrates were cleaned with a plasma treatment of O_2 thanks to which it is possible to burn any organic impurity left. The machine used was a plasma system coming from Diener Electronic.

The plasma treatment must be done immediately before the application of PFBT, since it is necessary have an ultra-clean surface in order to favor the formation of a SAM with good quality in terms of coverage and defects. Moreover, this process is exploited to have a good control on the change in work function of the metal electrode after the application of the PFBT. This is because the plasma treatment is able to remove any molecule physically absorbed on the gold surface, leaving the metal bare. Otherwise, if a layer of absorbed molecules is still present, the real value of the work function of the

metal is modified of an unknown extent (21), (40), making it not possible tune in a precise way the injection barrier with the application of PFBT.

3.2.1.2 Application of pentafluoro tiophenol (PFBT)

During the realization of transistors, after the plasma treatment and before the deposition of the semiconductor, a self-assembled monolayer of pentafluoro tiophenol (PFBT) bought from Sigma-Aldrich is applied on the gold electrodes in order to modify the metal work function and tune the injection barrier for "holes", as already explained in section 2.4.1 and 2.4.2. This was done supposing that the material has a higher tendency to behave as p-type way, as the greatest part of organic semiconductors. This hypothesis was actually supported by simulations of electrical transport and charge transfer processes performed by D. Fazzi et al. As illustrated in Table.5, the values of reorganization energy and transferring integral for holes are better than the ones for electrons, leading a difference of two orders of magnitude in the Marcus transfer rate.

Table 5. Values of reorganization energy, transferring integral and charge transfer rates for holes and electrons calculated by D. Fazzi et al. for two possible dimers.

	λ^h (eV)	λ^e (eV)	V_{ij}^h (eV)	V_{ij}^e (eV)	k^h (s^{-1})	k^e (s^{-1})
Dimer 1	0,366	0,495	0,045890	0,010645	$1,765 \cdot 10^{13}$	$2,955 \cdot 10^{11}$
Dimer 2	0,366	0,495	0,012913	-0,006354	$1,398 \cdot 10^{12}$	$8,293 \cdot 10^{11}$

PFBT was used for both BGBC and TGTC devices and during deposition-tests, in order to check the influence of the SAM on film morphology.

PFBT was applied immersing the substrates in a super clean Petri dish in which a solution of 10 ml of IPA and 6.7 μl of PFBT was prepared. The relative quantities were chosen according to a standard protocol in order to form a SAM with good quality. The Petri dish used was always the same and was not employed for any other process to avoid any residual contaminant. The substrates were left in the solution for some hours to allow the formation of the SAM. After this time, they are removed and dried with a nitrogen gun.
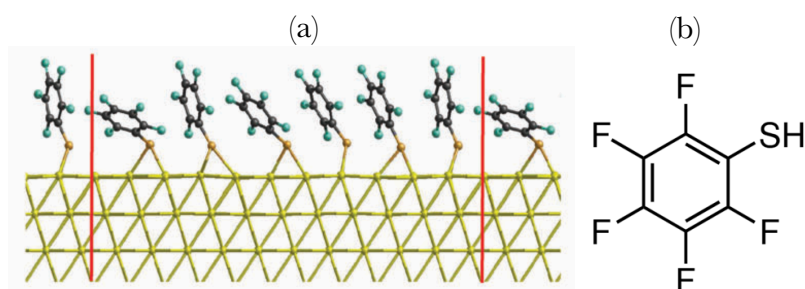
Figure 38. (a) Molecular packing of PFBT on gold (45). (b) Lewis formula of PFBT.

3.2.2   Top gate – Bottom contacts (TGBC)

For the TGBC architecture, the transistors were realized on square glass substrates where interdigitated patterns of gold contacts were created by lithography. These patterns are equal to the ones of BGBC devices, a part for the channel width that was changed from 1 cm to 2 mm. After the cleaning process, the application of the PFBT and the deposition the active material, a polymeric dielectric was applied (parylene) by chemical vapour deposition (CVD) with a thickness of $\sim 500 - 1000$ nm. Then, gates made of aluminium were fabricated by physical evaporation (40 nm). The lithographic process for the creation of gold contacts was also used for the production of some substrates for the deposition-tests to see the effect of gold on the film growth.
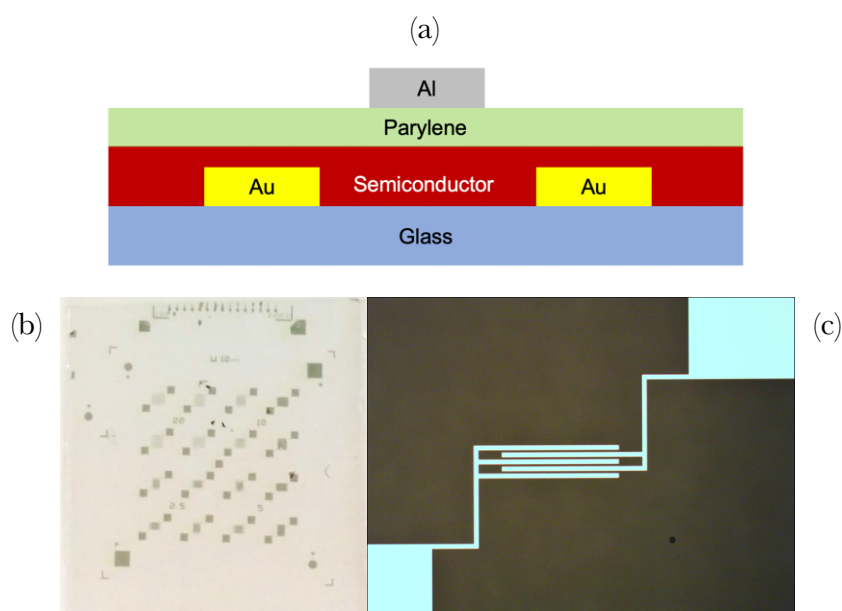
Figure 39. (a) Schematic representation of the TGBC architecture. (b) Lithographed substrate. (c) Geometry of a single transistor transistor.

3.2.2.1   Contact fabrication

The starting point of the fabrication of TGBC devices are corning glass substrates, which are cut into small square like pieces using a diamond tip. Then, these glass substrates were cleaned with the same procedure illustrated in section 3.2.1.1 using acetone and IPA with ultrasounds and by oxygen plasma. After the cleaning process, a first layer of resist LOR5B was applied by spin-coating. This material was chosen due to its good adhesion and optimized dissolution rate for maximum undercut control. Spin speed must be between 2.500 and 4.500 rpm to ensure best coating uniformity. After the application of LOR5B, the real photoresist was deposited, again by spin-coating, with a speed equal to 3000 rpm, which correspond to a thickness of about $1,2 - 1,3$ μm according to the providers Rohm and Haas. The material chosen was MICROPOSIT S1813, which is a positive photoresist that ensures excellent adhesion and uniformity. After the deposition, the mask was aligned mechanically and put in contact with the photoresist, paying attention not to damage it. Then, the resist was exposed to UV light for 7 seconds, during which it is selectively modified to change its dissolution rate toward the developer. After the exposure, the resist was developed in MF-319 for 30 seconds. Then, the process is blocked putting the substrates in water for others 30 seconds. As last step, gold was deposited uniformly (without a mask) by thermal evaporation, with the same procedure used for the aluminium gates, which will be presented in section 3.2.2.3. After the deposition there is the lift-off step.

The application of LOR5B is fundamental to form an undercut between the resist and the glass. If only the photoresist is used, due to the high difference in dissolution rates between lateral and vertical direction (which ensures an anisotropic dissolution), regular rectangular wells would be created, without any undercut. This would be a problem, because the deposited metal would form a continuous film, which makes the lift-off impossible. LOR5B, thanks to its isotropic dissolution, is instead able to produce undercuts in a controlled way, which makes it possible to remove the resists without damaging the contacts. In Fig.40 the whole process is summarized by steps.
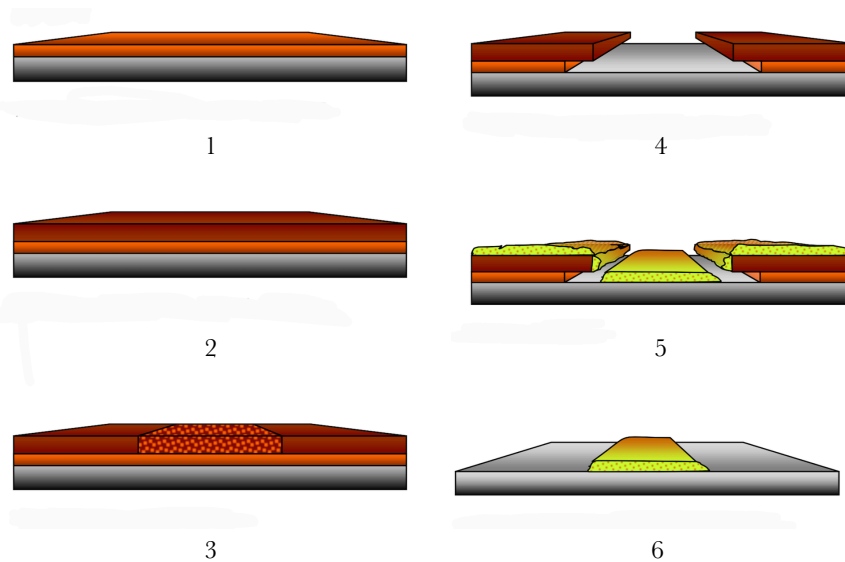
Figure 40. Fabrication of gold contacts by lithography. (1) Deposition of LOR5B. (2) Deposition of MICROPOSIT S1813. (3) Exposure of the photoresist to UV light. (4) Develop of the photoresist. (5) Gold deposition. (6) Lift-off.

3.2.2.2   Dielectric application

After the deposition of gold contacts, PFBT and active material, a polymeric insulating dielectric was applied. Parylene was chosen as dielectric since it can be the only available that could be deposited by vacuum techniques, which allow the formation of an uninform deposit in terms of surface profile and thickness, more than other polymers deposited by solution methods. The main problem of solution techniques is the possible partial dissolution of *[3]ph* in the solvent used to deposit the dielectric, which is unwanted to create a good interface (orthogonality problem). This arises because the solubility of the semiconductor is known only for some specific solvents. Moreover, depositing from solvent, an annealing process is often needed which could cause degradation of the material in the solid state. Parylene is known also to create a good semiconductor-dielectric interface avoiding formation of defects and interdiffusion. The polymer is deposited by chemical vapour deposition (CVD) starting from the corresponding dimer using "Speciality Coating System PDS 2010". The thickness of the dielectric varies from 500 nm up to 1 μm to limit surface unevenness before the application of the gate. This problem arises since parylene is conformal and replicates the surface pattern of the semiconductor (layer below) which can be far from being flat,

especially if fibres are formed. The application of parylene follows a protocol in which the deposition parameters (deposition rate, pressure and chamber temperature) were already specified to have a good film quality. After the positioning of the substrates in the vacuum chamber, the right quantity of dimer is placed in the vaporizer, where it is vaporized; from there, it goes through a furnace, kept at 720°C, where the pyrolysis takes place. The highly reactive monomers will then flow into the chamber passing through a tube, and the deposition takes place. The substrate is put in rotation to have good uniformity of the deposit.

The monomers polymerize when they reach the substrate. In Fig.41(a) the chemical process is shown.

                (a)   (b)
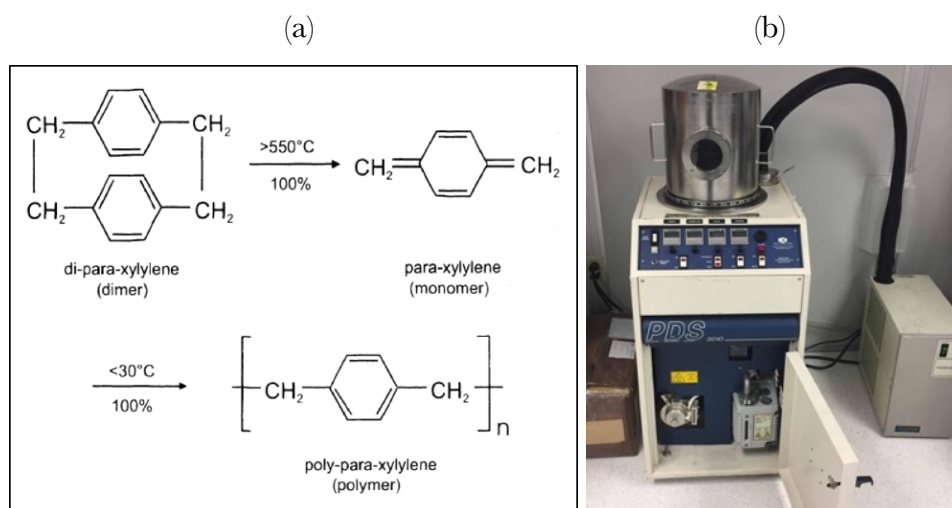
Figure 41. (a) Deposition process of parylene. (b) Coater used for the deposition (Speciality Coating Systems PDS 2010).

3.2.2.3   Gate deposition

After the application of the dielectric, aluminium gates were deposited by thermal evaporation using "PROvap Glovebox Integrated M-braun Thermal Evaporator". Al was chosen since it is cheap, simple to be evaporated and compatible with most organic materials. To deposit the gates, a specific mask compatible with the contacts pattern has been used. The mask was manually aligned using an adhesive, checking each time its relative position with respect to the substrates with an optical microscope. Then, the substrates are put in a holder which is placed inside the vacuum chamber, above the shutter. After this, a strip of Al (few centimetres) is wrapped around itself and put inside a boat (crucible) made of tantalum which is fixed between two metallic bridges. Later,

the chamber is closed and brought in vacuum until a pressure around $2 \cdot 10^{-6}$ mbar is reached (high vacuum level HV). At this point, the source is turned on and the electrical power is raised gradually until the metal starts to be evaporated. When, the evaporation rate and the pressure are almost constant (the rate must be around $0,2 - 0,4$ Å/s), the shutter is opened and the deposition starts. When the thickness of the film is equal to 40 nm (high enough to avoid surface disuniformity), the prosses is stopped, closing the shutter.

(a) (b) (c)
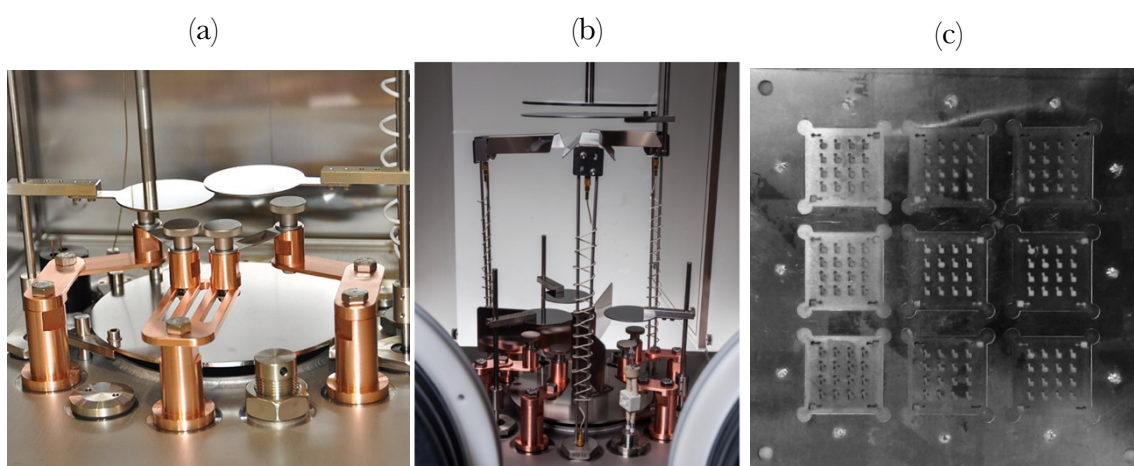
Figure 42. (a) and (b): Vacuum chamber and source dispositions. (a) Mask used to deposit the gates in aluminum.

3.3 Blend preparation and deposition

The blend was prepared in clean room in the following way. *[3]ph* and a-PS were weighted using a microbalance and put inside two separated glass vials. Then, the two materials were dissolved in a common solvent. The solution of *[3]ph* assumes a yellow colour, while the a-PS one is transparent. The solvent mainly used to realize the electrical devices was 1,2-dichlorobenzene (DCB), with concentration of 20 mg/ml, even if during the deposition-tests also toluene and dichloromethane (DCM) were used. At the beginning, DCM was used since the solubility of *[3]ph* is not known for the most part of organic solvents, a part for some specific cases for which few tests were performed in the past. In Table.6 a list of the solubility of *[3]ph* in some solvents is presented.

Table 6. Values of solubility in g/ml of *[3]ph* in some solvent, showing also the relative boiling points.

Solvents	Solubility (mg/ml)	Boiling Temperature (°C)
Acetone	0,8	56
Ethanol	0,07	78
Hexane	0,15	68
DCM	12,6	39
Toluene	6,07	110

As it is possible to see, DCM is the solvent for which *[3]ph* has the higher solubility. For this reason it was selected for the first tries, and a concentration of 4 mg/ml was used for both *[3]ph* and a-PS, far from the solubility limit of *[3]ph*. In these conditions, it is quite easy to dissolve the material, without the need of heating the solutions (which would be a problem since the boiling point of DCM is quite low). A magnetic stirrer was used to help the process. After both materials were completely dissolved, the same volume of solution was taken with a micropipette from both vials and put in a third one to form a blend with concentration 1:1 of *[3]ph* and a-PS.

The second solvent considered was toluene, for which the solubility is half of the one in DCM. The choice was done because of its relatively high boiling point, which allows a better control of the evaporation rate. In particular, depositing the material at room temperature, in the same conditions used for DCM, the evaporation rate is much lower, allowing to obtain bigger crystals. Moreover, the high boiling point allows to change the deposition temperature of a given extent to study what are the effects on film morphology, in order to obtain a better understanding of the kinetics of the process and to find out what are the processing conditions needed to obtain the best performances. The concentration used was still 4 mg/ml, as for DCM. In this case, to help the dissolution of *[3]ph*, in addition to the stirrer, the solution was heated using a metal plate, at temperatures between 50 and 60 °C, until a clean yellow solution is obtained. Usually it takes few minutes. This process is fundamental since a non-complete dissolution would lead to an unbalanced blend concentration.

The last solvent tried was DCB for which the solubility was not known a priori. It was

selected for two reasons. The first one is that it is a common solvent used to deposit many organic semiconductors and for this reason the solubility was expected to be good enough. The second one is related to its very high boiling point (180°C), which allows to extend further the range of processing temperatures. At the beginning the concentration used was 2 mg/ml. Then, since the dissolution was easy, it was raised to 10 mg/ml and 20 mg/ml. The latter is probably close to the solubility point of *[3]ph* since the solution appears turbid. Also for a-PS the dissolution is difficult, showing many undissolved parts. However, using a stirrer and heating the vials at $65 - 70$°C for $5 - 10$ minutes it was possible to have complete dissolution for both materials. If the solution of *[3]ph* is left at room temperature, there will be the formation of precipitates; for this reason, it is better prepare new solutions for every experiments.

The greatest part of the blends were prepared in ratio 1:1 of polymer and small molecule. However, during the deposition-tests this parameter was changed to see the minimum amount of *[3]ph* needed to create a uniform film.

The blend was always deposited in air, mainly with two techniques, drop-casting and bar-coating, even if during the deposition-test, also spin-coating was tried. As the blend preparation, also the deposition was performed in clean room.

3.3.1   Drop-casting

Drop-casting was chosen as first deposition technique since it is simple and fast, useful to perform first studies of morphology and electrical properties, before moving to more complex methods. Moreover, high viscosity is not required for this technique, so it is possible to deposit a solution of pure *[3]ph*, without polystyrene, which is useful for a comparison between films with and without PS, in order to see the beneficial effects of the blend for both film morphology and electrical performances.

In this case, 12 μl of solution is dropped over the substrates and left to dry for an amount of time dependent on type of solvent and substrate temperature. For transistors, just few trials were done at the beginning by drop-casting and they were carried out at room temperature with DCM. In this case, the dry time was very short, tens of seconds. During the deposition-tests, the same trials were done with toluene and DCB, both at room temperature and at 70°C. In the case of toluene, the drying at room temperatures

takes some minutes, while for DCB it goes up to tens of minutes. At 70°C instead, the evaporation rate is faster and just tens of seconds are needed for both solvents.

The drawback of drop-casting is the low level of control in the deposition process, which leads very often to low uniformity, low reproducibility and high device-to-device variation in the performances.

3.3.2   Bar-coating

Bar-coating is a widely spread technique used for the deposition of organic semiconductors in many applications. It allows the production of films characterized by good uniformity. This technique was used for both the realization of the greatest part of the electrical devices and for the deposition-tests. Compared to blade-coating, the solution under the bar is less confined near the contact line, minimizing the effects induced by the blade edges. Moreover, in appropriate conditions, it can be possible to give a preferential crystalline orientation. During the deposition, due to the so-called Marangoni effect, there is a mass flow of solute from low surface tension regions to high surface tension regions. Hence, because of a surface-tension gradient near the contact line, the molecules will diffuse toward the meniscus, where the solidification takes place, avoiding a coffee-ring growth which is a characteristic of drop-casting and spin-coating. However, if the Marangoni effect is not well controlled, disuniformity can be induced in the film. For example, a lean supply of molecules at the contact line can cause defects and voids. Moreover, when the deposition is performed at high temperatures, usually to have a better uniformity thanks to the temperature dependence of surface energy, there can be an opposite effect. Since the surface tension of most organic solvents decreases with temperature, the solution further away from the substrate will have a surface tension higher than that of the solution near the contact line. Hence, solute will flow away from the contact line, where the temperature is higher, leading to disuniformity in the deposition (46). If this happens, different strategies can be adopted, like using an appropriate combination of different solvents.
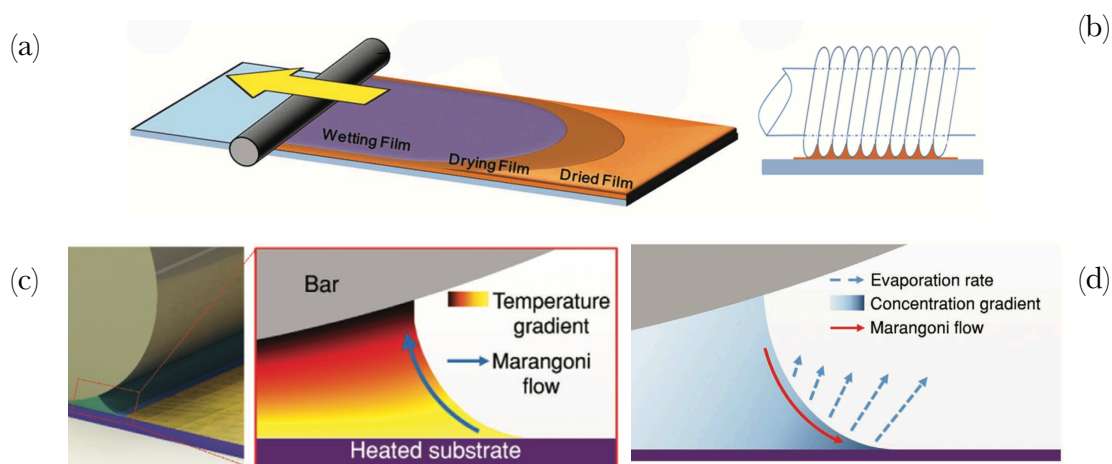
Figure 43. (a) Bar-coating process (47). (b) Formation of the meniscus in correspondence of the contact line for a spiral wire bar (47). (c) Unwanted Marangoni flow induced by temperature effects (46). (d) Right Marangoni flow (46).

To bar-coat the material and avoid de-wetting phenomena, it is always necessary blend *[3]ph* with PS, to increase the viscosity of the solution. The coater used for the deposition was a "TQC Automatic Film Applicator" while the bar was a spiral round wire bar AB3057 made in stainless steel with a wire diameters of 20 μm, coming from TQC Sheen.

For the deposition, the substrates are positioned on a metal block over the coater platform. To fix their positions and avoid unwanted displacements, a silicon or glass piece with the same thickness of the substrates is fixed with an adhesive right in front of the substrates. Then, the distance between bar and substrate is manually adjusted. The substrate must be almost in contact with the bar, but a small line of air between them must be still visible. In this condition the deposition is governed by Marangoni effect that occurs in the meniscus formed at the contact line thanks to capillarity. If the distance is too high, the bar will not assist the growth of the film and will act just as a brush, dragging the solution.

To deposit the material, 12 μl of solution are dropped on the bar in correspondence of the substrate and, immediately after, the bar moves automatically, spreading the solution in a uniform way. The speeds used during the deposition-tests were 2, 30 and 100 mm/s to select the best condition, which turned to be 30 mm/s. Hence, the devices were fabricated only at this velocity.

The kinetics of solidification strongly depends on many parameters but the only one that was changed during this work was the processing temperature, which was ranged from

RT up to 110°C with steps of 10°C. The solidification can take from few seconds up to some minutes. Sometimes it starts during the deposition itself (at high T), while other times after (at low T). The only solvent used to produce transistors by bar-coating was DCB, while during the deposition-tests also toluene was tried but only at 70°C.

Very important is to clean the bar after any deposition with the same solvent used to deposit the material to avoid modification of the bar surface energy. The bar used was employed only for the deposition of the blend and not for other processes, to avoid any possible contaminations.

For the hot depositions, it is important that a homogenous temperature is reached both on the bar and on the substrate, limiting uncontrolled changes in surface energy. To check locally the temperature, an IR thermography camera was used.

(a) (b)
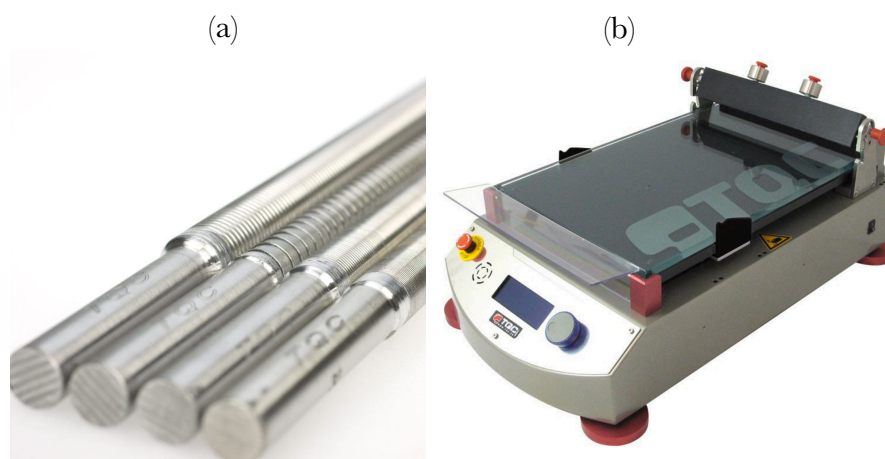
Figure 44. (a) Spiral wire bars. (b) TQC Automatic Film Applicator.

3.4 Characterization techniques

Many characterization techniques have been used in this work to obtain different types of information regarding both *[3]ph* and the semiconducting blend. In this section, they will be illustrated explaining the motivations of their use, the kind of information that we would like to obtain and the experimental procedure. Details about the experimental set up and a little explanation of the physical principles for some techniques will be provided, even if most of them are widely used nowadays to characterize new materials.

3.4.1 Optical polarized microscopy and Scanning Electron Microscopy (SEM)

Optical cross polarized microscopy is the first technique that has been used to study the morphology and the types of crystalline structures of the semiconducting film. The instrument is composed of a standard optical microscope with the addition of two important components, a polarizer filter, able to polarize the light coming from the source, and an analyser, which is a second filter placed after the sample at 90° with respect to the first one, so that, if nothing is placed between the two, the light cannot pass through. If a crystalline anisotropic material is observed, the transmitted light will be split in two rays out of phase with respect to each other due to the birefringence, and they will recombine at the analyser, determining the final colour of the light observed, also called "interference colour". This parameter is mainly affected by the difference in phase of the two rays (which can be correlated to the thickness of the material). If the material is perfectly isotropic or amorphous, the image will be dark, in the first case is because the two rays have the same phase and will give destructive interference, while in the second one because amorphous materials do not show birefringence. Hence, with this technique, it is not only possible to have an image of the film morphology at the micro scale, but also to distinguish between amorphous and crystalline domains. Since only *[3]ph* can crystallize, this is fundamental to distinguish between what is *[3]ph* and what is a-PS. Hence, the information obtained are:

1. Morphology of the film at the microscale (mainly at the top surface).
2. Classification of types of crystalline structures (constituted predominantly by *[3]ph* even if a given amount of PS can be present since the degree of crystallinity is not known a prori).

Scanning Electron Microscopy (SEM) was used to study more in details the different types of crystalline structures in terms of size and geometry, thanks to images with resolution at the naoscale. In this way it was possible observe features of the film that

cannot be seen using a normal microscope, such as types of segregations at gran boundaries, location of nucleation sites, sub-structure of the crystalline domains, presence of multi or single layers, vertical dimension of fibres, etc. In principle other information can be obtained with a proper use of the processing parameters, but in this work the technique was used only to have a better understanding of film morphology and topography. The microscope used was a "FE − SEM (Field Emission Scanning Electron Microscope) in high vacuum Zeiss Supra 40" equipped with GEMINI column and maximum resolution of 1 nm. The microscope is equipped also with a microanalysis apparatus for EDS element analysis and a STEM module. The imagines were obtained with extra-high tension acceleration voltage (EHT) of 3.00 and 5.00 KV. The types of detector used were:

1. In-lens detector (annular SE detector) for which the signal is given by secondary emitted electrons (SE), both SE1 and SE2. SE1 are electrons that leave the surface of the specimen directly at the spot where the primary electron beam impacts on the surface. SE2 are electrons generated after multiple scattering events inside the interaction volume that leave the sample at a greater distance from the primary beam's impact point. This detector is mainly used to study surface structure.

2. ET-SE (Everhart-Thornley detector) for which the output signal is given only by SE2 electrons. This detector is mainly used to study topography and surface structure.

It was not so trivial to obtain these images sometimes because of the presence of PS, which is an insulating material that can accumulate charges interacting whit the incoming electron beam, thus affecting the contrast. The information extracted from SEM images in this work were:

1. Morphology and topography of the film at the micro-nanoscale.
2. Dimensional analysis of crystalline structures.
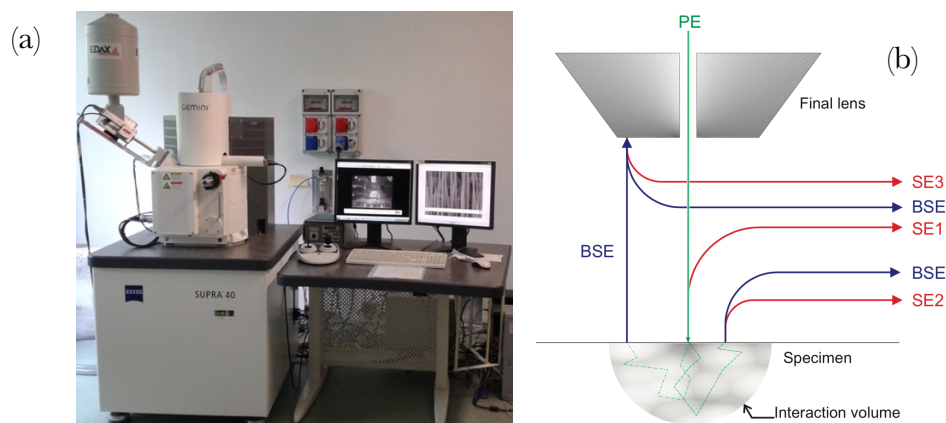
Figure 45. (a) SEM apparatus. (b) Types of signals.

3.4.2 Mechanical profilometer

A mechanical profilometer was used to estimate the roughness profile and uniformity in terms of film thickness, since it is a very simple and low time consuming instrument. Moreover, it is very useful to investigate large areas and samples in which there are abrupt changes in thickness and the use of AFM can be complex. The instrument used was an "Alpha-Step IQ surface profilometer" which works in contact mode. To perform the measurements a scratch was done on pre-selected samples coming from the deposition-tests with the help of metallic tweezers, to remove the material a leave the surface bare. The scratch must be visible so that it is easy to put the samples in the right position on the stage. The selected spot must be distant from the scratch some tens of µm, so that the tip, moving for few hundreds of µm, is able to measure the difference in thickness between where there is material and where it has been removed. Usually the scan distance ranges from 100 µm to 800 µm, while the selected speed was 10 µm/s. The measurements were performed on samples deposited on glass at different temperatures to see the difference in surface profile and uniformity between the different morphologies. Hence, the information obtained are:

1. Rough estimation of the film thickness.
2. Surface profile and roughness of the deposit.

3.4.3 UV-vis spectroscopy

UV-vis spectroscopy is a very useful technique to study the energy levels of electrons in organic molecules upon photo excitation. Many information can be deduced from the resulting spectrum. The first one is the determination of the band gap by looking at the value of wavelength relative to the onset of the lowest energy transition, which can be extrapolated considering the tangent of the peak. This property was already investigated for *[3]ph*. However, to do a comparison between the spectrum of the molecule in solution and in the solid state, the UV-vis spectra was measured again. To do this a "U.V. − 1800 Shimadzu spectrometer" was used. A solution of *[3]ph* in DCM was prepared with concentration of about ~1,5 mg/ml. The solution was placed inside a quartz cuvette, paying attention not to touch the lateral walls. After the positioning of the sample, the measurements can be done. To distinguish the contribution of the solvent, a sample of pure DCM was measured. The range of wavelength selected was limited from 200 up to 500 nm, since the region of absorption was already known from the data of Tykwinski et al. and by the calculations performed by Milani et al.

The solid state measurements were instead performed on selected samples coming from the deposition-tests on glass substrates. In this case, the experiments were performed using "Lambda 1050 UV/VIS/NIR spectrometer". By doing a comparison between the spectra related to the isolated molecule and those of the films it is possible to recognize some modifications, like the appearance of new bands or a shift of the main peak. This can be related to solid state interactions between molecules, that change the molecular orbitals and the energy levels of electrons depending on the type of aggregates formed. Recognizing the type of aggregate is fundamental to have a better understanding of the nature of transport in the active material, and can be used as a starting point for theoretical simulations. Moreover, comparing samples produced at different temperatures, which show different morphologies, it is possible to see if there are changes in terms of molecular interactions. For solid state experiments, an integrating sphere set up was used, which is able to collect also the scattered light along with the transmitted one. In this case the samples were attached using parafilm at the entrance of the sphere. The sources used were both a tungesten and D2 lamp, to cover a larger range of wavelengths.

3.4.4   X − Ray diffraction

X – ray diffraction is an important technique to study crystalline materials. Different kind of information can be obtained, depending on the set up and the type of sample. In this work, this technique it was used to confirm the crystalline structure of *[3]ph* in the solid state, doing a comparison between the pattern obtained from a drop-cast on a silicon substrate and the one already present in literature (44). The sample was prepared drop-casting a solution of 4 mg/ml in DCM in controlled atmosphere, which turns out to be a simple way to obtain single crystals. Then, some measurements were performed on semiconducting blend films bar-coated at different temperatures, to observe possible differences in the degree of crystallinity between the different structures from a qualitative point of view. The detector used was Zero-D type detector and the measurements were performed in grazing incidence mode. The sample and the source were kept fixed while the detector moves of an angle of 2θ, going from very low angles up to 90°. The experiments were performed using a "Bruker DS Advance Diffractometer".
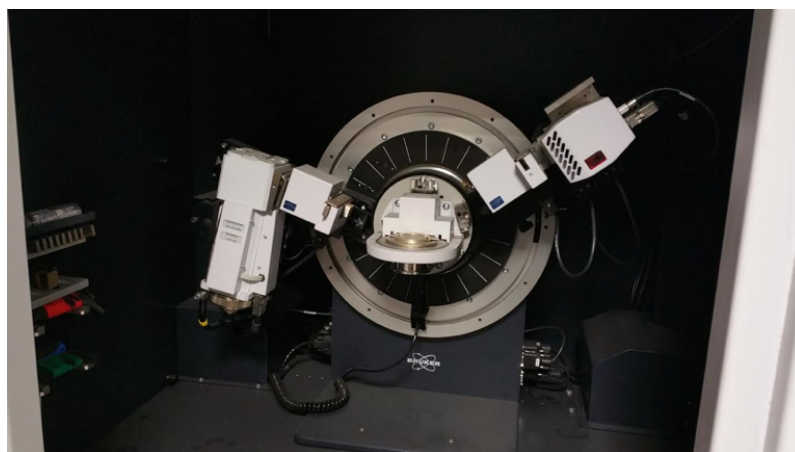
Figure 46. Bruker DS Advance Diffractometer.

3.4.5 Raman and SERS spectroscopy

As already mentioned in section 1.2, Raman spectroscopy is a useful technique to characterize carbon based materials such as *sp* carbon. In this work, Raman was used for two purposes:

1. To go from a BGBC configuration to a TGTC one, a partial phase segregation must occur in the blend. The presence of a semiconductor rich layer at the bottom surface is verified by the electrical characterization itself. However, from the images obtained at the microscope it seemed that crystalline domains were present also at the top surface and, moreover, there must be a connection between the two interfaces because sometimes a relation between electrical response and directionality of the film at the top surface could be found. However, to be sure of the presence of *[3]ph* at the top interface, Raman measurements of the blend were performed, allowing an easy recognition of the presence of *sp* carbon at the surface.

2. Doing a comparison between the Raman and SERS spectra it is possible get important information about charge transfer processes from metal electrodes to the active material and the nature of the charge carriers themselves, in terms of distribution of excess of charge.

In principle, other information like the value of the BLA and band gap could be obtained, but in our case they were already known. The measurements were performed using a "Renishaw Invia Raman Spectrometer" with single grating and notch filters. The system is equipped with an optical microscope to do Micro-Raman measurements. The two possible wavelengths of the Argon Ion Laser are 457 nm (blue) and 514 nm (green). Both of them were used to perform the measurements, even if in the wavelength at 457 nm was problematic probably due to photoluminescence phenomena that can cover the Raman signal.

To perform Raman measurements a calibration step was done with a small Si substrate, checking that the resulting peak is in correspondence of 521 cm^{-1}. If not, the value must be corrected. Then, the samples are measured extending the range of wavenumber from 100 up to 3500 cm^{-1}. The power of the laser can be changed depending on the need from 5 up to 100 mW, while the number of accumulations selected to have a good spectrum was usually 10. Before the measurement it is important to select the "cosmic ray removal" option and turn off the light of the room. To perform the experiments on the raw material, the samples were prepared just taking a bit of powder and putting it

on a Si substrate, while for the blend, the material was deposited on glass substrates in clean room.

In case of SERS measurements, the only difference is the sample preparation. A solution of *[3]ph* in DCM with concentration of 2 mg/ml was deposited on a prefabricated active substrate made of silver. The solution was deposited by drop casting in controlled environment.
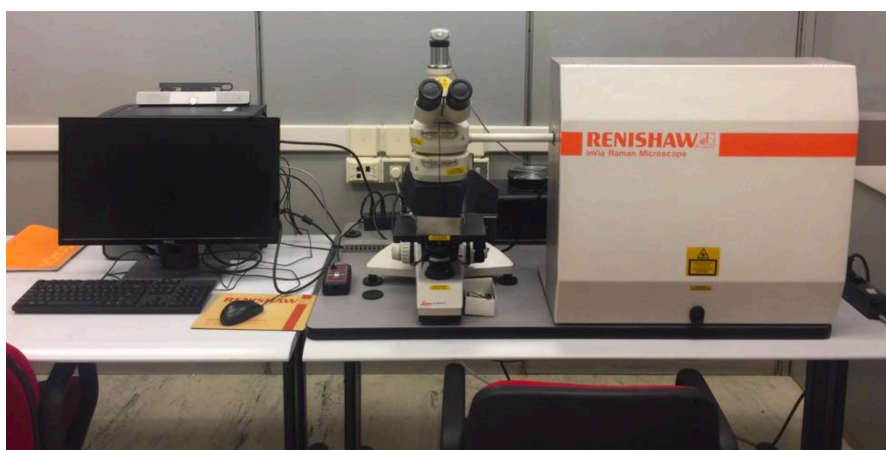
Figure 47. Raman apparatus.

3.4.6   Semiconductor parameters analyzer (SPA)

The electrical measurements were performed using a Semiconductor Parameter Analyzer (SPA) "Agilent Technologies B1500A Semiconductor Device Analyzer" with a current resolution of 0,1 fA. It is connected to a four-probe stage, equipped with an optical microscope, inside a glove box, so that the tests can be performed in controlled nitrogen atmosphere, with a low level of oxygen and concentration of H_2O less than 1ppm, to avoid degradation and instability phenomena. In the second part of the work, tests in atmosphere and in vacuum, using a cryoprobe, were performed in order to study the stability of the system and to better analyze the role of the blend. Experiments are carried out contacting the three terminals of the transistors to three probes with the help of the microscope. To contact the gate in case of BGBC devices a scratch must be done laterally, at the edge of the chip, using a metallic tweezers, while for the TGBC ones gates are deposited on top of each transistor.

The primary information obtained are the transfer and output characteristics. The transfer curves for the BGBC devices were obtained with a sweep of the gate voltage from 2 to -10 V. It was not necessary go further since the ideality of the transistors was quite high, with field effect mobility not bias dependent but constant as soon as the device is turn on. Moreover, going toward higher voltages, there is the risk of causing bias stress and degradation. The measurements were done both in linear and saturation regime, changing the drain voltage from -2 to -10 V. For the TGBC devices, because of the higher dielectric thickness, the range of gate voltage was extended from 5 to -22 V, changing also the drain voltage (-5 for the linear and -22 for the saturation regime).

For the output curves, the drain voltage was varied continuously from 0 to -10 V, while the gate voltage was changed from 0 up to -10 V with steps of 2 V.

From the transfer characteristic, many parameters have been extracted such as field effect mobility, ON-OFF ratio, subthreshold slope, threshold voltage and reliability factor with a procedure that will be explained in section 4.3. The output curves were instead used to discuss the nature of the semiconductor-metal contact and to have a qualitative idea of the magnitude of the contact resistance.
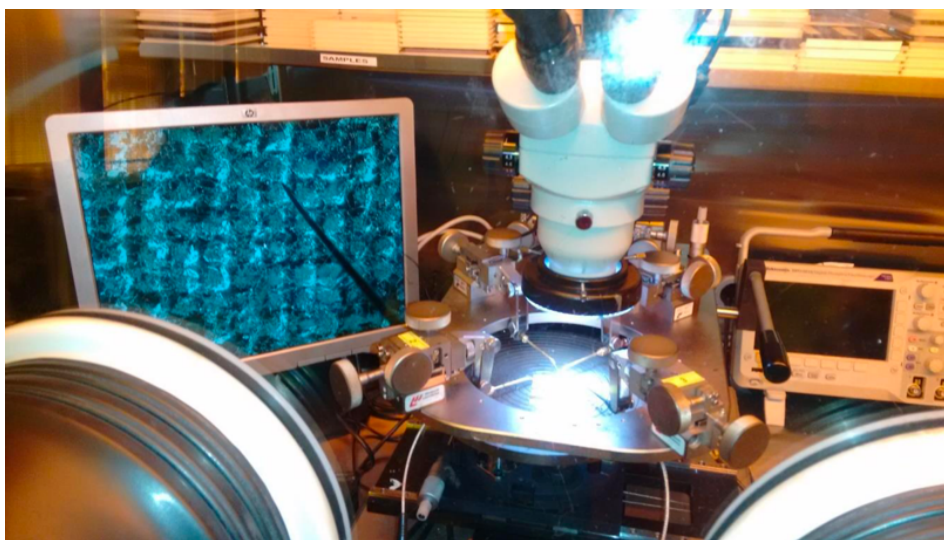
Figure 48. Glove box prober.

4. Experimental results

4.1 Morphology and structures of the conducting film

In this section, all the types of crystalline structures obtained during this work will be illustrated. As it will be possible to see, by changing different processing parameters like solvent temperature, concentration, type of deposition technique and surface energy, different morphologies can be obtained, from isolated single crystals to highly oriented fibres or spherulite-like domains. Having a good understanding of film growth is fundamental to have a good control on the deposition of the active material and to be able to realize a uniform and reproducible thin film, which is important requisite for an OFET.

4.1.1   Molecular packing

From experimental data coming from X − ray diffraction measurements performed in the '70s by Ziva Berkovitch-Yellin at al. (44) it was possible to simulate the molecular packing for an ideal infinite crystal made of *[3]ph*. Even if these data are related to crystals of only *[3]ph*, without polystyrene, they are anyway important to have an idea of how the molecules of semiconductor are arranged in space at thermodynamic equilibrium. Moreover, since the crystalline domains also in the blend are formed mainly by *[3]ph*, the molecular packing could be preserved. Fig.49(a), (b) and (d) show the unit cell of *[3]ph* and how it is repeated in space along the three directions x,y and z. As it is possible to see, the cell is formed by two molecules in a lamellar stacking mode (almost parallel) from the point of view of the main chain that, as previously mentioned,

is slightly bent. Looking at how the cell is repeated in space, *[3]ph* appears to be ordered in a layered structure. If the molecules are imagined as rigid segments, each layer will be constituted by segmented lines parallel to each other formed by an alternation of *[3]ph*. The position of phenyl rings belonging to neighbouring molecules of adjacent cells along the y direction is another interesting feature. They are packed in a herringbone way because of interactions between C–H groups of neighboring rings, as frequently happens also for others aromatic structures. In Fig.49(c) there is a comparison between the X − ray diffraction pattern of Ziva Berkovitch-Yellin at al. and the one obtained during this work on a drop-cast of *[3]ph* in DCM with concentration 4 mg/ml on a clean silicon substrate. This turned out to be an easy way to produce a random network of single crystals with needle-like geometry.
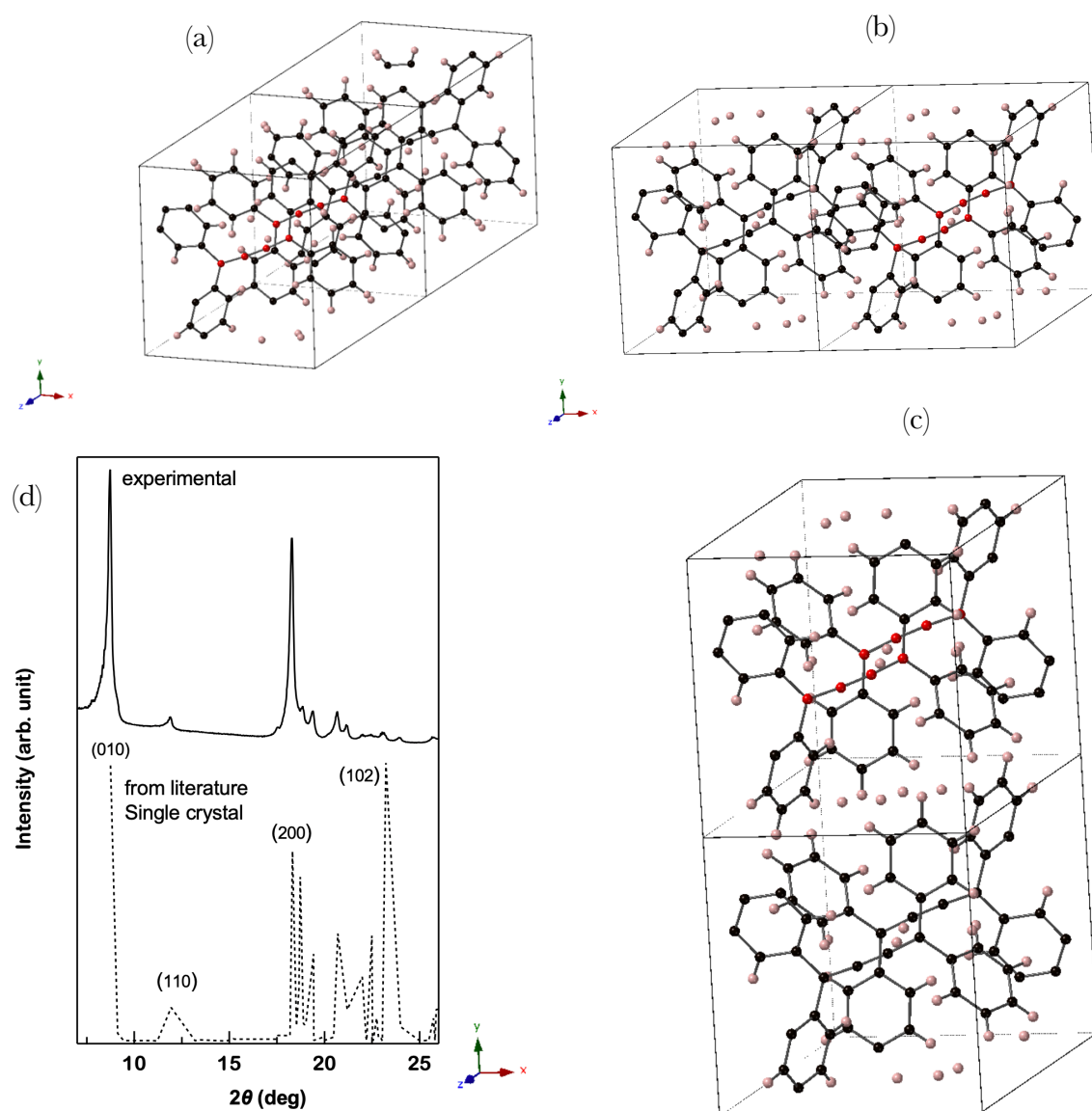
Figure 49. (a), (b) and (d) Unit cell of *[3]ph* simulated from X − ray diffraction data coming from experiments performed by Ziva Berkovitch-Yellin at al. on single crystals of *[3]ph* (44). (c) Comparison between diffraction patterns of single crystals obtained from a drop-cast of *[3]ph* in DCM with concentration of 4 mg/ml on silicon and the one obtained by the data of Ziva Berkovitch-Yellin at al. (44).

As it is possible to see in Fig.49(c), the (102) diffraction is missing in the pattern coming from our experiments. This peak is related to neighboring interactions between adjacent molecules belonging to different cells, along the zy plane as shown in Fig.50(a). This could be attributed to local molecular disorder in the crystals obtained by drop-casting that makes it difficult to see diffractions corresponding to very low intermolecular distances. Another possibility could be that this reflection is totally in-plane, making it impossible to see with our set-up.

(a)   (b)
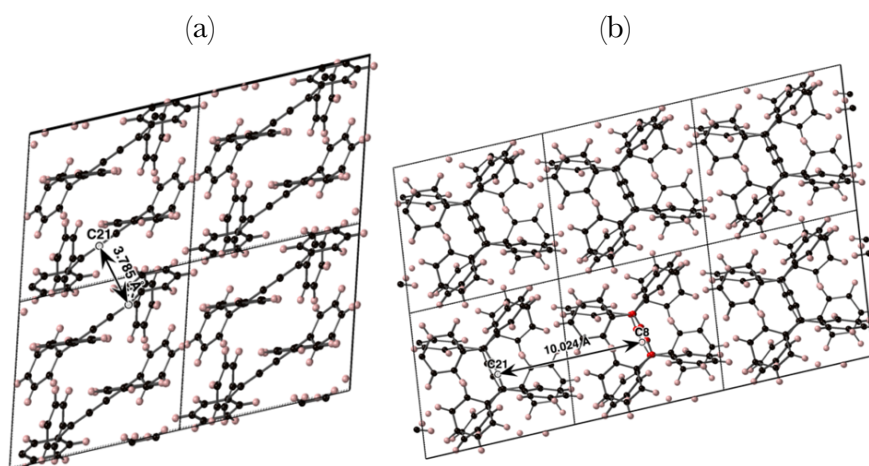
Figure 50. Intermolecular distances corresponding to the 102 (a) and 010 diffraction (b).

4.1.2   Types of crystalline structures

As mentioned before, depending on the processing conditions, the morphology and structure of the semiconducting film changes a lot. This is typical of organic semiconductors. In this section, all the types of structures obtained in this work during the deposition-tests will be presented. Many trials were done in order to obtain a film with the desired requirements. Type of solvent, concentration and deposition technique were changed, until the best condition was selected. The latter corresponds to bar-

coating a solution of *[3]ph* and PS with ratio (1:1) and concentration of 20 mg/ml in DCB. Now, in a chronological order, the results of all the tests in terms of structures will be presented.

Fig.51 shows a deposition by drop-cast of a 4 mg/ml pristine solution of *[3]ph* in DCM on a glass substrate. This type of deposit was the starting point. As it is possible to see, a film is not formed, but rather a multitude of isolated needle-like single crystals, with a well defined geometry.
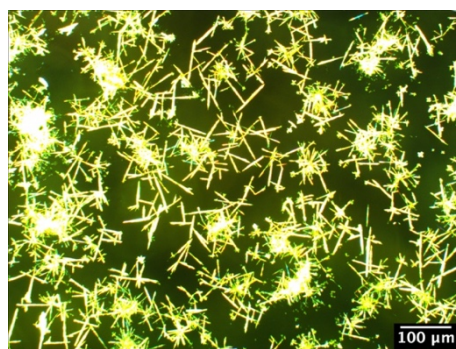
Figure 51. Optical polarized image of a film obtained by drop-casting a solution of *[3]ph* in DCM with concentration of 4 mg/ml.

The length of the crystals ranges from 50 up to 80 μm. In this case, the coverage is very low and the film has no uniformity. Due to the fast evaporation rate, the deposition shows a marked solidification ring at the edges, where the crystals appear to be bigger and more elongated. For an OFET this situation must be avoided since the "film" is not reproducible and highly non-uniform, leading to device-to-device variation in the final performances. However, despite these drawbacks, the degree of crystallinity of each crystal is very high. For this reason, the initial idea was to try to obtain a more compact film with bigger crystals, preserving the high crystallinity.

The solvent was changed, in order to obtain bigger crystals, from DCM to toluene, which has a higher boiling point, leading to a lower evaporation rate and a slower deposition. Even if the solubility in toluene is lower than in DCM, the concentration was kept equal to 4 mg/ml. The obtained drop-casted structures were very similar to those obtained with DCM. Also in this case, the films were formed by small isolated needle-like crystals.

The next step was the addition of an insulating polymer to increase the film-forming properties and thus the uniformity. To do that, atactic polystyrene (a-PS) was selected.

In Fig.52(a),(b) and (c) the result of a drop-cast solution made of *[3]ph* and PS in toluene with ratio (1:1) and concentration of 4 mg/ml is shown. In this case, apart from the edges, the deposition is more uniform and compact with a higher coverage. The small crystals of *[3]ph* have a dendritic-like shape with a lot of branches. The length of the dendrites usually ranges from 10 up to 80 µm, even if the greatest part of them have a size of about 50 µm. However, at the edges of the drop it is still possible to notice the presence of big single crystals with length of $150 - 250$ µm due to ring-like evaporation.

(a)   (b)   (c)
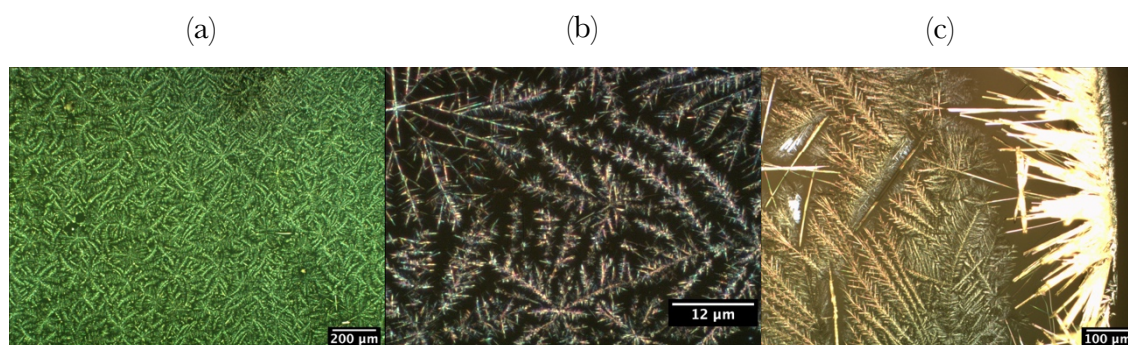
Figure 52. Optical polarized images of films deposited by drop-casting a solution made of *[3]ph* and PS (1:1) in toluene with concentration 4 mg/ml. (a) and (b) Center of the drop (c) Edge of the drop.

If the glass substrate is tilted manually during the deposition, it is possible impose a directionality to the crystals, which are also more elongated, compact and less branched, as it is possible to see in Fig.53(a) and (b). This trial was important to appreciate the possibility of having crystals along a preferential direction, which could be interesting for charge transport.

(a)   (b)
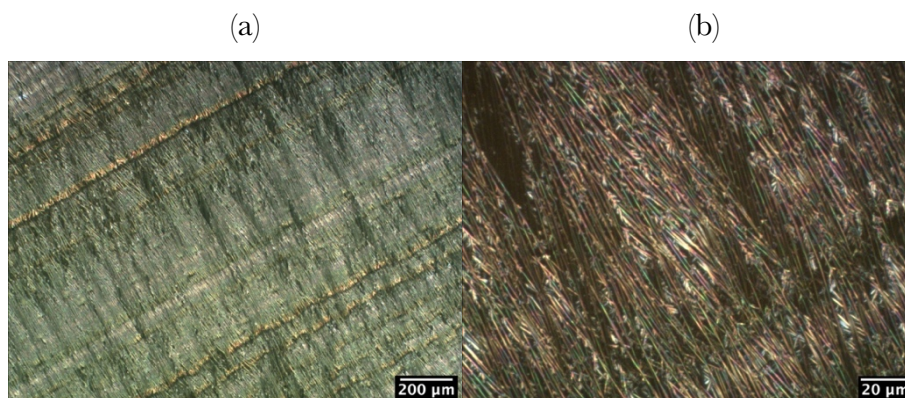
Figure 53. (a) and (b) Optical polarized images of a film deposited by drop-casting a solution made of *[3]ph* and PS (1:1) in toluene with concentration 4 mg/ml on a tilted glass substrate.

Sometimes, as presented in Fig.54(a) and (b), also bigger crystalline domains with a feather-like shape can be formed, especially when the substrate is tilted. Their formation is always located at the beginning of each coffee-stain line.

(a)   (b)
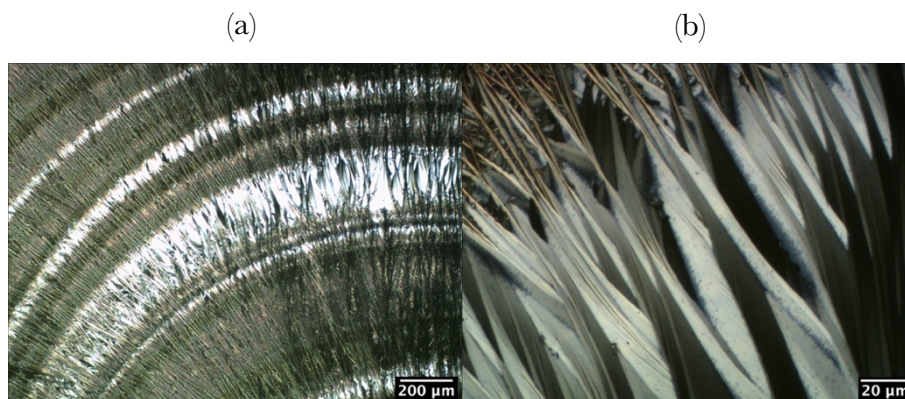
Figure 54. Big feather-like crystalline domains at the coffee-stain lines.

By drop-casting, films always appear as non-homogeneous and hardly reproducible. To increase uniformity and reproducibility, and to avoid the ring or coffee stain-like evaporation, it is necessary change the deposition technique. Some trials by spin-coating were done, but the solution always de-wetted from the substrate, probably because the viscosity was not high enough. However, the solution in toluene was successfully bar-coated. In Fig.55(a) and (b) a film obtained with a solution made of *[3]ph* and PS (1:1) in toluene with concentration of 4 mg/ml bar-coated at 70°C is shown. This was the first time in which a uniform film was produced. Small crystalline domains with a spherulite-like shape were formed.

(a)   (b)
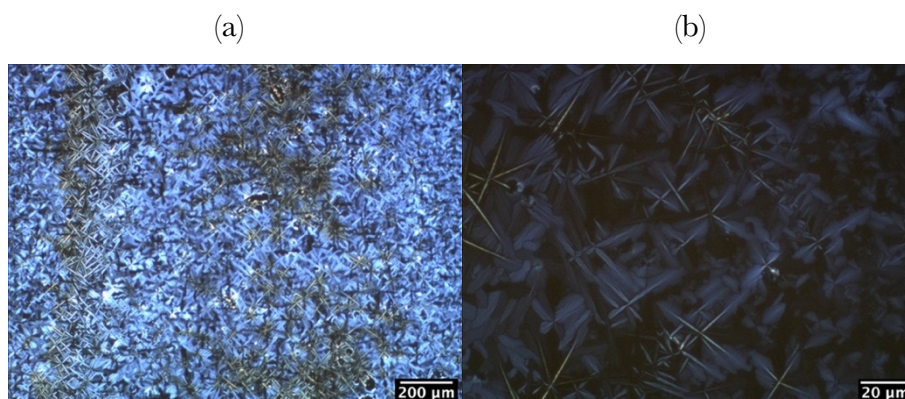
Figure 55. (a) and (b) Optical polarized images of a film deposited by bar-coating of a solution made of *[3]ph* and PS (1:1) in toluene with concentration 4 mg/ml at 70°C.

After toluene, DCB was chosen as alternative solvent. The molecule was successfully dissolved up to concentrations of 20 mg/ml. The choice of DCB, as previously mentioned, was made for two reasons. First, due to the high boiling point, by depositing the solution at ambient temperature, a very low evaporation rate, fundamental to obtain big crystals, it is expected. Second, it is possible extend a lot the range of processing temperatures in order to find out the best processing condition. Fig.56(a) and (b) illustrate the results of a deposition by drop-casting a solution made of *[3]ph* and PS (1:1) in DCB with concentration of 10 mg/ml at room temperature and 70°C. In the first case, big isolated single crystals are formed with length of about $50 - 150$ μm, while in the second one, at the centre, large crystalline domains with a spherulite-like shape were found. However, in some cases also dendritic fibres were observed, similar to the case of toluene.

(a)   (b)
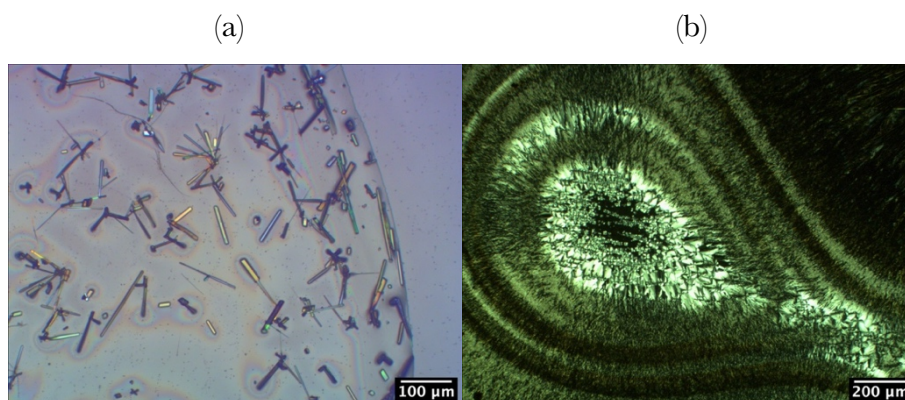
Figure 56. Optical polarized images of a film deposited by drop-casting a solution made of *[3]ph* and PS (1:1) in DCB with concentration 10 mg/ml at (a) room temperature and (b) at 70°C.

After some trials by drop-casting, the solution was deposited by bar-coating with concentration of 20 mg/ml at different processing temperatures (which turns out to be the most influencing factor). Since it was possible to obtain a vast variety of morphologies, including a uniform, reproducible film, this method was chosen as the best one to realize field effect transistors. In the next sections a detailed description of the influence of different parameters follows, including the effect of temperature, deposition speed, concentration and changes in the surface energy due to the presence of gold contacts with and without PFBT.

Below a list of the types of structures obtained with the corresponding images is presented. All of them are related to film deposited by bar-coating a solution made of *[3]ph* and PS (1:1) in DCB with concentration 20 mg/ml.

1. Isolated big single crystals. Fig.57(a) and (b).
2. Branched dendritic-like fibres with low directionality. Fig.58(a) and (b).
3. Highly oriented rod-like fibres, non-branched. Fig.59(a) and (b)
4. Spherulite-like crystalline domains with fibrillar structure. Fig.60(a) and (b)
5. Spherulite-like crystalline domains with lamellar structure. Fig.61(a) and (b).
6. Small crystalline domains with polygonal geometry. Fig.62(a) and (b).

(a)　　　　　　　　　　　　　　　　(b)
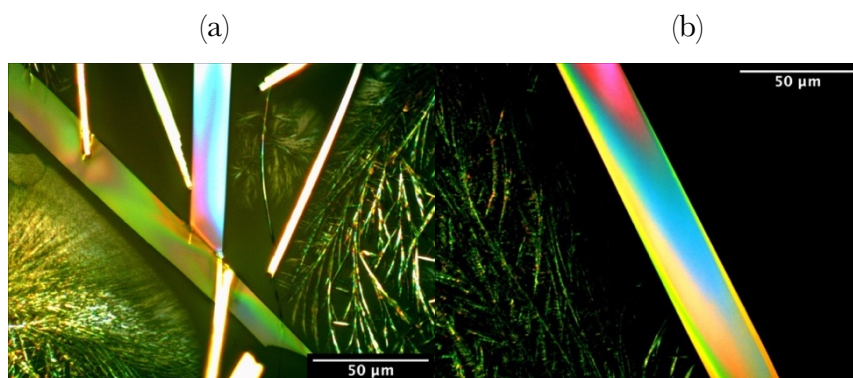
Figure 57. Optical polarized images of single crystals on a glass substrate.

(a)　　　　　　　　　　　　　　　　(b)
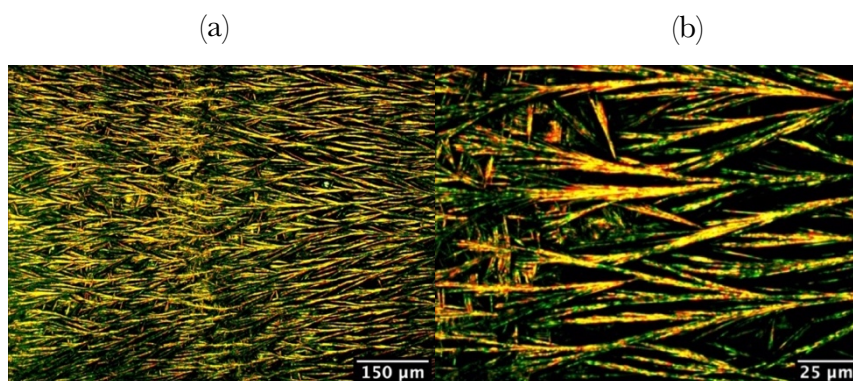
Figure 58. Optical polarized images of dendritic-like fibres on a glass substrate.

(a)　　　　　　　　　　　　　　　　(b)
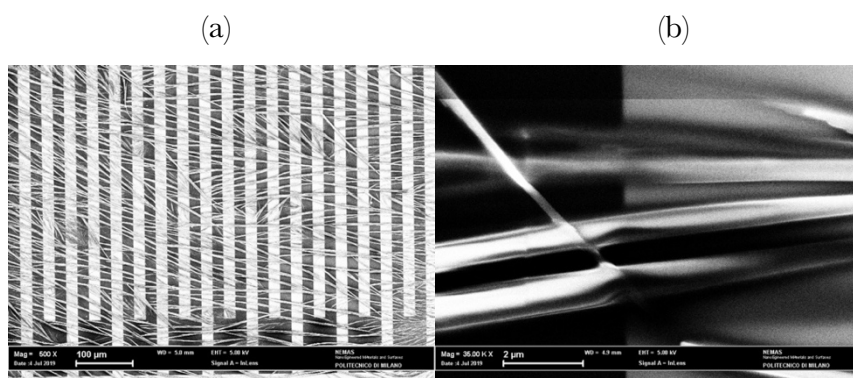
Figure 59. SEM images of oriented rod-like fibres on prefabricated BGBC transistors.

(a)   (b)
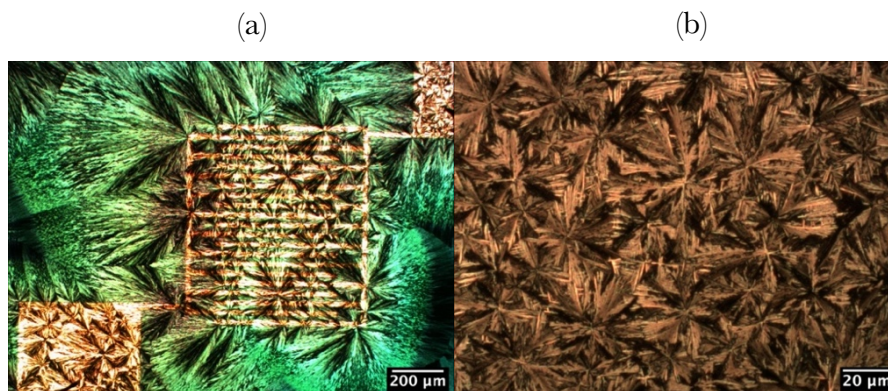
Figure 60. Optical polarized images of spherulite-like crystalline domains with fibrillar structure on prefabricated BGBC transistors.

(a)   (b)
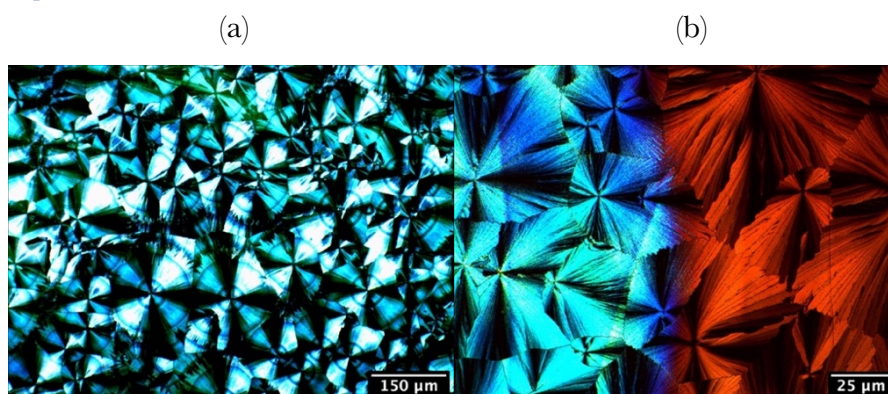
Figure 61. Optical polarized images of spherulite-like crystalline domains with lamellar structure on a glass substrate.

(a)   (b)
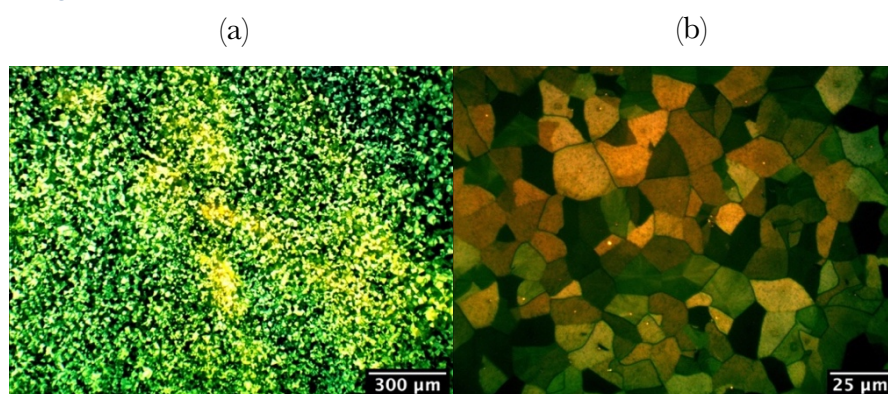
Figure 62. Optical polarized images of small crystalline domains on a glass substrate.

4.1.3   Effect of the deposition technique

Drop-casting is a useful technique to perform first studies on new materials since it is very simple. However, the films produced were highly non-uniform due to ring or coffee-stain evaporation. At the edge of the drop, the structure was always different from the centre and, moreover, very often the deposit often presented marked solidification fronts at which the morphology changes drastically. In the same deposit the shape of the

crystals was observed to change a lot, from small dendrites to long fibres and big crystalline domains. In addition, even if sometimes the films show a good coverage and compactness, usually there were many regions not properly covered. Such technique has limited control and is affected by too many environmental parameters. This not only leads to non-uniform films, but also to low level of reproducibility. For this reason, even if sometimes the structures obtained are interesting, it is not useful in the prospective of producing electrical devices. By bar-coating, instead, the films obtained were much more uniform and predictable, because the deposition is more controlled and less affected by little changes in the environment. In this case, the role of processing parameters, like temperature, speed, concentration and type of solvent, can be more easily identified. Instead, in the case of drop-casting, the relation between structure and deposition conditions results highly elusive. Furthermore, bar-coating offers the possibility to produce oriented structures, which is important to study anisotropicity in the charge transport. Due to all these considerations, apart from the deposition-tests and some trials at the beginning, all the devices were produced by bar-coating.

4.1.4   Solvent and concentration effects

The type of solvent used play an important role during the deposition since its evaporation affects the solidification rate, which is a crucial parameter in determining the type and shape of structures as well as the size of the crystals. Going from low boiling point solvents to high boiling point ones, the dimensions of the crystals were observed to increase, when the depositions were performed at the same temperature. For example, passing from DCM to DCB, the length of the single crystals changes from ~ 50 μm to 200 μm, in average, and they are also wider.

(a)   (b)
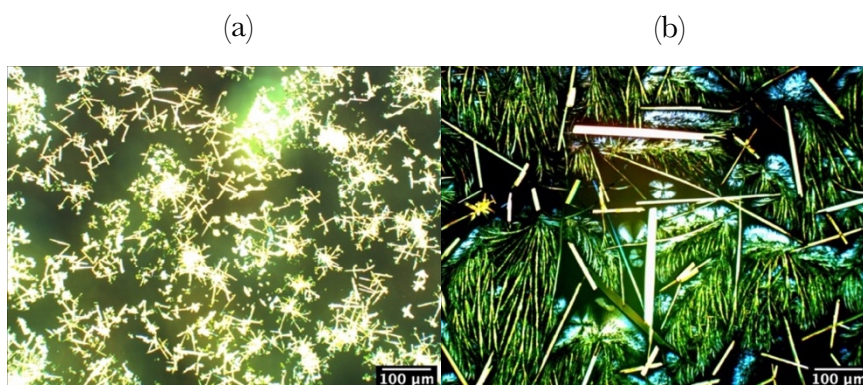
Figure 63. Optical polarized images of: (a) a film deposited by drop-casting a solution of *[3]ph* in DCM with concentration 4 mg/ml at room temperature, (b) a film deposited by bar-coating a solution of *[3]ph* and PS in DCB with concentration 4 mg/ml at 30°C.

Also, the concentration plays a little role. Increasing the content of material, the film often tends to have an higher compactness, covering in a more uniform way all the substrate. However, this effect is not so marked, because sometimes even with low concentrations it was possible to obtain good films. This can be noticed just comparing Fig.55(a) and Fig.61(a). The two films were deposited both by bar-coating at 70°C, one in toluene with concentration of 4 mg/ml, while the second in DCB with concentration of 20 mg/ml. As it is possible to see, apart from the size of the crystals, the shape and uniformity of the deposit are very similar.

The role of the relative ratio between *[3]ph* and PS is more interesting. Changing the percentage of semiconductor it could be possible to verify if a thin uniform crystalline layer of *[3]ph* can be formed also with a low quantity of small molecule. In principle, for the functioning of the devices, it is not important to have a thick layer of semiconductor, but it is enough to have a thin layer, since the transport will take place in a layer close to the dielectric interface. In Fig.64 the relative amount of *[3]ph* is changed in the following way: 100%, 75% and 25%. As it is possible to see, there must be a minimum amount of *[3]ph* needed to from a uniform layer at the surface of the film, around 50%.

(a)   (b)   (c)
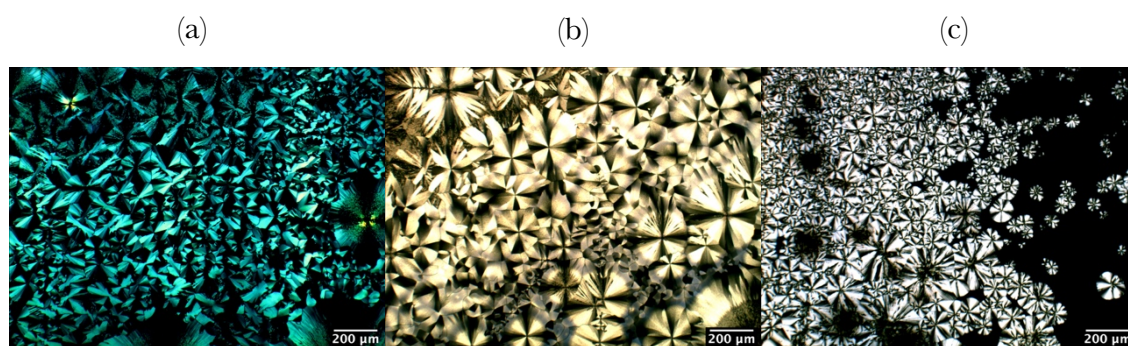
Figure 64. Optical polarized images of films deposited by bar-coating a solution of *[3]ph* and PS in DCB with concentration of 20 mg/ml with percentage of *[3]ph* equal to: (a) 100%, (b) 75% and (c) 25%.

4.1.5   Influence of the processing temperature and bar speed.

Thanks to the high boiling point of DCB, it was possible to deposit the blend by bar-coating in a wide range of substrate temperatures. The processing temperature strongly affects the kinetics of the film growth, determining the evaporation rate of the solution. At low temperatures, the solidification can take some minutes, while at high temperatures few seconds. The deposition temperatures can be classified in four main classes:

1. $30 - 40 \ °C$ (low temperatures)
2. $50 - 60 \ °C$ (medium temperatures)
3. $70 - 80 - 90 \ °C$ (high temperatures)
4. $110°C$ (temperature above T_g of polystyrene)

At low temperatures $(30 - 40 \ °C)$, the film starts to solidify after the passage of the bar. The deposit obtained is quite similar to the one produced by drop-casting, except for the presence of the ring-like solidification. Big isolated single crystals, with size of tens up to few hundreds of micrometres are formed. Sometimes, highly branched dendritic fibres, without any directionality, are generated. The higher is the temperature (from 30 up to 50°C), the higher will be the amount of fibres with respect to the one of single crystals. In this temperature range, the film is always characterized by a low level of coverage. In Fig.65(a) and (b) films obtained by bar-coating at 30 and 40°C are shown.

(a)   (b)
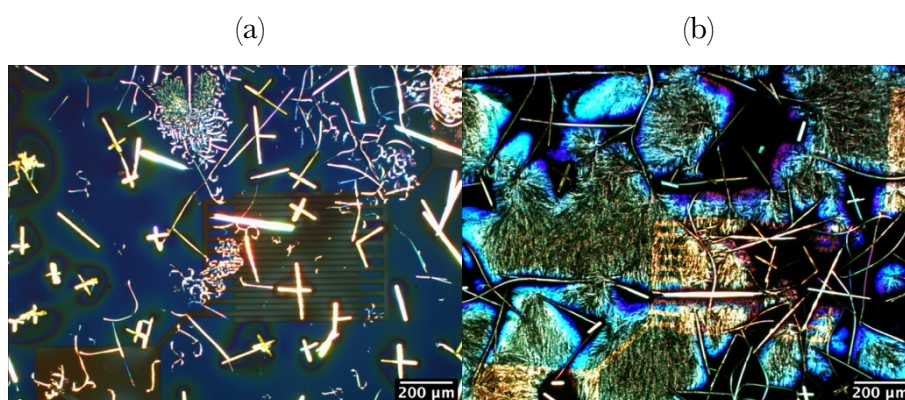
Figure 65. Optical polarized images of films deposited by bar-coating a solution of *[3]ph* and PS (1:1) in DCB with concentration of 20 mg/ml on prefabricated BGBC transistors at (a) 30°C and (b) 40°C.

At medium temperatures $(50 - 60 \ °C)$, the solidification starts during the deposition itself. In this case the films obtained were constituted by a uniform compact deposit

made of small oriented dendritic-like fibers with high level of coverage, as it is possible to see in Fig.66(a). Sometimes highly oriented rod-like fibers can be formed in some regions of the film, probably thanks to an assisted growth induced by the bar. In this case, the coverage is lower, since there is a lot of space between the fibers, but the degree of directionality is very high, as also their dimension. The length of these rod-like fibers ranges between 100 up to 400 μm, as shown in Fig.66(b).

(a)   (b)
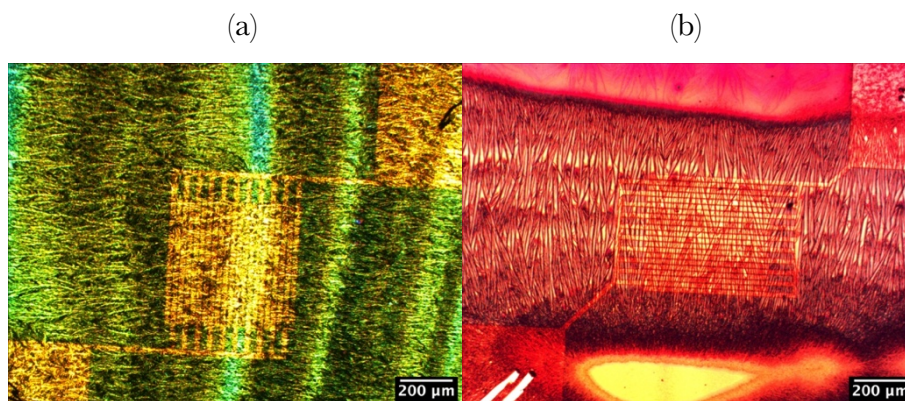
Figure 66. Optical polarized images of films deposited by bar-coating a solution of *[3]ph* and PS (1:1) in DCB with concentration of 20 mg/ml on prefabricated BGBC transistors at 60°C.

At high temperatures (70 − 90 °C), the solidification takes place in few seconds. Thanks to the high evaporation rate, the films are highly uniform over all the substrate. They are constituted of crystalline domains with variable dimension and shape that resemble the one of spherulites, due to the presence of a Maltese cross, like in case of semi crystalline polymers. They usually have a fibrillar structure. The size of these domains decreases increasing the processing temperature. At 90°C the domains are so small that it is no longer possible to see the Maltese cross and they appear as little crystals with a polygonal shape. The coverage obtained with spherulite-like domains is very high. However, the degree of crystallinity of each single domain should be investigated more in details since probably they contain not only *[3]ph* but also a fraction of PS.

(a)   (b)
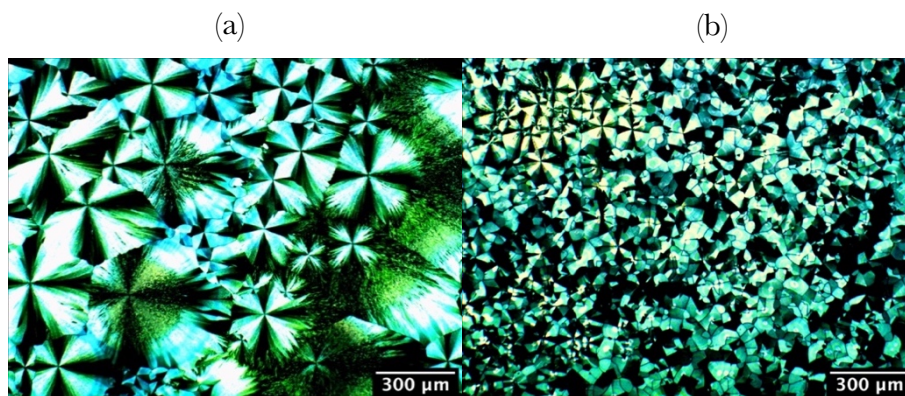
Figure 67. Optical polarized images of films deposited by bar-coating a solution of *[3]ph3* and PS (1:1) in DCB with concentration of 20 mg/ml on a glass substrate at (a) 70°C and (b) 90 °C.

At 110 °C, the spherulites are bigger and wider with respect to what expected. This could be attributed to the fact that the working temperature is above the T_g of PS. Since polystyrene remains in a liquid viscous state during the formation of the crystals, the small molecules of *[3]ph* are more mobile and this compensate for the fast evaporation rate, which has an opposite effect.

For what concerns the bar speed, during the deposition-tests the films where deposited at three different velocities: 3 mm/s, 30 mm/s and 100 mm/s. It was observed that at high speed, the films always appear as non-homogeneous. Many morphologies were present on the same substrate, dividing it in different regions separated by marked solidification fronts. At low speed, instead, the bar dragged the solution leading to not fully covered regions. Moreover, the solidification was more susceptible to little changes in the external pressure. At intermediate speed, instead, the films were more reproducible. For this reason the transistors were fabricated at 30 mm/s.

4.1.6   Effect of gold and PFBT

During both the realization of transistors and the deposition-tests, bar-coating the solution of semiconducting blend at high temperatures a change in morphology and dimension of the crystals was observed depending on the type of substrate. When the films were deposited on glass, very large spherulite-like domains were formed with a compact and uniform lamellar structure. Their growth starts from a nucleation point from which the crystals expands radially in all the directions in form of lamellae, until grain boundaries are formed when the domains meet each other. Form SEM imagines it

was possible to notice the presence of segregations at the boundaries between spherulites, formed by small single crystals similar to those originated at low temperatures. These types of segregations were observed also inside each spherulite between the lamellae, which have probably a lower content of *[3]ph*, and at the nucleation point. The latest suggests either that these spherulite-like domains starts to growth from few single crystals formed during the first moments of the deposition, or that the segregation phenomena involve also the center. In the images, the black color of the inner parts of the lamellae suggest also that a given amount of PS is present, since this should lead to an accumulation of charges during the SEM measurements.

(a)   (b)
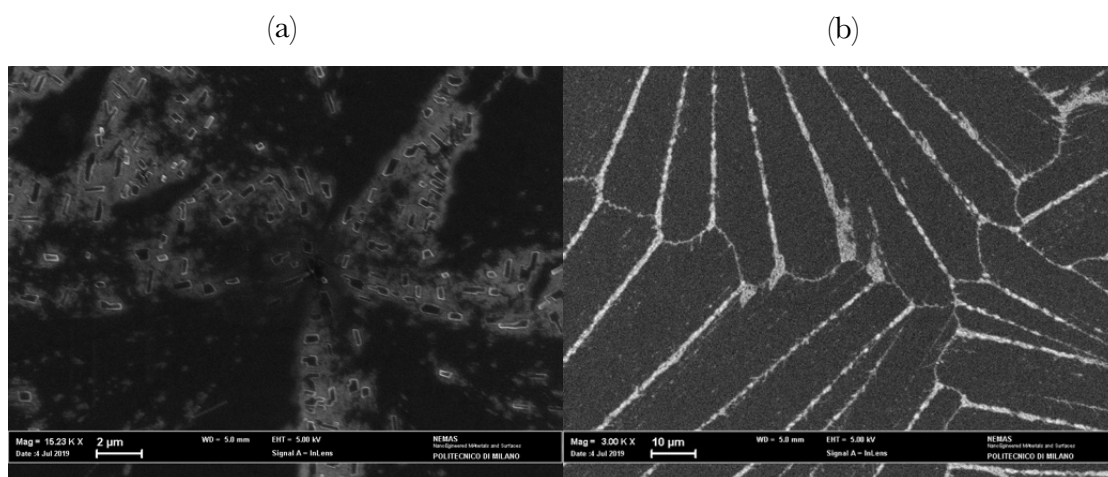
Figure 68. SEM images of spherulite-like domains on glass substrate obtained by bar-coating at 70°C. (a) Center of a spherulite. (b) Intersection between different domains.

(a)   (b)
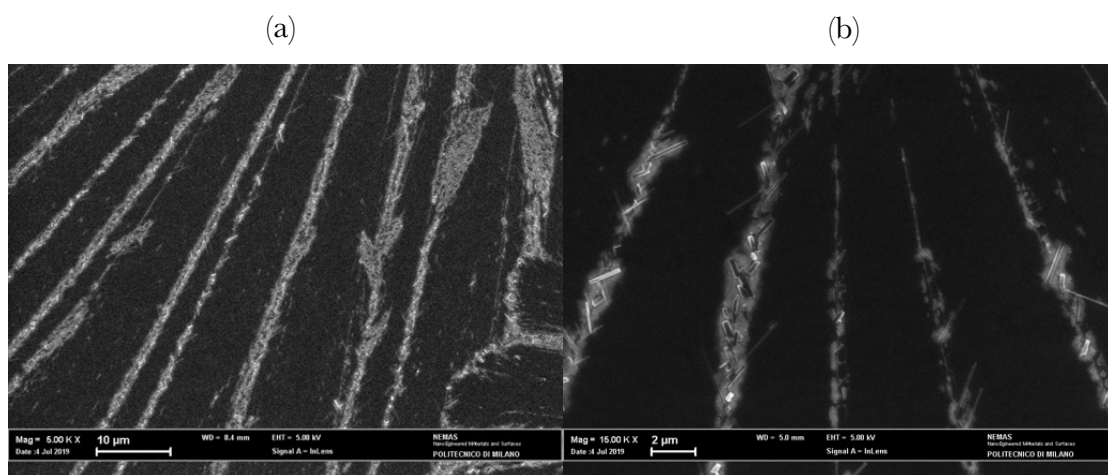
Figure 69. SEM images of lamellae of spherulite-like domains on glass substrate obtained by bar-coating at 70°C.

However, when there is gold on the substrate, the spherulites are much smaller all around the metal. This is due to the change of surface energy from glass to gold, which favors the nucleation of the domains. In Fig.70(a) and (b) it is possible to notice that the

nucleation points of the spherulites close to the metal are always located on the gold-glass interface. For this reason, when an interdigitated pattern is created, the spherulites all around the contacts will be smaller, since many crystals start to nucleate leaving little space for their growth.

(a)   (b)
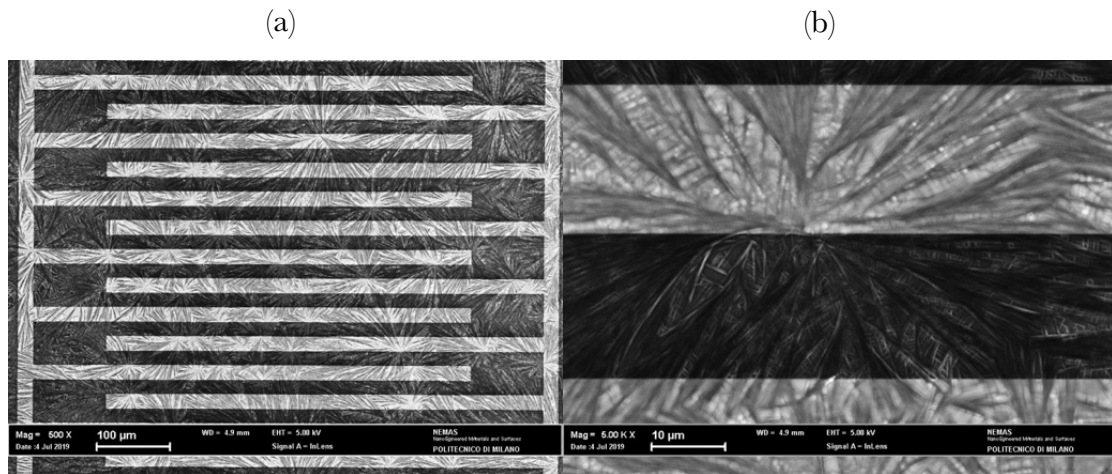
Figure 70. SEM images of a film made of spherulites deposited at 80 °C on prefabricated BGBC transistors, with also application of PFBT.

The role of plasma treatment was also considered, since it is able to change the surface energy of the substrate, but no relevant difference in the shape and dimension of the crystals was observed.

During the realization of the transistors, it was noticed that it is very difficult, if not impossible, to obtain lamellar-spherulites, as the ones formed during the deposition-tests, apart for regions far from the contacts. The generated domains can still be called spherulites because of the Maltese cross, but the structure is completely different. They have fibrillar structure and seem to be formed by branched fibers that growth radially. This effect cannot be attributed to gold, but is probably caused by the presence of PFBT. It is well known that the presence of a SAM affects the growth of the film, determining the final morphology. For example, it was shown that a film made of pentacene can change the structure from a flat lamella-spherulite one to rod-like small grains, when on gold or copper contacts a thiol-based SAM is applied (41). In Fig.71 the change in structure of spherulites is shown. As it is possible to see, only on gold treated with PFBT the spherulites have a fibrillar structure, while on glass and on gold without PFBT they have a lamellar shape.

(a) – (d)   (b) – (e)   (c) – (f)
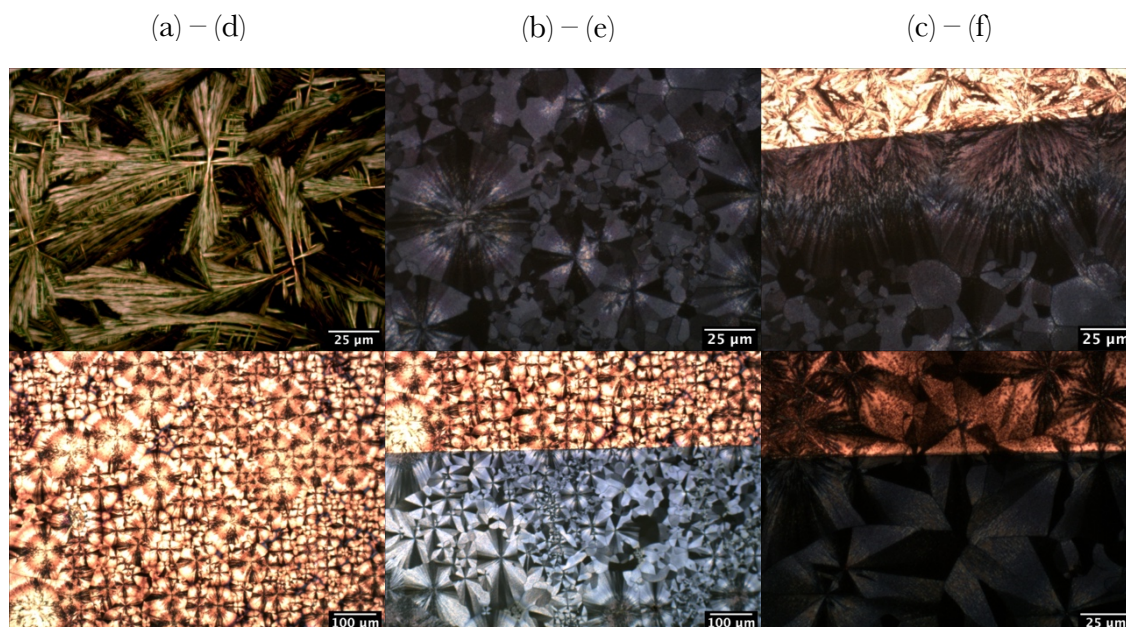
Figure 71. Optical polarized images of two films made of spherulites deposited at 80°C on glass substrates with gold patterns: (a), (b) and (c) with PFBT, (d), (e) and (f) without PFBT. (a) and (d) Spherulites on gold, (b) and (e) spherulites on glass. (c) and (f) Interface between gold and glass.

4.1.7   Film characterization

As seen before, bar-coating a solution of *[3]ph* and PS (1:1) in DCB with concentration of 20 mg/ml, three types of films were obtained, with a completely different morphology:

1. Single crystals at low temperatures.
2. Oriented fibres (with a dendritic or rod-like structure) at medium temperatures.
3. Spherulite-like crystals (with a fibrillar or lamellar structure) at high temperatures.

Even if sometimes there are variations, it is convenient to group all of the morphologies in these three main categories. In the first case, as said many times, the deposit is highly non-uniform and characterized by a low coverage that varies between $5 - 15\%$, depending if some fibers are formed along with single crystals. Also, the reproducibility is very low, since the disposition of the crystals in the film is completely random. An example of surface profile for a film produced at 40°C is shown in Fig.72(b). As it is possible to see, there are strong variations in the profile probably due to the presence of

some fibers. Then, in correspondence of single crystals, there are abrupt flat peaks of hundreds of nm. In the example the height measured is around 600 nm while the width about ~1 μm. The shape of the peak indicate a well regular geometry.
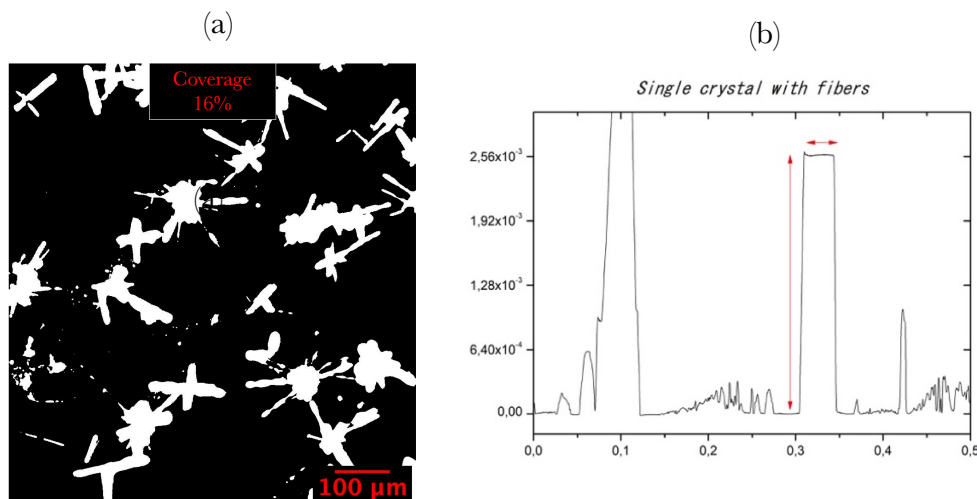
Figure 72. (a) Coverage estimation for a film made of single crystals deposited at 30°C. (b) Surface profile obtained by mechanical profilometer of a film deposited at 40°C made of single crystals with some fibers.

Looking at the profile, it seems that the crystals lie on top of a film probably formed of polystyrene and, in some regions, by fibers of *[3]ph*. However, since the devices works also in BGBC configuration, the single crystals cannot be just disposed on top of the film, but penetrate inside PS reaching also the bottom surface. Form optical images no information can be deduced about the organization in depth. The film thickness cannot be measured due to the low uniformity in the surface profile.

In case of fibers, at the macroscale the films appear uniform and compact with a relative good level of coverage, around 70 − 80%, even if sometimes it can be less than 50% when long rod-like fibers are formed. The level of directionally can change depending of the particular type of crystals. The films produced in this way are also reproducible.
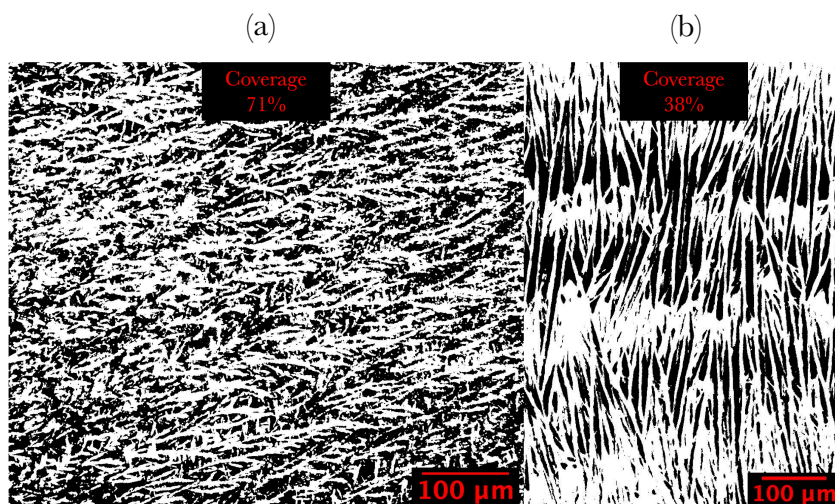
Figure 73. Estimation of coverage of a film made of fibers. (a) Dendritic (b) Rod-like.

However, at the microscale, analyzing the surface profile with the mechanical profilometer, it was easily noticed a high level of discontinuity in the thickness, related to a high of surface roughness. There are abrupt changes of hundreds of nm, which could be an indication of the fiber thickness. Different from the single crystals, the peaks have a non-uniform shape with many humps and tails, probably related to the presences of branches. From these results and from SEM images, we can speculate that the film could be constituted by a three dimensional network of fibers superimposed along the vertical direction, with PS present in the spacing between them. In Fig.74(b) it is possible to see layers of fibers disposed at different depths, making a communication between top and bottom surface possible.
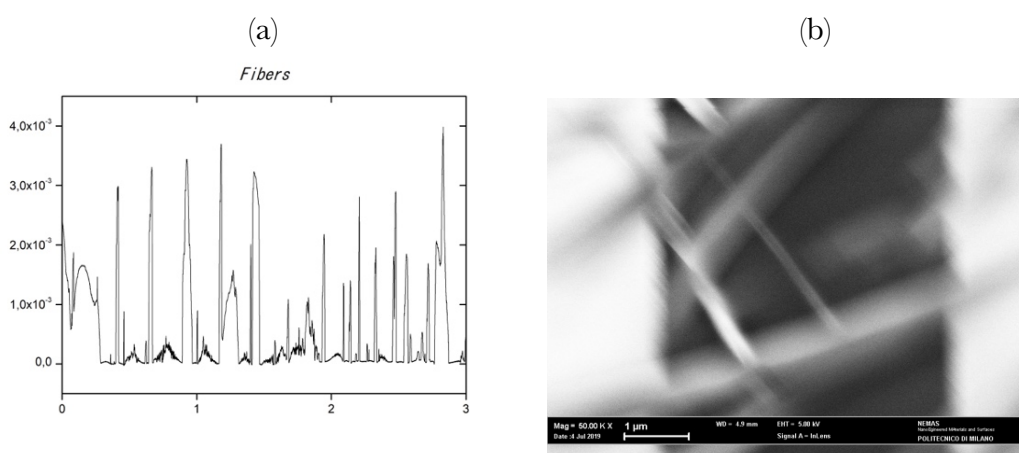
Figure 74. (a) Surface profile obtained by mechanical profilometer of a film deposited at 50°C made of fibers. (b) SEM image of a film deposited at 60°C made of dendritic fibers.

In the case of spherulites, the films appear uniform both at both the macro and microscale. Looking at Fig.75(a) and (b), it is possible to notice that the surface profile is

103

much more flat than in case of fibers (the spikes are attributable to external noise). This indicates a low level of roughness, ideal when another material is deposited on top. The film thickness can be easily measured doing a scratch. Usually it is in the order of 100 nm with little variations of 20 nm. The values corresponding to the figures below are equal to (a) 140 and (b) 120 nm. This type of deposit is also the most reproducible one and is characterized by the highest level of coverage, around 90%. In Fig.76(a) and (b) there is an estimation of coverage but it is not precise due to the fact that many regions of the spherulites appear dark even if there is material, due to the presence of the Maltese cross.
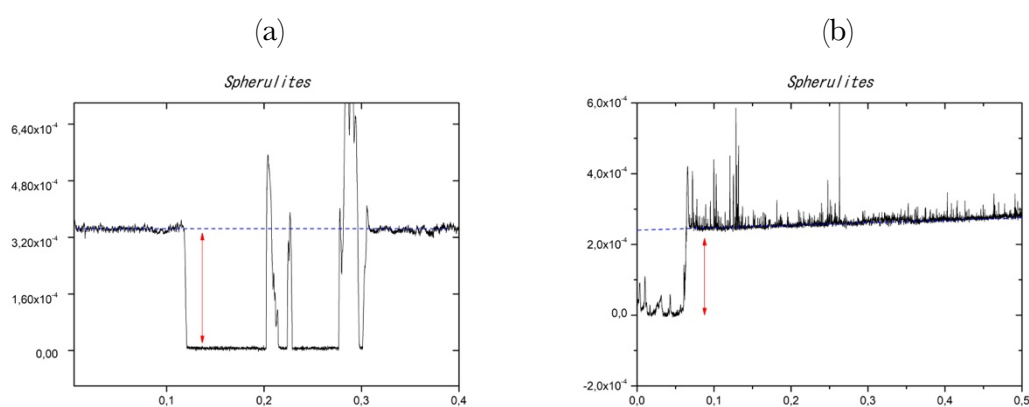
Figure 75. Surface profile obtained by mechanical profilometer of a film deposited at (a) 70°C and (b) 90°C made of spherulites.
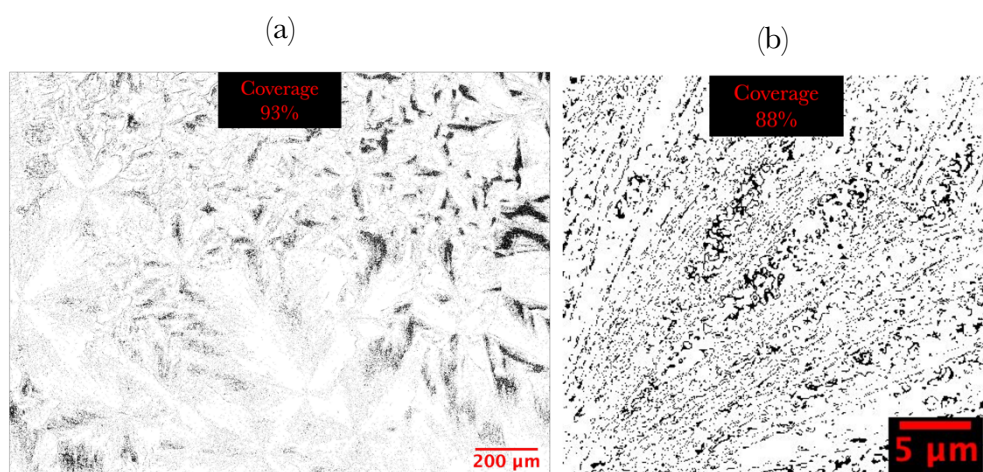
Figure 76. Estimation of coverage of: (a) a film made of spherulites, (b) a portion of a single spherulite formed by many lamellae.

In case of spherulites, it is more difficult to make a hypothesis on the film structure along the vertical direction. Since the devices works both in BGBC and TGTC configurations, there must be a layer rich of semiconductor at both interfaces. One possibility could be

a vertical stratification in three regions: two formed of spherulites (top and bottom surface) and one intermediate constituted mainly of PS. Another possibility could be the presence of a single uniform layer of spherulites, where the polymer is present in a given amount inside each semi-crystalline domain.

To have a better idea of the film structure, a compositional analysis should be done for all the types of morphologies. In Fig.75 a comparison between the Raman spectrum of three samples is presented: *[3]ph* deposited by drop-casting in DCM on a silicon substrate, a film formed of fibres made of *[3]ph* and PS deposited by drop-casting in toluene on glass, and a film formed of spherulites made of *[3]ph* and PS deposited by bar-coating at 70°C in DCB on glass. As it is possible to see, in case of spherulites, a high peak corresponding to *sp* carbon is detected, indicating the presence of cumulene molecules at the top surface. However, also a broad band in the sp^2 region is revealed, probably related to both the phenyl rings of *[3]ph* and the presence of amorphous polystyrene. This supports the idea that the film could be formed of just a single layer with both materials, without a proper stratification, and that the spherulites are semi-crystalline domains with a given content of a-PS. The sample in toluene does not show a broad band attributable to a-PS. This probably because in that case the film was constituted by a compact network of fibres at the surface, while the polymer is present in little amount in the spacing between them and probably below. The measure also confirms that fibres are only formed by cumulene molecules.
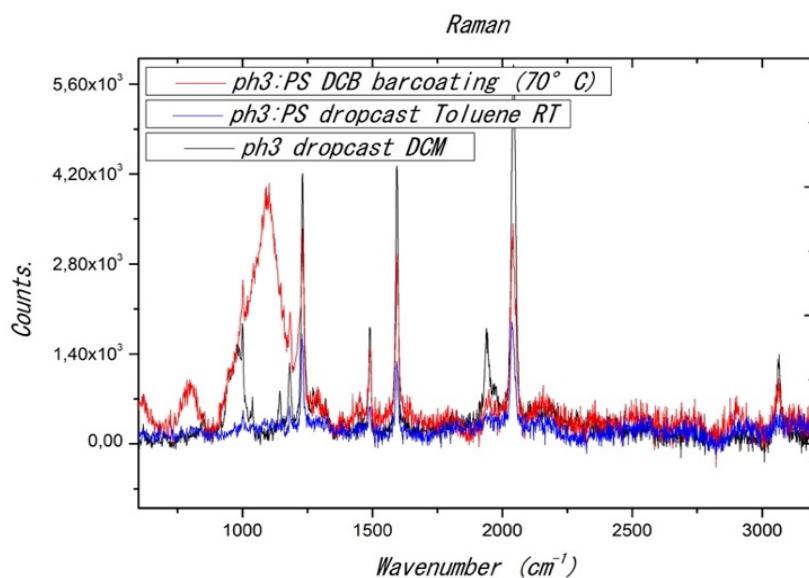
Figure 77. Raman measurements of: *[3]ph* deposited by drop-casting in DCM on a silicon substrate, a film made of *[3]ph* and PS deposited by drop-casting in toluene on glass formed of fibers, and a film made of *[3]ph* and PS deposited by bar-coating at 70°C in DCB on glass formed of spherulites.

To make a comparison between the degree of crystallinity of different structures, X-ray diffraction measurements were performed on bar-coated films at different temperatures. However, since the measurements were very noisy and just one peak was detected, no information was derived from these results.

UV-vis spectroscopy was carried out on samples produced bar-coating a solution of *[3]ph* and PS in DCB (1:1) with concentration 20 mg/ml on glass substrates at three different temperatures: 50°C, 70°C and 90°C with velocity equal to 30 mm/s. At 50°C, the film was formed of single crystals and fibres, while at 70 and 90°C of spherulites. Form Fig.78(a) and (b) it is possible notice that the main peak of absorption is always split in two sub-peaks. This is easily seen at high temperatures where the two peaks are well defined, while at 50°C they are not distinguishable anymore. However, fitting the plot with two gaussian functions in correspondence of the two peaks, it is possible to see that the absorption band can be always well decomposed in two mini-bands with a good precision, also at low temperatures. From the fitting, the two peaks have a λ_{max} of 404 nm and 450 nm, while the onset of absorption is around at $\sim 450 - 460$ nm for peak one and at 490 nm for peak two.

(a)   (b)
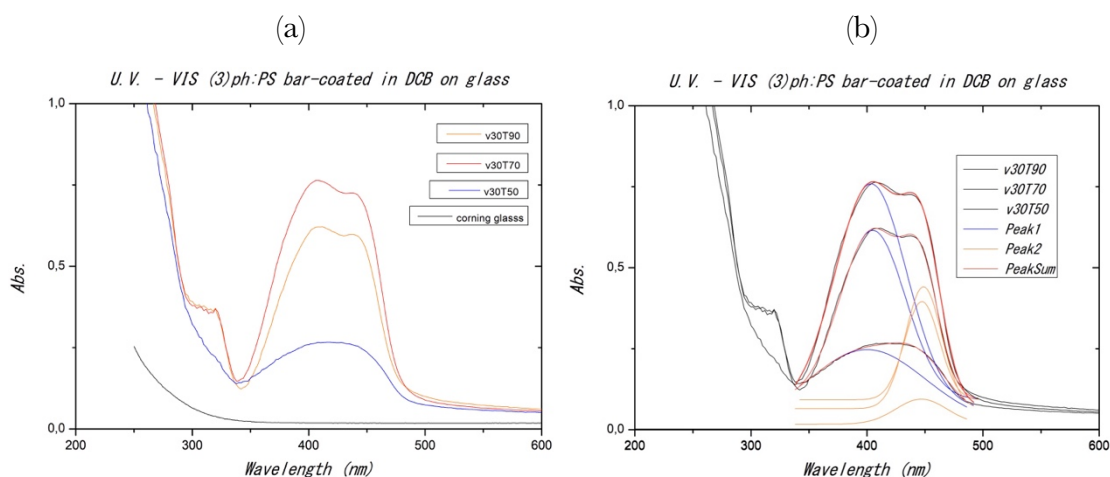
Figure 78. (a) UV-vis spectra of films bar-coated at 50, 70 and 90°C. (b) Fitting of the main absorption band with two gaussian functions.

In Fig.79 (a) and (b) the spectrum in solution of *[3]ph* drop-casted in DCM at concentration 4 mg/ml and a comparison with the one of a film bar-coated at 70°C is shown.

(a)   (b)
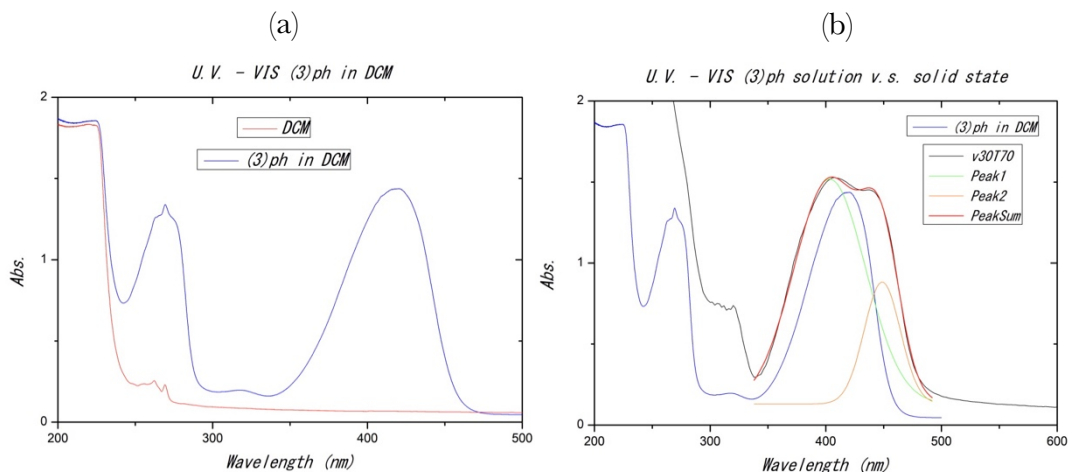
Figure 79. (a) UV-vis spectra of *[3]ph* in DCM (b) Comparison between the spectrum in solution and in the solid state.

The main peak in solution is at 420 nm, while the onset of absorption around ∼ 455 nm. From these data it is clear that the first peak of the band observed in films is attributable to the main peak related to the isolated molecule. In energy, the two values are 2,72 eV for the spectrum in solution and 2,75 − 2,69 eV for the ones in the solid state. These values correspond to the bad gap of *[3]ph*, as said in section 3.1. The second peak is red-shifted at lower energies and it corresponds to 2,5 eV. The origin of this peak can be attributed to solid state interactions among molecules that form different types of aggregates such as dimers and trimers. In exciton theory, aggregates associated to a shift to longer wavelengths are called J − aggregates. They are formed of a certain number of parallel molecules stacked in a tail-to-tail arrangement. However, to be sure of this conclusion, theoretical simulations of the molecular orbitals related to the aggregate should be done.

4.2 Charge transfer simulation by SERS

To model charge transfer phenomena between a metal and *[3]ph* molecules, SERS measurements were performed in the solid state, depositing a solution of semiconductor

on an active substrate. In Fig.80 a comparison between SERS and Raman spectra of two samples prepared by drop-casting a solution of *[3]ph* 4 mg/ml in DCM on silicon and on a prefabricated nanostructured silver substrate, is shown. The two spectra are very similar concerning the shape of the peaks. However, the intensity changes a lot, showing an enhancement of $\sim 10^2$ in the case of silver, which is a clear indication of SERS effect.
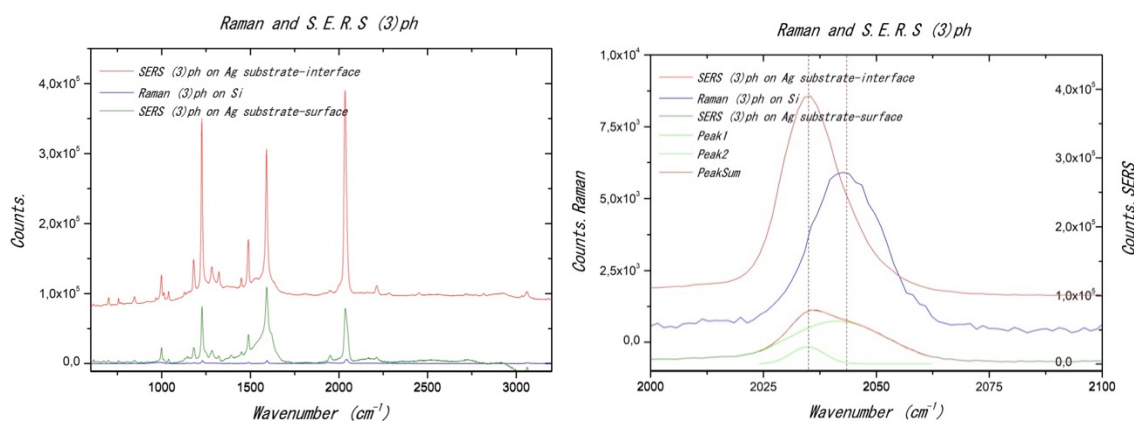
Figure 80. Raman and SERS spectra of two samples deposited by drop-casting a solution of *[3]ph* with concentration 4 mg/ml in DCM on silicon and on a prefabricated nanostructured silver substrate.

The red and green spectra in both figures are related to SERS measurements but with a different focus. In the first case, we focused on the silver surface in order to probe the material present at the interface, which is also the one that should interact more with the noble metal. In the second case, we focused on the top surface of the deposit, where there is less probability of interaction. As expected, the enhancement changes, passing from 10 to 100. Looking at Fig77(b), it is possible to observe for the red spectrum a shift of the *sp* carbon peak at lower wave numbers with respect to the blue spectrum that corresponds to the Raman measurement. The shift is about 10 cm^{-1}. It is not so marked but high enough to be relevant. In the green spectrum it seems that the peak at 2000 cm^{-1} is split in two due to the presence of a marked hump. Fitting with two gaussian functions, which are better than the Lorentzian for solid crystals according to Raman theory, it is possible decompose the band in two peaks with good approximation. The centre of the peaks correspond with good agreement to the ones of the red and blue spectra, confirming that the shift is not an artefact. The presence of both peaks in the

green spectrum is not so strange since we are focusing a portion of material less interacting with the metal.

Regarding the other regions of the spectra, there is no particular difference between SERS and Raman. Some peaks are slightly shifted to both lower and higher wave numbers, but the shift it too small to be reliable. Some other signals, instead, remain exactly in the same position.

From the results obtained it seems that, due to charge transfer phenomena, as illustrated in section 1.2, the molecule of *[3]ph* stabilizes the excess of charge with a molecular distortion that leads a lower value of BLA. Hence, the charged molecule should tend to a more equalized structure, concerning the main chain. However, in the main chain of *[3]ph* there are just two *sp* carbon atoms, separated by one bond. For this reason, it is more difficult to define the concept of BLA as bond length alternation between adjacent bonds, unless also the two atoms at the extremities, which are hybridized sp^2, are considered. For this reason, the peak at 2000 cm^{-1} cannot be properly attributed to a collective BLA oscillation between only *sp* carbons, since also the sp^2 carbon must be included to define the BLA. We could consider in first approximation that the peak at 2000 cm^{-1} is related to a simple stretching mode between the two *sp* carbons present in the molecule; however, also in this case Raman theory claims that a shift to lower wave number corresponds to an higher value of bond length, indicating that the chain tends to a more cumulene-like configuration.

From theoretical calculations performed, charging the molecule, the BLA value and the bond length of middle bond should increase and decrease respectively, indicating a more alternated structure.
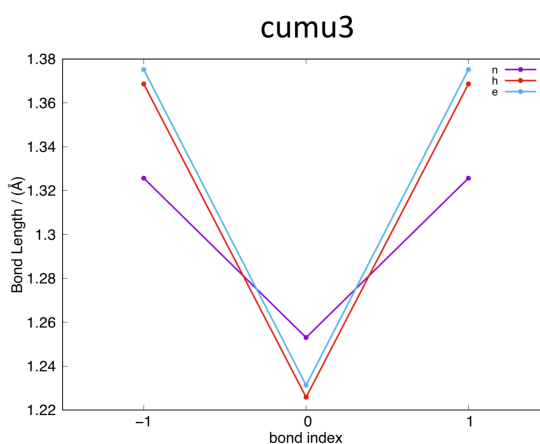
Figure 81. Variation on bond length simulated along the chain of *[3]ph* for the neutral, negatively and positively charged molecule.

To have a better understanding of how the molecule deforms upon charge transfer from Raman measurements, a simulation of each normal modes of *[3]ph* should be done, to do a better peak assignment.

4.3 Electrical measurements and parameter extraction

For each electrical device the transfer characteristic was measured both in linear and saturation regime. From the shape of the curve it is possible recognize some non idealities such as: presence of an hysteresis cycle, false or dual switching, high current leakages, voltage instabilities, long switching rate, etc. Some electrical parameters were extracted from these data using the Schottky equations, which is a common way to describe a transistor. In particular, these parameters were extracted from the transfers curves:

1. **Field − effect mobility** in saturation and linear regime ($\mu_{sat.}$ and $\mu_{lin.}$). The formula used for the calculations were the following:

$$\mu_{lin.} = \frac{L}{WCV_{D\ lin.}} \left| \frac{\partial |I_{D\ lin.}|}{\partial V_G} \right|$$

$$\mu_{sat.} = \frac{2L}{WC} \left(\frac{\partial \sqrt{|I_{D\ sat.}|}}{\partial V_G} \right)^2$$

2. **Threshold voltage** in saturation and linear regime ($V_{T\ lin.}$ and $V_{T\ sat.}$). $V_{T\ lin.}$ was calculated linearly fitting the drain current as a function of gate voltage, while for the saturation regime, by fitting the square root of the drain current as a function of gate bias. The intersection with the voltage axis give us an indication of V_T. For the linear regime, also the transconductance change

method (TC) has been used. In this case, V_T is given by the peak in a plot of the second derivative of I_D with respect to V_G as a function of the gate bias.

3. **ON/OFF ratio**. It is simply estimated as the ratio between the OFF and ON currents.

4. **Subthreshold swing** (**SS**). It is calculated plotting the logarithm of I_D as a function of V_G in linear regime. In the subthreshold region, a linear fit is performed and, by estimating the reciprocal value of the maximum slope of the curve, SS is extracted.

5. **Reliability Factor** (**r**) in saturation and linear regime. It was calculated to estimate the device ideality and quality of the of field-effect mobilities extracted. It was estimated with the following formula:

$$r_{sat.} = \left(\frac{\sqrt{|I_{D\,max.}|} - \sqrt{|I_{D\,(V_T)}|}}{|V_{G\,max.} - V_{Tsat.}|} \right)^2 \Bigg/ \left(\frac{WC}{2L} \mu_{sat.} \right)$$

$$r_{lin.} = \left(\frac{|I_{D\,max.}| - |I_{D\,(V_T)}|}{|V_{G\,max.} - V_{Tlin.}|} \right) \Bigg/ \left(\frac{WCV_{D\,lin.}}{L} \mu_{lin.} \right)$$

Output characteristics have been used to get a qualitative estimation of the contact resistance. This can be done by looking at the shape of the $I_D - V_D$ curve. If the contact is Ohmic and the contact resistance is low, the curve in the linear regime should resemble a straight line. However, if the contact resistance is high, the shape at low voltages changes, from a straight line to an S-like shape.

4.3.1   BGBC configuration

At the beginning some transistor was realized by drop-casting a solution of *[3]ph* in DCM 4 mg/ml. Then, after the work done to improve film properties, all the other devices were fabricated by bar-coating a solution of *[3]ph* and PS (1:1) in DCB 20 mg/ml.

4.3.1.1   Analysis of the transfer and output curve

In Fig.82, the transfer characteristics of BGBC transistors deposited in two different conditions are shown. The blue and green curves correspond to linear and saturation regime. Fig.82(a) is related to a drop-cast of only *[3]ph* in DCM at room temperature, while Fig.82(b) is related to a device produced bar-coating *[3]ph* with polystyrene at high temperatures. As it is possible to notice, without PS, the curve presents different negative features such as: a marked hysteresis cycle at low voltages, slow switching speed, high leakage current and low ON/OFF ratio, which is in the order of 10^5. When PS in added and the film is deposited at temperatures that allow to obtain an uniform film $(50 - 110°C)$, the shape of the curve is more ideal and the hysteresis is reduced. Moreover, there is an abrupt change in the current as soon as the device is turned on, indicating a high switching speed. The leakage current is reduced with respect to the drain current, that now is increased of two orders of magnitude, reaching values around $1\ \mu A$ in linear and $10\ \mu A$ in saturation regime. The ON/OFF ratio is also improved, reaching $10^6 - 10^7$.
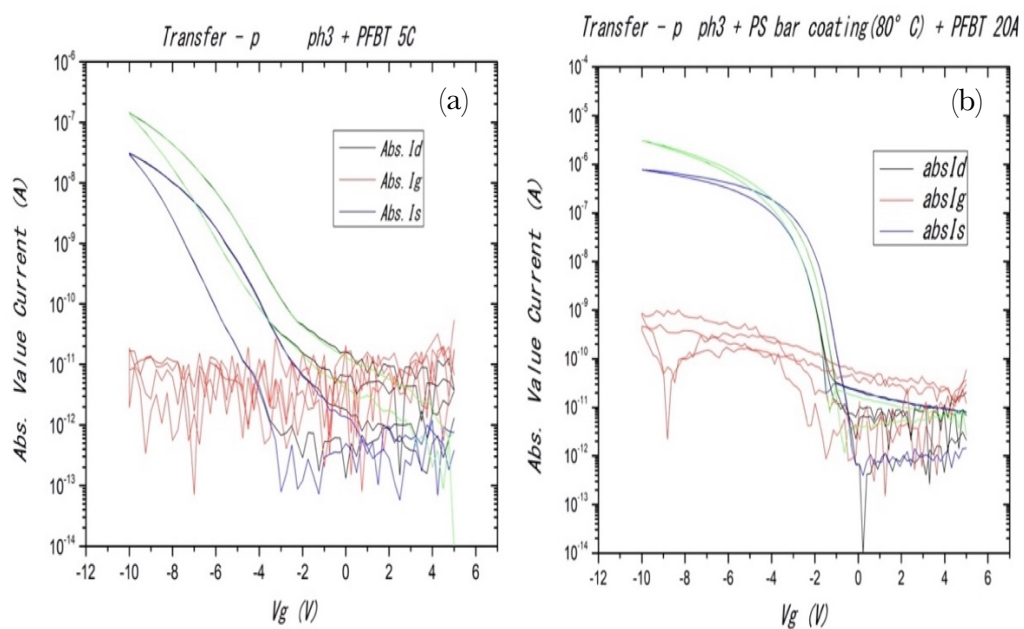
Figure 82. Transfer curves. (a) *[3]ph* deposited by drop-casting in DCM 4 mg/ml (b) *[3]ph* and PS bar-coated at 80°C in DCB 20 mg/ml.

These improvements are related to the formation a uniform crystalline deposit with good coverage with respect to a situation with just few randomly disposed single crystals. In fact, if the temperature of bar-coating is not sufficiently high, the curve is very similar to the one obtained by drop-casting without PS. The output curves, unlike the transfer ones, do not show a particular difference changing the processing parameters. A difference can be found comparing transistors with different channel length. In Fig.83(a) and (b) the output characteristics for two devices produced in the same conditions and different channel lengths, 2,5 and 20 μm, are presented. In the first case, the curves show some non idealities, for example there is no real saturation of drain current increasing the drain voltage. Moreover, the shape resembles an "S", which is an indication of high contact resistance. In the second case, usually the curves are ideal, with a well-defined plateau of the drain current in saturation regime and a linear dependence in the linear regime. The linear dependence of the output in the linear regime for high channel lengths is an indication that the device is no more contact − limited, because the contact resistance is no more the dominant term in the total resistance of the device.
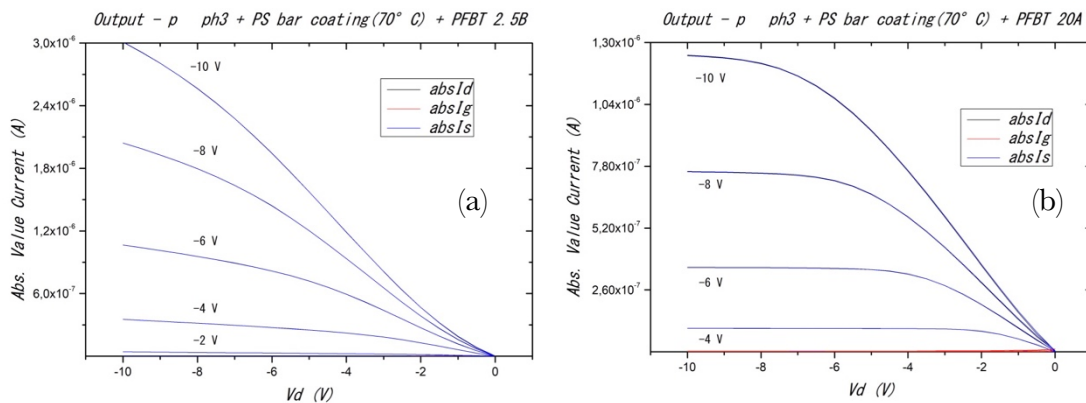
Figure 83. Output curves obtained bar-coating *[3]ph* and PS at 70°C in DCB 20 mg/ml.

4.3.1.2 Field − effect mobility

Field-effect mobility is a common parameter to define the performances of an OFET. It is an indication of how fast the induced charges move in the semiconducting channel. As the name said, it is not an intrinsic property of the material but rather a property of the transistor. For an ideal device, the values in linear and saturation regime should be

relatively close and not voltage dependent. Of course, while the transistor is switching-on the mobility increases with V_G, since the concentration of majority carriers is enhanced. A clear mark of non-ideality is a bias depended mobility that does not saturate rapidly. In Fig.84 a comparison between field-effect mobility of two devices is shown: (b) drop-casting of *[3]ph* in DCM at room temperature, (c) bar-coating of *[3]ph* with polystyrene at high temperatures.
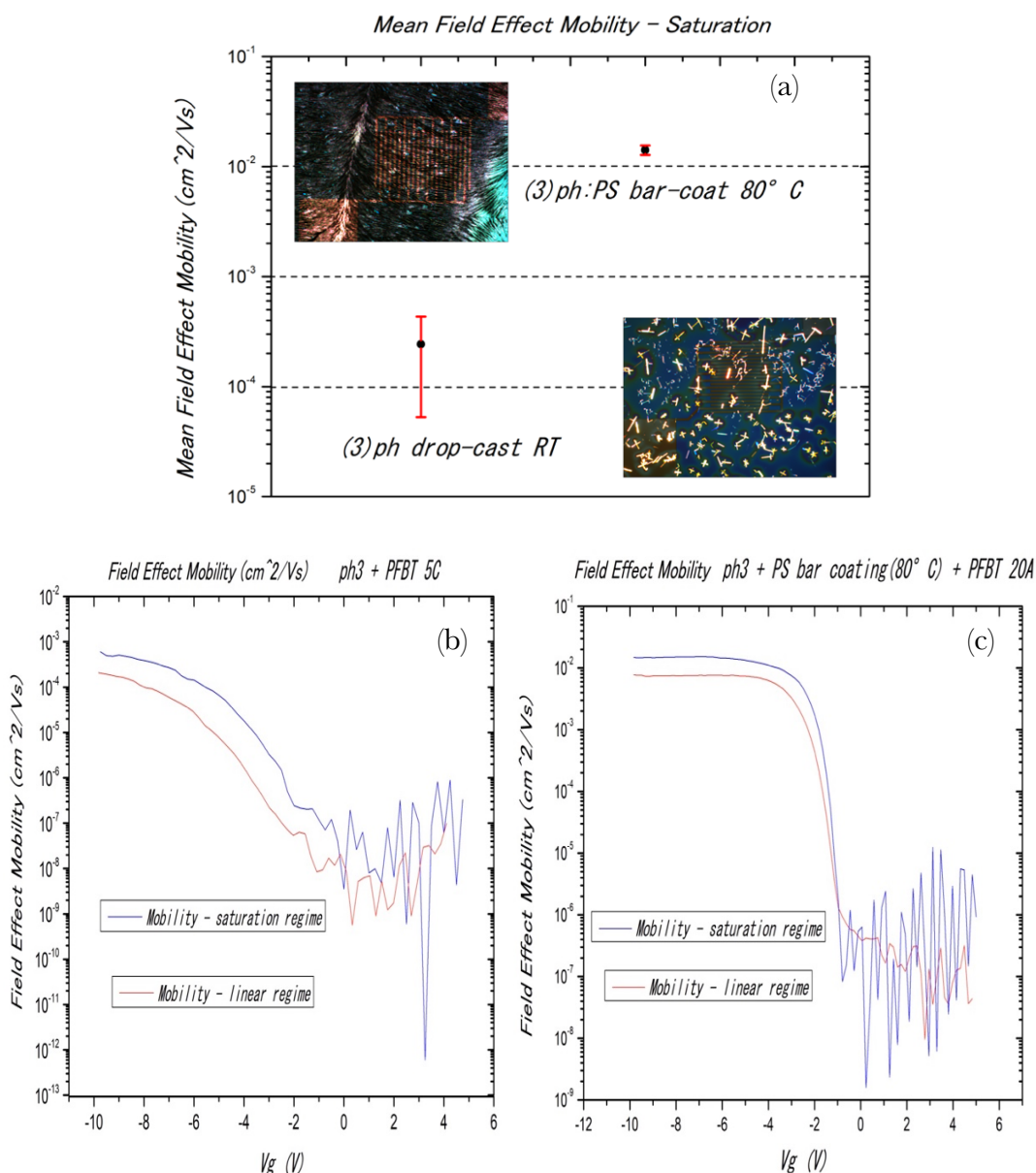
Figure 84. (a) comparison between field − effect mobility of two BGBC transistors with and without PS. (b) Field − effect mobility curve for (c) isolated single crystals deposited drop-casting a solution of *[3]ph* in DCM (b) a compact film deposited bar-coating a solution of *[3]ph* and PS in DCB.

As it is possible to see, in the first case the mobility never reaches a plateau but continuously increases, ranging from 10^{-6} to 10^{-4} cm²/Vs, making it difficult to estimate a single mobility value. Fig.84(a) shows the large range of variation with mean value around $3 \cdot 10^{-4}$ cm²/Vs.

In the second case, the mobility rapidly increases during the transistor turn-on and then remains almost constant, without a marked bias dependence. This is a clear indication of device ideality and that the extracted values are much more reliable. In Fig.84(a) it is possible to appreciate how narrow the range of variation is and how much the mobility it is increased with respect to the previous case. There is an improvement of at least two order of magnitudes, reaching values of $2 \cdot 10^{-2}$ cm²/Vs.

The difference in performances is related again to the film structure. In the first case, just few isolated crystals contribute to the electrical transport. Moreover, many of them are not fully in contact with the gold electrodes, because they overlap each other. For this reason, the active area is very limited. In the second case, thanks to the formation of a compact uniform film, the electrical properties are improved.

In Fig.85 the change in mean field − effect mobility in saturation regime with processing temperature, from 30°C up to 110°C for BGBC transistors produced bar-coating a solution of *[3]ph* and PS in DCB 20 mg/ml, is shown. Each value was estimated doing an average in a range of voltage higher than the threshold voltage. As it is possible to notice, there is a clear trend related to the change in film morphology. At low temperatures, below 50°C, the film is similar to a drop-cast with many isolated single crystals and limited coverage. As expected, the mobility is quite low ($10^{-5} \div 10^{-4}$ cm²/Vs) and highly voltage-dependent, meaning that the devices are not ideal and the values extracted not so reliable. At intermediate temperatures, the films starts to be uniform and compact with high level of coverage, mainly formed by dendritic fibres. The mobility increases of one order of magnitude, around 10^{-3} cm²/Vs, and it is no more be bias dependent, meaning that the devices are more ideal and the data obtained are reliable. At high temperatures, the films are highly uniform and mainly formed by spherulite-like crystalline domains. The mobility increases further of one order of magnitude, reaching values around 10^{-2} cm²/Vs. The values obtained have a narrow range of variation meaning that the mobility is constant and voltage independent. In this condition, the highest value of mobility obtained is equal to $3,5 \cdot 10^{-2}$ cm²/Vs.

A particular exception is represented by the case of long rod-like fibres. When they are formed, even if the coverage is much lower than spherulites, the values of mobility are always very high, around 10^{-2} cm²/Vs, if they are oriented orthogonally to the channel.
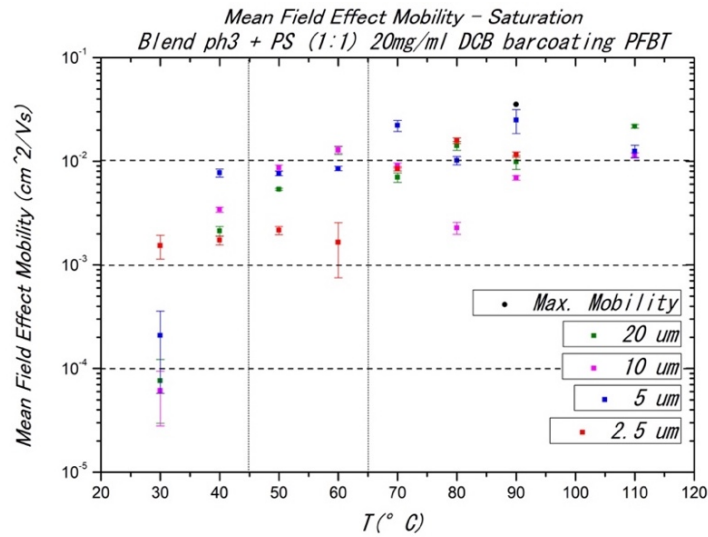
Figure 85. Saturation mean field – effect mobility as a function of processing temperature for BGBC transistors bar-coated in DCB 20 mg/ml.

Fig.86 shows the same concept with linear mobilities. The trend is the same but with lower mobility values, as expected for organic semiconductors.
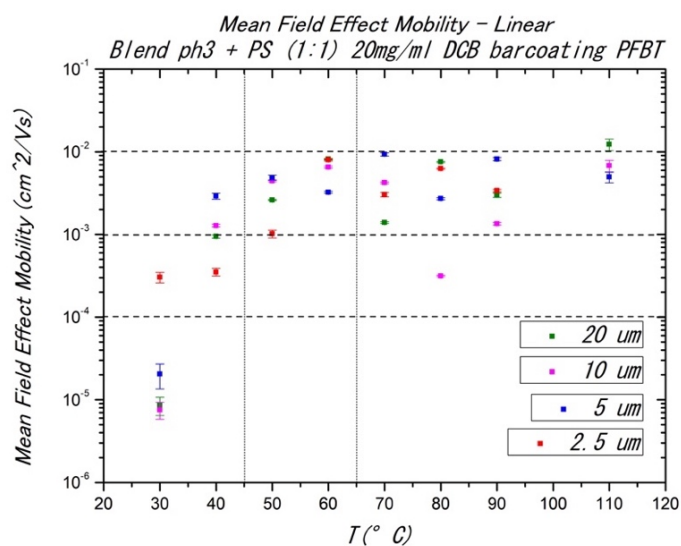
Figure 86. Linear mean field – effect mobility as a function of processing temperature for BGBC transistors bar-coated in DCB 20 mg/ml.

In Fig.87, the values of mean mobility in saturation are corrected taking into account the morphological coverage. In this way, the highest mobility value is equal to $5 \cdot 10^{-2}$ cm²/Vs. Since there are little variations, the percentages of coverages used are average values, equal to:

1. $10 - 20\%$ for single crystals (depending if some fibres are present).
2. 40% for rod-like fibres.
3. 70% for dendritic fibres.
4. 80% for fibrillar spherulites.
5. 90% for lamellar spherulites.

As it is possible to see, the values of mobility increase a lot at medium − high temperatures ($50 - 70°C$) where long highly oriented rod-like fibres are formed. Instead, in the case of dendritic fibbers and spherulites, there is a lower change. In the case of spherulites, the real coverage is not known since the electrically active area could be much less that the one expected, unlike for fibres for which the morphological and electrical coverage should coincide. Then, at low temperatures (<50°C), since the covered area is below 30%, the mobility increases a lot but these values are not so reliable because the device is not ideal.
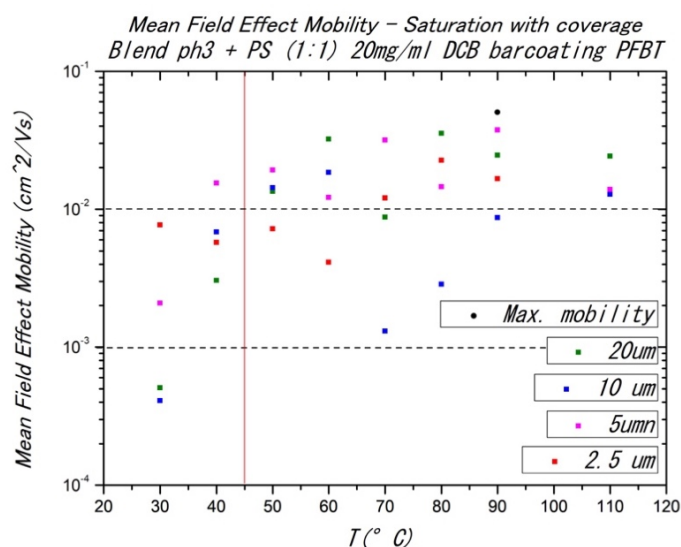
Figure 87. Values of saturation mean field − effect mobility corrected with the morphological coverage.

4.3.1.3   Threshold   voltage   and

subthreshold swing.

The threshold voltage is an indication of the value of V_G that needs to be applied to either turn-on or off the device. In our case, due to the presence of a marked hysteresis cycle, there is always a shift of V_T to higher negative values between forward and backward sweeps, as expected for a lower BCS hysteresis. The shift depends on the magnitude of the hysteresis. For small hysteresis, it is usually around 1V, while for large hysteresis it can go up to 3V. This can be easily seen using the transconductance change method as shown in Fig.88(a) and (b).

(a)   (b)
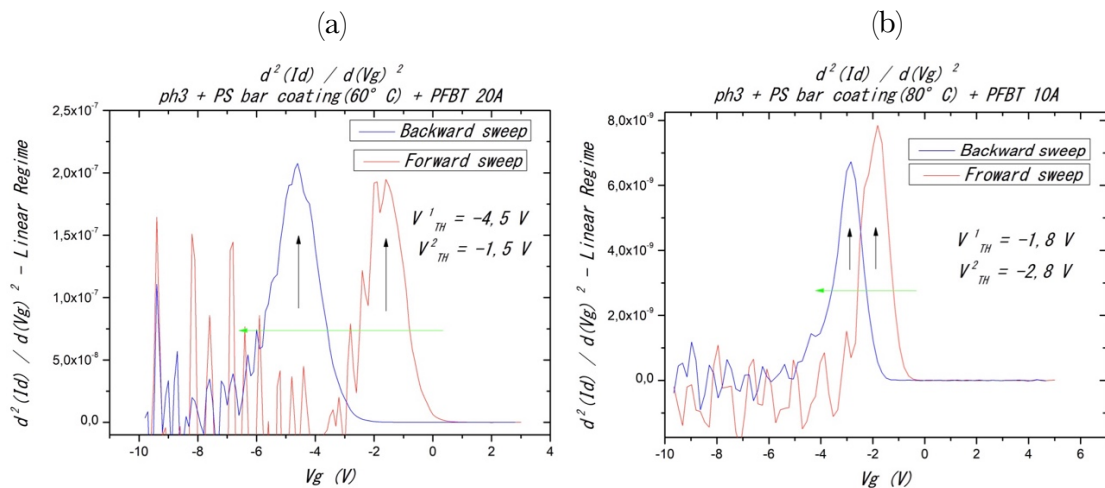
Figure 88. Threshold voltage extraction in linear regime with transconductance change method.

This means that the device will never turn-off at the same voltage needed to turn it on. To have an idea of the voltage needed to switch-on the transistors, V_T was always calculated from the forward sweep. Doing a linear fitting, as shown in Fig.89(a) and (b), it was found that V_T ranges from -1,5 V to -3,5 V for both linear and saturation regime. For the greatest part of the devices it is close to -2 V.
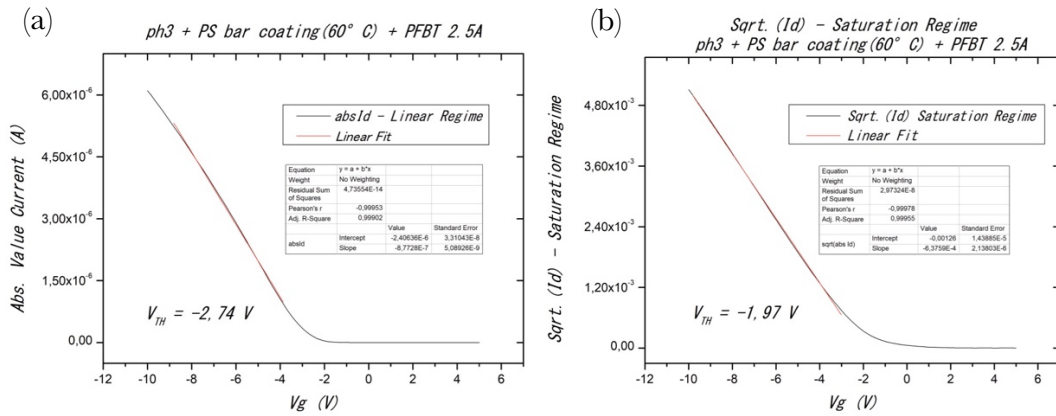
Figure 89. Threshold voltage extraction in linear (a) and saturation (b) regime.

The subthreshold slope is defined as the increase of drain current per decade of voltage in the of subthreshold region, just below V_T, where ideally I_D should be linearly dependent with respect to the gate voltage. Its reciprocal is called subthreshold swing (SS) and is measured in V/dec. It is an indication of how fast the transistor goes from the OFF to the ON sate. It is a very important parameter to qualify the performance of a FET. Usual values of SS for OFETs range from 5 to 1 V/dec. However, in the last years values below 1 V/dec have been reached. Best values of SS are in range of 0,9 – 0,1 V/dec and recently, the world record is equal to 0,064 V/dec, approaching the thermodynamic limit of 0,059 V/dec (48). In our case, the values of SS range between 0,6 – 0,4 V/dec, with the best performing devices showing values around 0,2 and 0,1 V/dec. In particular, the best value of subthreshold swing obtained is 115 mV/dec.
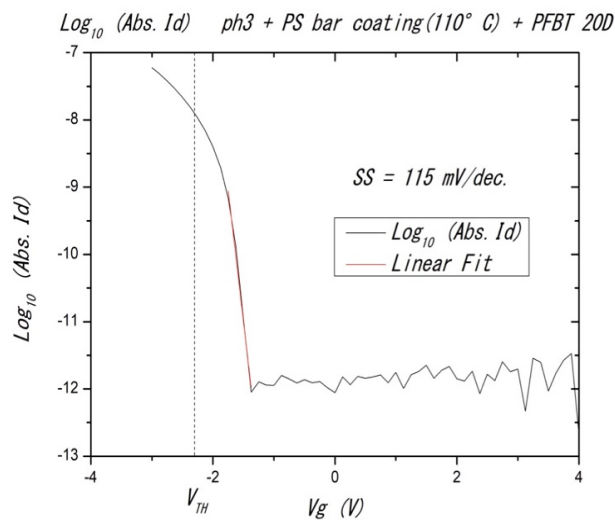
Figure 90. Extrapolation of SS in linear regime.

The transistors fabricated in this thesis are thus characterized by a very steep sub-threshold slope, even if the values of mobility are not particularly high.

4.3.1.4   Reliability factor and contact resistance

The reliability factor is very important to avoid a wrong estimation of device parameters since the use of the Schottky equations should be done carefully, keeping always in mind that they are based on some assumptions not always valid for organic semiconductors. Without a proper consideration of device ideality, there is the possibility of under or overestimate field effect mobility. This error is very common in literature.

The reliability factor was estimated both in linear and saturation regime. For transistors bar-coated at temperatures enough high to obtain a uniform compact film ($50 - 110°C$), the values of r are usually in a range of $60\% - 80\%$ in saturation and $70\% - 85\%$ in linear regime. This means that the devices behaviour is close to ideality (a perfect agreement with the Schottky model would give r equal to 100%) and that the estimated values of field-effect mobility are reliable. At low temperatures (below $50°C$), as also for transistors realized without PS by drop-casting, the values of r oscillate more depending on which value of mobility is considered for the calculation. For example, considering the maximum value of mobility, r is in the order of $10\% - 40\%$. This indicates that the values of mobility are overestimated and that the device is far from an ideal condition. Instead, if the mean values of mobility averaging in a voltage range above V_T, are considered the value of r increases indicating that we are doing a better estimation of the actual mobility.

The estimation of the contact resistance from the output curves with the common transmission line method (TLM) was not possible for the devices produced. This method consist in plotting the total resistance of a series of transistors having different channel lengths at the same value of gate voltage and doing a linear fit, the intercept should correspond to R_C. The problem arises because of the marked S-shape of output curves, especially when the channel length is lower than $10~\mu m$, making it difficult to have a good estimate of the total resistance. The only thing that can be reliably said is that, despite of the presence of PFBT, the contact resistance is often very high.
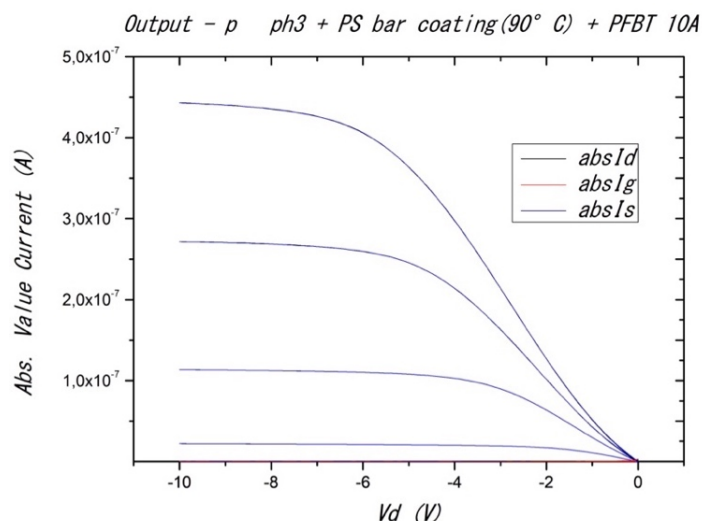
Figure 91. Output curves for a BGBC transistor bar-coated at 90°C with PFBT.

During the deposition-tests, it was noticed that PFBT changes the morphology of the film at high temperatures, from a spherulite-lamellar structure to a spherulite-fibrillar one. Because of this change, some transistors were fabricated also without PFBT at 70°C. Fig.92 shows an example of both transfer and output characteristics for devices bar-coated without SAM.
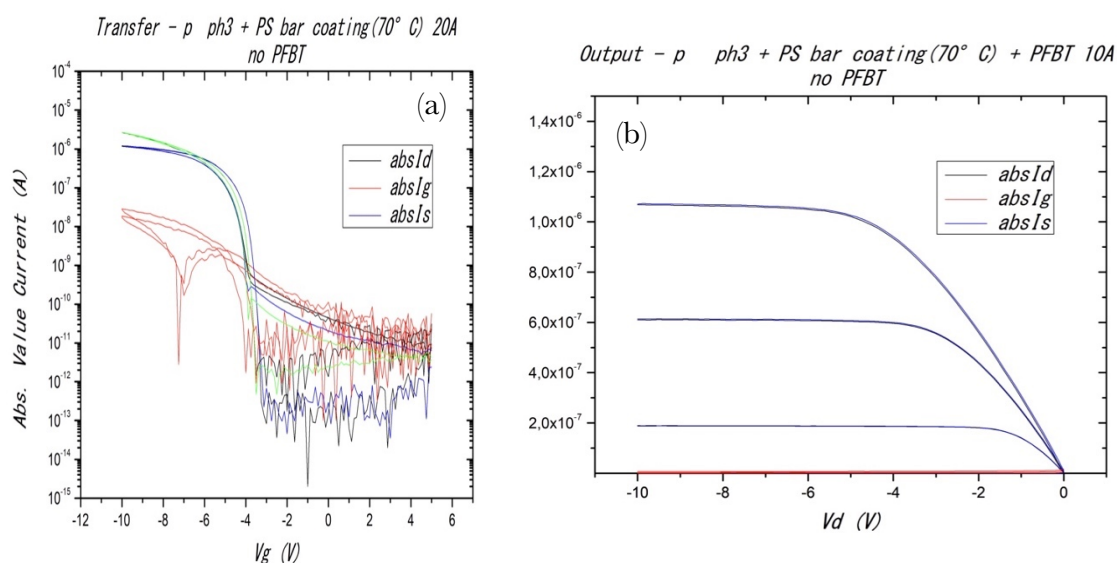
Figure 92. Transfer and output curves for a BGBC transistor bar-coated at 70°C without PFBT.

It is possible to notice that the transfer curve has all the positive features that also transistors with PFBT have. The mobilities related to the device, shown in Fig.90, are $1,5 \cdot 10^{-2}$ cm²/Vs and $9,2 \cdot 10^{-3}$ cm²/Vs, in saturation and linear regime respectively. Hence, the transistor works well even without the use of PFBT. From the output curve, surprisingly, it is possible to notice the absence of the S-shape also for low channel lengths. This means that the contact resistance is lower with respect to the case of devices with PFBT, even if the SAM should improve the injection. An explanation could be related to the change in crystalline structure. Probably, the lamellar structure have a facilitated injection with respect to the fibrillar one.

4.3.1.5 Hysteresis and instabilities

To prove the stability of the electrical devices, some tests were performed in vacuum, keeping the devices at a pressure of $7,7 \cdot 10^{-5}$ mbar overnight, and in air. In Fig.93 a comparison between transfer characteristics of the same transistor measured first in vacuum and then in air is shown.
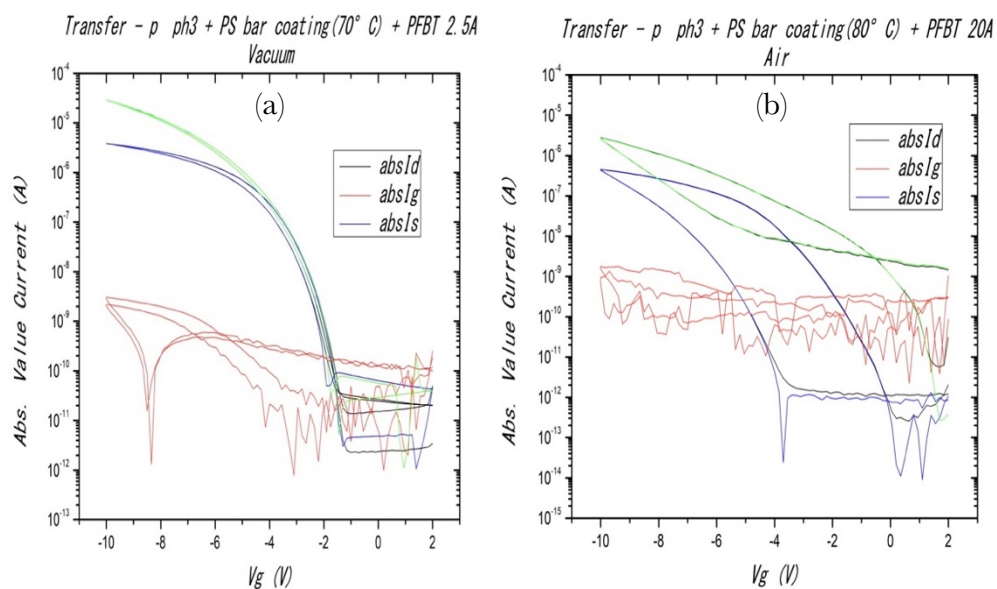
Figure 93. Transfer characteristics of BGBC transistors bar-coated at 70°C measured in (a) vacuum and (b) air.

As it is possible to see, before the exposure to the atmosphere the device is characterized by a reduced hysteresis with respect to the tests performed in glove-box, no threshold voltage instabilities and a high switching rate. The shape of the curve suggests good

device ideality. Then, during the test in air, the value of the drain current is reduced of one order of magnitude and the hysteresis becomes very large. This suggests that probably the origin of the hysteresis is related to some degradation phenomena or to the formation of charge traps while the device is working, due to oxygen and water present in the atmosphere.

To see if the stability of the blend is improved with respect to a film without PS, the same procedure was carried out on transistors containing only *[3]ph*. In this case, after the exposure in air, the devices stopped working or they showed much worse performances, as shown in Fig.94. This means that polystyrene is able to improve both the electrical performances and the stability of the transistors in air.
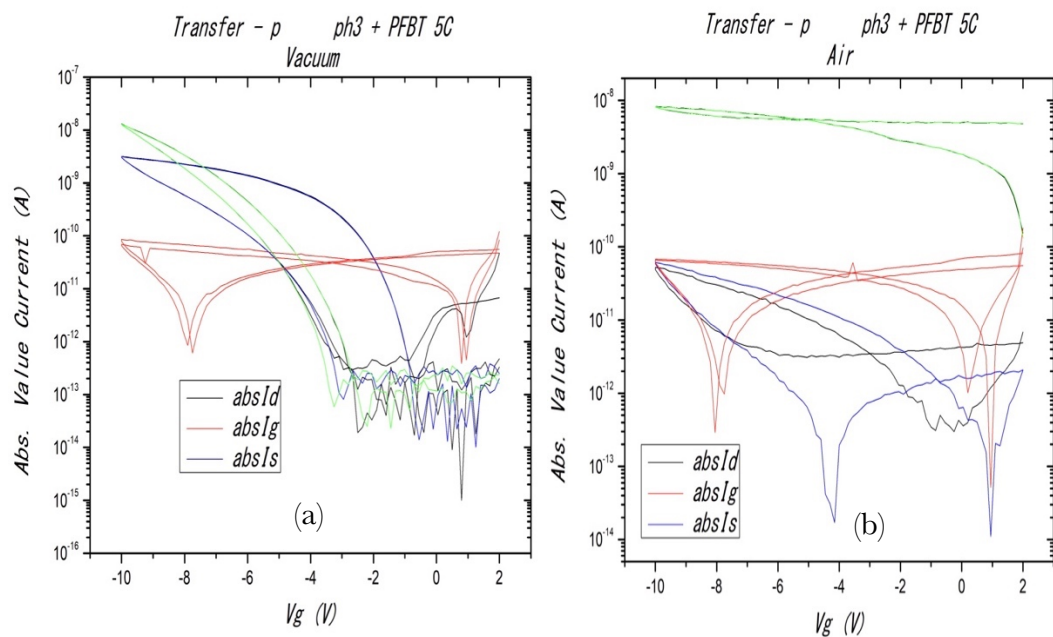
Figure 94. Transfer characteristics of BGBC transistors drop-casted without PS measured in (a) vacuum and (b) air.

4.3.2   TGBC configuration

At the end of this work an attempt in changing device configuration was done, from a BGBC architecture to a more promising TGBC one. Since the material is less exposed to the atmosphere, device stability and ideality should improve.

4.3.2.1   Analysis of the transfer and output curve

123

The transistors produced in TGBC architecture proved to work with also good performances, meaning that a layer rich of semiconductor is present at both surfaces. Moreover, since the conducting channel is still formed at the bottom interface, where the contacts are present, the induced carriers, created at the dielectric interface, must travel through the bulk to contribute to the drain-source current. This means that there can't be a net phase segregation, but at least the formation of gradients of the two materials in the film. In Fig.95, a comparison between transfer characteristics of two devices produced in the same conditions is shown. Fig.95(a) is related to a TGBC configuration, while Fig.95(b) to a BGBC one. As it is possible to see, the hysteresis is absent for TGBC devices in linear regime and this is because the thick layer of parylene acts as protection, limiting contaminations and a direct exposure toward oxygen and water. It sometimes happens that these devices show higher OFF current during the backward sweep; this can be explained considering that the accumulation takes place at the interface opposite to that of the contacts, and thus there is a bulk contribution to the drain current, which induces charges also far from the dielectric-semiconductor interface.

In some other cases, a small higher BSC hysteresis is formed, opposite to the case of BGBC devices, both in linear and saturation regimes. This could be due to charge injection from the gate into the dielectric, as explained in section 2.3.
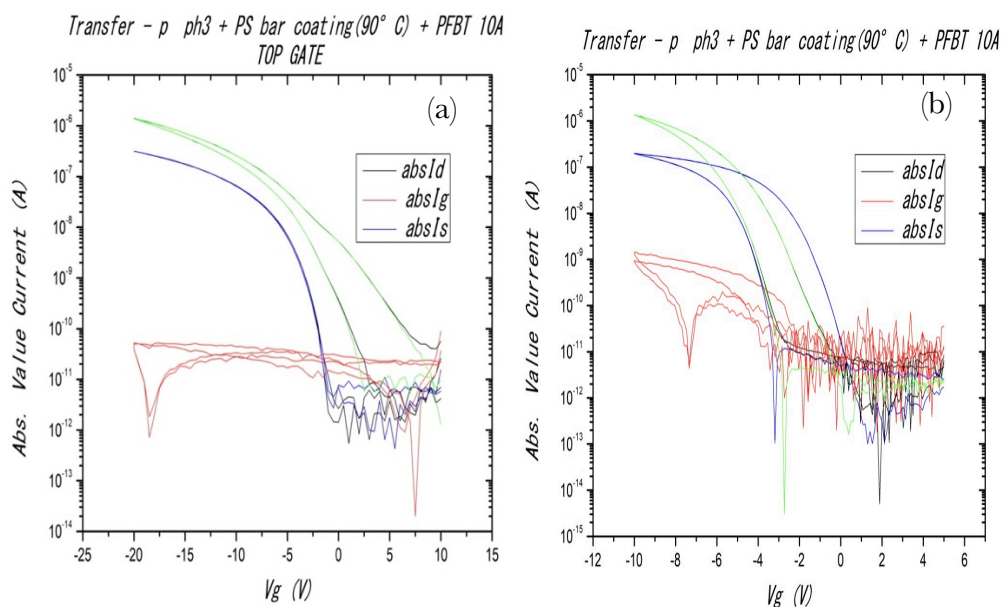
Figure 95. Transfer characteristics of (a) TGBC and (b) BGBC transistors both bar-coated at 90°C.

The values of mobility reached in TGBC transistors are equal to the ones obtained in BGBC devices, if the transistors are fabricated with same processing conditions.

Looking at the shape of the output characteristics, in case of TGBC devices the curves are always non linear, also at high voltages, showing a positive curvature, which is an indication of high contact resistance. Moreover, the current does not show a clear saturation in many devices. In Fig.96, a comparison between output curves of two devices produced in the same conditions is shown. Fig.96(a) is related to a TGBC configuration, while Fig.96(b) to a BGBC one.
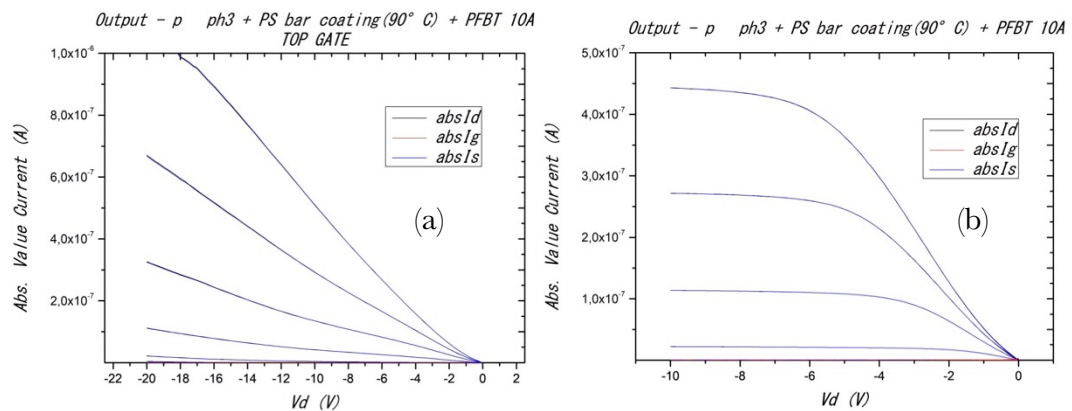
Figure 96. Comparison between output curves of two devices bar-coated at 90°C with TGBC (a) and BGBC (b) configuration.

Conclusions and future perspectives

During this work, the possibility to use *sp*-carbon based molecules, in particular cumulene-like systems, as active material in field-effect transistors was demonstrated. After many trials, a uniform, compact and reproducible crystalline film with high level of coverage was successfully deposited by bar-coating, at temperatures higher than 50°C. This was possible thanks to the use of atactic polystyrene, which is able to increase the film-forming properties of *[3]ph*. The final performances of the electrical devices improved with respect to the initial condition in which only *[3]ph* was deposited by drop-casting. In particular, it was possible to obtain bias independent field-effect mobility values increased of two orders of magnitude and reliability factors higher than 70%. The highest reported value of mobility is 0,05 cm^2/Vs. Furthermore, subthreshold swings of 0,2 – 0,1 V/dec were achieved, indicating a high switching rate. Device stability was enhanced, reducing the hysteresis as well as threshold voltage shifts. Finally, stability in air was improved, even if there are still signs of degradation.

At the end, the possibility to change device configuration, passing from a BGBC architecture to a TGBC one, was demonstrated. The transistors produced in this way have shown better stability and device ideality.

Regarding future work, the first thing to be studied more in details is the stability of *[3]ph*. To do that, the semiconductor should be deposited in a controlled environment, inside the glove-box and not in air, to limit as much as possible exposure to the atmosphere. Moreover, a deep investigation regarding possible degradation mechanisms should be done to understand if this limits the performances of the transistors.

An interesting investigation could be to change the polymer used to blend *[3]ph*. Eventually, also semiconducting polymers could be investigated to obtain films with better conductive pathways. Then, once the most promising polymer has been identified, a more detailed study of the influence of molecular weight and concentration should be performed, to obtain a better understanding of film growth.

Another possibility could be exploring other types of solvents, including the possibility of using two solvents with different solubility, which is often done in the literature to assist bar-coating deposition.

Moreover, one could investigate more into detail the TGBC configuration, trying to use different type of dielectric materials, to find the best one able to create a good interface with the semiconductor in terms of defects and uniformity. Additionally, the materials used for the electrodes could be changed, moving toward fully solution-processed devices.

For what concerns film characterization, precise $X-ray$ diffraction measurements should be carried out, as well as a compositional analysis along the depth, to study more precisely the film structure.

Finally, it would be of great interest to try other *sp*-carbon based molecules of longer chain length and different end-groups, in order to verify if a relation between thin film-conductivity and BLA exists.

Acknowledgments

I would like to thank all those who helped me in writing this thesis with suggestions, criticisms and observations. First of all, I thank professor C. Spartaco Casari, supervisor, and professor Mario Caironi, co-supervisor. Without their support and their assistance this thesis would not exist. I continue by mentioning Dr. Alberto Scaccabarozzi, Dr. Elena Stucchi, Dr. Sonia Peggiani and Stefano Pecorario for their great help during the laboratory activities.

A special thanks goes to my parents, my cousins and my friends who have always encouraged me and helped me to believe in myself, with friendship, kindness and love, even in moments of great difficulty.

Index of figures

Figure 18. Trend of field effect mobility over the years, indicating which values are reliable and which not, due to non-ideality of the device. (a) Comparison between p- and n-type materials for solution processed OFETs (22). (b) Comparison between solution and vacuum technology, indicating also when the material is in form of single crystal (22).

Figure 19. Examples of common thiophene based semiconducting polymers.

Figure 20. Examples of common semiconducting small molecules used in OFETs.

Figure 21. (a)-(b)-(c)-(d) Different morphologies obtained for a blend of TIPS-pentacene:PS deposited by drop casting with different concentrations of TIPS-pentacene: 25, 50, 75 and 100 % (31). (e) Effect of concentration of diF-TES ADT in a small molecule/polymer blend with PTAA deposited by spin coating (32).

Figure 22. Concentration profiles and optical images of a small molecule/polymer blend formed by diF-TES ADT with three different polymers: (a) PαMS, (b) PMMA and (c) s-PS (33).

Figure 23. Concentration profile of a blend formed by TIPS-pentacene with PTAA (34).

Figure 24. (a) Plot of the total energy of polyacetylene as a function of the BLA (37). (b) Schematic representation of a neutral soliton (37). (c) Energy diagram of all the type of solitons (neutral, positive and negative) (37).

Figure 25. (a) Formation of a positive polaron and bipolaron in case of polytiophene (36). (b) Possible molecular structures originated due to polaron formation in polytiophene (36). (c) Energy diagram for the pristine state, positive polaron and positive bipolaron (36).

Figure 26. (a) Potential wells of the neutral and charged molecule. (b) Change in ionization energy of the neutral molecule upon molecular deformation (37).

Figure 27. Split of the frontiers energy levels (HOMO and LUMO) of adjacent molecules upon dimer formation.

Figure 28. (a) Workflow form microscopic charge transfer simulations (39). (b) Fundamental ingredients for transport simulations in organic semiconductors (39).

Figure 29. (a) Schematic representation of the energy diagram for a metal-semiconductor interface of gold and pentacene when the two materials are not in contact (21). (b) Formation of injection barrier for a gold-pentacene junction (21).

Figure 30. Different types of charge injection mechanisms that can be active during charge − injection (21).

Figure 31. Examples of SAMs molecules used for contact engineering (41).

Figure 32. Types of hysteresis cycles in OFETs. (a) higher BCS hysteresis. (b) Lower BCS hysteresis.

Figure 33. Schematic representation of the different types of mechanisms that can lead to an hysteresis cycle (42).

Index of tables

Table 1. List of cumulenes that have been synthetized so far with different terminations and lengths (12).

Table 2. List of type of doping methods used for organic semiconductors with advantages and disadvantages.

Table 3. List of recent values of field effect mobility for solution processed OFETs based on small molecules/polymer blends.

Table 4. In the first two tables the energy values of the frontier molecular orbitals of *[3]ph* obtained by Tykwinski et al. are listed (on the left electrochemical measurements while on the right the optical ones). In the second table, the results of DFT calculation performed by Milani et al. using HSE06/cc-pVTZ as functional are listed.

Table 5. Values of reorganization energy, transferring integral and charge transfer rates for holes and electrons calculated by D. Fazzi et al. for two possible dimers.

Table 6. Values of solubility in g/ml of *[3]ph* in some solvent, showing also the relative boiling points.

References

(1) Casari CS, Milani A. Carbyne: from the elusive allotrope to stable carbon atom wires. MRS Communications 2018;8(2):207-219.

(2) Casari CS, Tommasini M, Tykwinski RR, Milani A. Carbon-atom wires: 1-D systems with tunable properties. Nanoscale 2016;8(8):4414-4435.

(3) Tommasini M, Fazzi D, Milani A, Del Zoppo M, Castiglioni C, Zerbi G. Effective hamiltonian for π electrons in linear carbon chains. Chemical Physics Letters 2007;450(1-3):86-90.

(4) Lambropoulos K, Simserides C. Electronic structure and charge transport properties of atomic carbon wires. Physical Chemistry Chemical Physics 2017;19(39):26890-26897.

(5) Lambropoulos K, Simserides C. Spectral and transmission properties of periodic 1D tight-binding lattices with a generic unit cell: an analysis within the transfer matrix approach. Journal of Physics Communications 2018;2(3):035013.

(6) Milani A, Tommasini M, Del Zoppo M, Castiglioni C, Zerbi G. Carbon nanowires: Phonon and π-electron confinement. Physical Review B 2006;74(15):153418.

(7) Milani A, Tommasini M, Fazzi D, Castiglioni C, Zoppo MD, Zerbi G. First-principles calculation of the Peierls distortion in an infinite linear carbon chain: the contribution of Raman spectroscopy. Journal of Raman Spectroscopy: An International Journal for Original Work in all Aspects of Raman Spectroscopy, Including Higher Order Processes, and also Brillouin and Rayleigh Scattering 2008;39(2):164-168.

(8) Milani A, Tommasini M, Russo V, Bassi AL, Lucotti A, Cataldo F, et al. Raman spectroscopy as a tool to investigate the structure and electronic properties of carbon-atom wires. Beilstein journal of nanotechnology 2015;6(1):480-491.

(9) Cataldo F. Simple generation and detection of polyynes in an arc discharge between graphite electrodes submerged in various solvents. Carbon 2003;13(41):2671-2674.

(10) Kudryavtsev YP, Heimann R, Evsyukov S. Carbynes: advances in the field of linear carbon chain compounds. J Mater Sci 1996;31(21):5557-5571.

(11) Heimann RB, Evsyukov SE, Kavan L. Carbyne and carbynoid structures. : Springer Science & Business Media; 1999.

(12) Wendinger D, Tykwinski RR. Odd [n] Cumulenes (n= 3, 5, 7, 9): synthesis, characterization, and reactivity. Acc Chem Res 2017;50(6):1468-1479.

(13) Chalifoux WA, Tykwinski RR. Synthesis of polyynes to model the sp-carbon allotrope carbyne. Nature chemistry 2010;2(11):967.

(14) Milani A, Tommasini M, Zerbi G. Connection among Raman wavenumbers, bond length alternation and energy gap in polyynes. Journal of Raman Spectroscopy: An International Journal for Original Work in all Aspects of Raman Spectroscopy, Including Higher Order Processes, and also Brillouin and Rayleigh Scattering 2009;40(12):1931-1934.

(15) Milani A, Barbieri V, Facibeni A, Russo V, Bassi AL, Lucotti A, et al. Structure modulated charge transfer in carbon atomic wires. Scientific reports 2019;9(1):1648.

(16) Lang N, Avouris P. Carbon-atom wires: charge-transfer doping, voltage drop, and the effect of distortions. Phys Rev Lett 2000;84(2):358.

(17) Artyukhov VI, Liu M, Yakobson BI. Mechanically induced metal−insulator transition in carbyne. Nano letters 2014;14(8):4224-4229.

(18) La Torre A, Botello-Mendez A, Baaziz W, Charlier J, Banhart F. Strain-induced metal−semiconductor transition observed in atomic carbon chains. Nature communications 2015;6:6636.

(19) Tanaka Y, Kato Y, Tada T, Fujii S, Kiguchi M, Akita M. "Doping" of Polyyne with an Organometallic Fragment Leads to Highly Conductive Metallapolyyne Molecular Wire. J Am Chem Soc 2018;140(32):10080-10084.

(20) Ravagnan L, Piseri P, Bruzzi M, Miglio S, Bongiorno G, Baserga A, et al. Influence of Cumulenic Chains on the Vibrational and Electronic Properties of s p− s p 2 Amorphous Carbon. Phys Rev Lett 2007;98(21):216103.

(21) Bao Z. Organic field-effect transistors. 2007; Available at: http://www.crcnetbase.com/isbn/9781420008012.

(22) Paterson AF, Singh S, Fallon KJ, Hodsden T, Han Y, Schroeder BC, et al. Recent progress in high-mobility organic transistors: a reality check. Adv Mater 2018;30(36):1801079.

(23) Wang C, Dong H, Hu W, Liu Y, Zhu D. Semiconducting π-conjugated systems in field-effect transistors: a material odyssey of organic electronics. Chem Rev 2011;112(4):2208-2267.

(24) Sirringhaus H. Device physics of solution-processed organic field-effect transistors. Adv Mater 2005;17(20):2411-2425.

(25) Xu Y, Liu C, Khim D, Noh Y. Development of high-performance printed organic field-effect transistors and integrated circuits. Physical Chemistry Chemical Physics 2015;17(40):26553-26574.

(26) Panidi J, Paterson AF, Khim D, Fei Z, Han Y, Tsetseris L, et al. Remarkable Enhancement of the Hole Mobility in Several Organic Small-Molecules, Polymers, and Small-Molecule: Polymer Blend Transistors by Simple Admixing of the Lewis Acid p-Dopant B (C6F5) 3. Advanced Science 2018;5(1):1700290.

(27) Paterson AF, Treat ND, Zhang W, Fei Z, Wyatt-Moon G, Faber H, et al. Small molecule/polymer blend organic transistors with hole mobility exceeding 13 cm2 V−1 s− 1. Adv Mater 2016;28(35):7791-7798.

(28) Soeda J, Okamoto T, Mitsui C, Takeya J. Stable growth of large-area single crystalline thin films from an organic semiconductor/polymer blend solution for high-mobility organic field-effect transistors. Organic Electronics 2016;39:127-132.

(29) Smith J, Hamilton R, Qi Y, Kahn A, Bradley DD, Heeney M, et al. The Influence of Film Morphology in High-Mobility Small-Molecule: Polymer Blend Organic Transistors. Advanced Functional Materials 2010;20(14):2330-2337.

(30) Smith J, Zhang W, Sougrat R, Zhao K, Li R, Cha D, et al. Solution-processed small molecule-polymer blend organic thin-film transistors with hole mobility greater than 5 cm2/Vs. Adv Mater 2012;24(18):2441-2446.

(31) Singsumphan K. Influence of polymer on morphological and optical properties of small molecules/polymer blend films. Materials Today: Proceedings 2017;4(5):6478-6484.

(32) Smith J, Heeney M, McCulloch I, Malik JN, Stingelin N, Bradley DD, et al. Percolation behaviour in high mobility p-channel polymer/small-molecule blend organic field-effect transistors. Organic Electronics 2011;12(1):143-147.

(33) Shin N, Kang J, Richter LJ, Prabhu VM, Kline RJ, Fischer DA, et al. Vertically Segregated Structure and Properties of Small Molecule–Polymer Blend Semiconductors for Organic Thin-Film Transistors. Advanced Functional Materials 2013;23(3):366-376.

(34) Hamilton R, Smith J, Ogier S, Heeney M, Anthony JE, McCulloch I, et al. High-performance polymer-small molecule blend organic transistors. Adv Mater 2009;21(10-11):1166-1171.

(35) Troisi A. Charge transport in high mobility molecular semiconductors: classical models and new theories. Chem Soc Rev 2011;40(5):2347-2358.

(36) Coropceanu V, Cornil J, da Silva Filho, Demetrio A, Olivier Y, Silbey R, Brédas J. Charge transport in organic semiconductors. Chem Rev 2007;107(4):926-952.

(37) Bredas JL, Street GB. Polarons, bipolarons, and solitons in conducting polymers. Acc Chem Res 1985;18(10):309-315.

(38) Shuai Z, Wang L, Song C. Theory of charge transport in carbon electronic materials. : Springer Science & Business Media; 2012.

(39) May F. No title. Charge-transport simulations in organic semiconductors 2012.

(40) Natali D, Caironi M. Charge Injection in Solution-Processed Organic Field-Effect Transistors: Physics, Models and Characterization Methods. Adv Mater 2012;24(11):1357-1387.

(41) Liu C, Xu Y, Noh Y. Contact engineering in organic field-effect transistors. Materials Today 2015;18(2):79-96.

(42) Egginger M, Bauer S, Schwödiauer R, Neugebauer H, Sariciftci NS. Current versus gate voltage hysteresis in organic field effect transistors. Monatshefte für Chemie-Chemical Monthly 2009;140(7):735-750.

(43) Gawel P. No title. Functional cumulene-based synthetic molecular materials 2015.

(44) Berkovitch-Yellin Z, Leiserowitz L. Electron density distribution in cumulenes: an X-ray study of tetraphenylbutatriene at 20° C and–160° C. Acta Crystallographica Section B: Structural Crystallography and Crystal Chemistry 1977;33(12):3657-3669.

(45) Fenwick O, Van Dyck C, Murugavel K, Cornil D, Reinders F, Haar S, et al. Modulating the charge injection in organic field-effect transistors: fluorinated oligophenyl self-assembled monolayers for high work function electrodes. Journal of Materials Chemistry C 2015;3(13):3007-3015.

(46) Zhang Z, Peng B, Ji X, Pei K, Chan PKL. Marangoni-Effect-Assisted Bar-Coating Method for High-Quality Organic Crystals with Compressive and Tensile Strains. Advanced Functional Materials 2017;27(37):1703443.

(47) Khim D, Han H, Baeg K, Kim J, Kwak S, Kim D, et al. Simple Bar-Coating Process for Large-Area, High-Performance Organic Field-Effect Transistors and Ambipolar Complementary Integrated Circuits. Adv Mater 2013;25(31):4302-4308.

(48) Zhao J, Tang W, Li Q, Liu W, Guo X. Fully solution processed bottom-gate organic field-effect transistor with steep subthreshold swing approaching the theoretical limit. IEEE Electron Device Lett 2017;38(10):1465-1468.